Investigating the Spatiotemporal Variation in Functional Markers, Gut Metabolites and Ethanol Toxicity in *In Vitro* Cultures of the Rat Jejunum and Hepatocytes

Anjaney Kothari

Dissertation submitted to the faculty of Virginia Polytechnic Institute and State University

in partial fulfillment of the requirements for the degree of

Doctor of Philosophy

in

Biomedical Engineering

Chair: Padmavathy Rajagopalan

Khalil N. Bitar

Rich F. Helm

Xiang-Jin Meng

Scott Verbridge

September 19th, 2019

Blacksburg, VA

Keywords: Intestine, Liver, Integrated Cultures, Spatiotemporal, Ethanol Toxicity, Metabolites

Investigating the Spatiotemporal Variation in Functional Markers, Gut Metabolites and Ethanol Toxicity in *In Vitro* Cultures of the Rat Jejunum and Hepatocytes

Anjaney Kothari

ABSTRACT

The small intestine and the liver regulate several physiological functions together including the absorption and bioavailability of drugs and bile and nitrogen homeostasis. It is important to study these two organs together to gain a holistic understanding of their communication with each other. However, there is a lack of culture models that investigate the use of primary cells/tissues from the liver and the intestine to study their interaction and importance in manifestation of drug toxicity. The studies described in this dissertation were conducted using inverted rat intestinal explants obtained from three regions of the jejunum, named as the proximal, medial and distal jejunum. Markers of enterocyte, goblet cell and Paneth cell function in the jejunum followed *in vivo* – like spatial trends reported for the entire small intestine. Jejunum explants were integrated with hepatocytes to model the intestine-liver axis. Integration of jejunum explants from the proximal region with hepatocytes had a beneficial effect on both hepatocyte urea secretion and jejunum mucin secretion, hinting at communication between these organs in culture. Integrated cultures of the rat jejunum and hepatocytes were used to investigate ethanol toxicity *in vitro*. Trends in activities of enzymes involved in ethanol metabolism and mucus secretion in integrated cultures with proximal jejunum explants corroborated with *in vivo* reports on ethanol toxicity. Various metabolites secreted and metabolized *in vitro* were also identified using mass spectrometry. Spatial trends in concentrations of several lipids including bile acids, lysophosphatidylcholines and fatty acids corroborated with *in vivo* reports of lipid metabolism. The integrated intestine-liver cultures can be used as a platform for future investigations of drug toxicity, lipid metabolism and inter-organ communication.

Investigating the Spatiotemporal Variation in Functional Markers, Gut Metabolites and Ethanol Toxicity in *In Vitro* Cultures of the Rat Jejunum and Hepatocytes

Anjaney Kothari

GENERAL AUDIENCE ABSTRACT

The small intestine and the liver perform several functions together. The small intestine is responsible for the digestion of food, absorption of nutrients and metabolism of oral drugs. The liver is involved in the metabolism of glucose, protein, lipids and drugs. It is important to study these two organs together to gain a holistic understanding of their communication with each other. However, there is a lack of culture models that investigate the use of cells/tissues directly obtained from animal liver and intestine to study their interaction and importance in manifestation of drug toxicity. The studies described in this dissertation were conducted using tissues obtained from three regions of the jejunum segment of the rat small intestine. Functional markers of various cell types in the jejunum followed *in vivo* – like spatial trends reported for the entire small intestine. Jejunum tissues were integrated with liver cells to model the intestine-liver axis. Integration of jejunum tissues from the proximal region with liver cells had a beneficial effect on both liver and intestinal markers, hinting at communication between these organs in culture. Integrated cultures of the rat jejunum and liver cells were used to investigate alcohol toxicity *in vitro*. Trends in activities of enzymes involved in alcohol metabolism and mucus secretion in integrated cultures with jejunum tissues corroborated with *in vivo* reports on alcohol toxicity. Various metabolites secreted and metabolized *in vitro* were also identified using mass spectrometry. Spatial trends in concentrations of lipids including bile acids, lysophosphatidylcholines and fatty acids within the jejunum corroborated with *in vivo* reports of lipid metabolism. The integrated intestine-liver cultures can be used as a platform for future investigations of drug toxicity, lipid metabolism and inter-organ communication.

Acknowledgements

I sincerely thank my advisor, Prof. Padma Rajagopalan, for her immense support, guidance and patience throughout my time in her lab that made this work possible. She not only guided me out of several tough spots in my experiments, but also assisted with surgical and cell isolation procedures when it was required. I want to thank my committee members Dr. Khalil N. Bitar, Dr. Richard F. Helm, Dr. X. J. Meng and Dr. Scott S. Verbridge for their support and guidance at various stages of my doctoral studies. Their time has been an asset for me. I sincerely appreciate Dr. Helm's support towards my last project on metabolite analysis. Judith Jervis and Dr. Sherry B. Hildreth have given so much of their time to teach me sample preparation for mass spectrometry as well as LCMS data analysis. For this, I thank them sincerely.

I want to thank my family - my parents, my brother and Garima Lohiya - without whom I would not have the courage to be here, several thousand miles away from my home, to work towards my PhD. Their support and encouragement helped me thrive during all these years.

I thank the previous and current members of the Rajagopalan lab: Dr. Sophia Orbach, Dr. Andrew Ford, Lauren Wills, Rosalyn Hatlen and Zachary Johnson. I especially want to thank Dr. Sophia Orbach for training me on several experimental techniques, including rat surgeries that were essential to my projects. I am also grateful to Lauren Wills and Zachary Johnson for assisting me with rat surgeries.

I thank my friends Japsimran Singh, Eshwari Someshwara K, Scott Saverot, Dr. Ishan Goswami, Amogh Jalihal, Brittany Boribong, Dr. Jewel Cary, Abhishek Parihar and Somayajulu Dhulipala for all the fun times we shared together.

I would also like to thank Ms. Haiyan Zhang at the VT Metabolic Phenotyping Core for her help in cryosectioning my experimental samples over the course of my graduate studies. I sincerely thank

Mr. Michael Vaught and Mr. Kevin Holshouser at the Chemical Engineering Machine Shop for their help with drilling Transwell inserts that were crucial to my experiments. I express my sincere gratitude towards Ms. Amanda Covey, who has been an incredible support system by always being available to happily answer any and every question that I had.

I gratefully acknowledge financial support from the National Science Foundation (NSF: CBET-1510920), ICTAS Center for Systems Biology of Engineered Tissues at Virginia Tech, and the Interdisciplinary Graduate Education Program in Computational Tissue Engineering at Virginia Tech.

Table of Contents

List of Figures

List of Tables

List of Abbreviations

Abbreviation	Meaning
AA	Arachidonic Acid
AB	Alcian Blue
ADH	Alcohol Dehydrogenase
ALDH	Aldehyde Dehydrogenase
ALP	Alkaline Phosphatase
ALT	Alanine Aminotransferase
ANOVA	Analysis of Variance
BSA	Bovine Serum Albumin
CS	Collagen Sandwich
CYP	Cytochrome P450
DHA	Docosahexaenoic Acid
DMEM	Dulbecco's Minimal Essential Medium
EGF	Epidermal Growth Factor
ELISA	Enzyme-Linked Immunosorbent Assay
EMRT	Exact Mass Retention Time Pair
ENS	Enteric Nervous System
ESI	Electrospray Ionization
EtOH	Ethanol
FA	Fatty Acid
FBS	Fetal Bovine Serum
GC	Gas Chromatography
GI	Gastrointestinal
H & E	Hematoxylin and Eosin
HEPES	(4-(2-hydroxyethyl)-1-piperazineethanesulfonic acid)
HSB	Hue Saturation Background
HSC	Hepatic Stellate Cell
IACUC	Institutional Animal Care and Use Committee
IL-1β	Interleukin-1β
IL-6	Interleukin-6
KC	Kupffer Cell
LCMS	Liquid Chromatography- Mass Spectrometry
LPC	Lysophosphatidylcholine
LSEC	Liver Sinusoidal Endothelial Cell
MS	Mass Spectrometry
NAD+	Nicotinamide Adenine Dinucleotide (Oxidized)
NADH	Nicotinamide Adenine Dinucleotide (Reduced)

NMR	Nuclear Magnetic Resonance
NPC	Non-Parenchymal Cell
OCT	Optimal Cutting Temperature
PAS	Periodic Acid/Schiff's Base
PBS	Phosphate-Buffered Saline
PC	Phosphocholine
PCA	Principal Component Analysis
PCIS	Precision Cut Intestinal Slice
PCLS	Precision Cut Liver Slice
PDMS	Polydimethylsiloxane
PLA	Phospholipase A
pNP	para-Nitrophenol
pNPP	para-Nitrophenol phosphate
SPE	Solid Phase Extraction
TNF-α	Tumor Necrosis Factor-α
ZO-1	Zonula Occludens-1

Chapter 1: Introduction and Background

1.1 The Gastrointestinal Tract

1.1.1 Physiology

The gastrointestinal (GI) tract is primarily involved in the digestion of food, absorption of nutrients and excretion of waste products (1-4). The upper section of the GI tract includes the mouth, esophagus, stomach and the small intestine, where food is taken in and digested (**Figure 1.1**) (2, 4, 5). The lower GI tract includes the large intestine (colon) (2-4). The small intestine performs several functions including digestion, absorption and biotransformation of ingested substances (2, 6-8). The large intestine is involved in the reabsorption of water and electrolytes (2-4). The small intestine is divided into three segments: duodenum, jejunum and ileum (**Figure 1.2**) (2, 4, 9). Several properties of the small and large intestines exhibit spatial variation along their lengths (10-13).

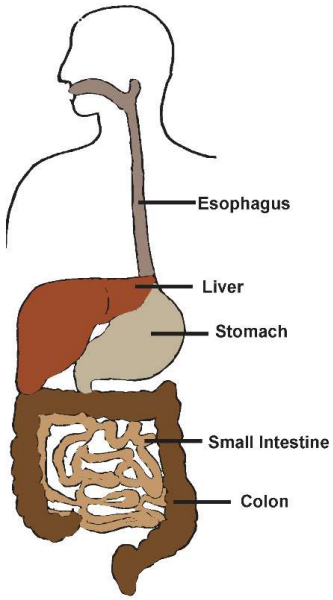

Figure 1.1: The gastrointestinal tract. Food ingested through the mouth is transported to the stomach through the esophagus. The stomach mixes and digests the food, and further digestion

and absorption takes places in the small intestine. The large intestine or colon absorbs water and electrolytes before the waste materials are excreted from the body.

The duodenum is the first part of the small intestine immediately distal to the stomach (2-4). It is the shortest segment and helps neutralize the acidic chyme that enters the small intestine from the stomach through Brunner's glands that secrete bicarbonate ions (14-16). It is also involved in the breakdown of food received from the stomach through pancreatic enzymes and helps in emulsification and absorption of fats through bile (4, 17). The duodenum also expresses phase I and phase II drug-metabolizing enzymes (8, 18). The jejunum is involved in the digestion of food as well as absorption of nutrients such as sugars, fats and amino acids (4, 19). Moreover, the jejunum has the highest abundance of several phase I and phase II drug metabolizing enzymes among the three segments (18). The third segment; ileum is involved in absorption of bile salts and vitamin B_{12} (19, 20). It is also characterized by the presence of Peyer's patches. These are lymphoid tissue patches that function as immune sensors in the intestine (2, 6, 21).

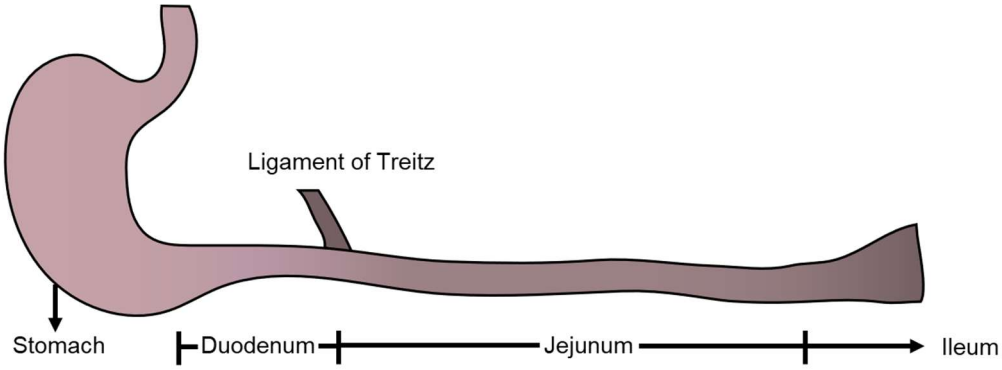

Figure 1.2: Segments of the small intestine. Longitudinally, the small intestine is divided into the duodenum, the jejunum and the ileum. The duodenum is the segment between the stomach and the ligament of Treitz. It is the site of neutralization of acidic chyme and digestion. The jejunum is the primary site of digestion, absorption and metabolism. The ileum helps in the absorption of bile salts and vitamin B_{12} as well as the modulation of the intestinal immune response.

1.1.2 Layers of the small intestine

The small intestine is composed of 4 different layers organized radially: mucosa, submucosa, muscularis externa and serosa/adventitia (**Figure 1.3**) (2, 9, 19, 22). The mucosa is the innermost layer which encounters the food and other ingested substances in the intestinal lumen (9, 19). Therefore, it is the primary layer responsible for absorptive and secretory functions. It also metabolizes any orally administered toxicants (1, 9). The submucosa is where blood vessels, lymphatic vessels and nerves are located (2, 22). The muscularis externa is composed of two layers of smooth muscles. The inner of these layers is the circular smooth muscle layer, followed by the outer longitudinal layer (2, 22). The serosa forms the outermost layer and serves as connective tissue (2, 22).

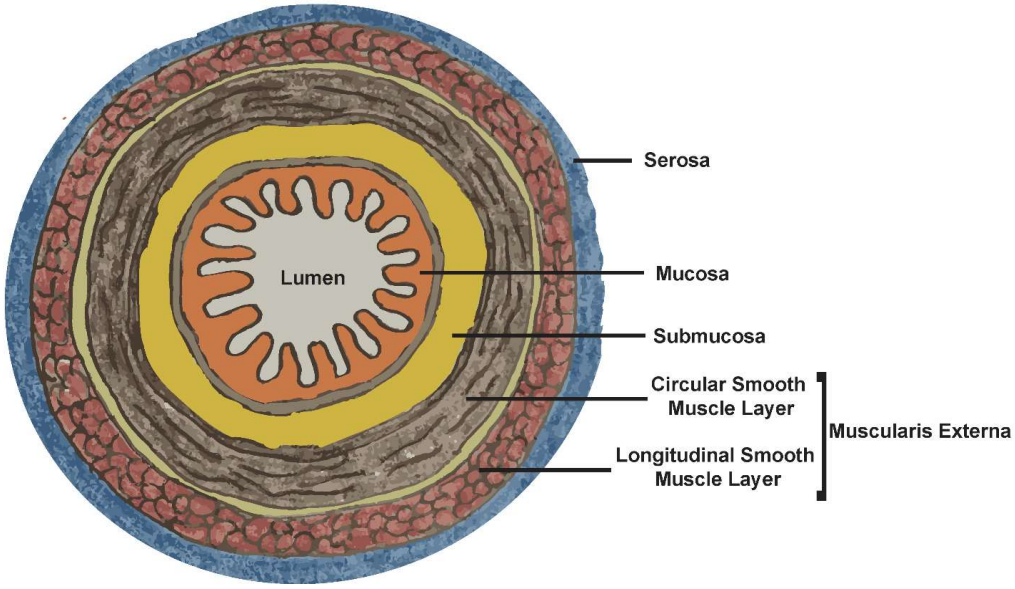

Figure 1.3: Layers of the small intestine. Radially, the small intestine has 4 different layers. The mucosa is the innermost layer, followed by the submucosa, the muscularis externa and the serosa.

1.1.3 Cell types of the small intestinal mucosa

The mucosal layer of the small intestine is organized into finger-like projections known as villi and invaginations called crypts of Lieberkühn (**Figure 1.4**) (1, 6, 23). The villi are populated by three

cell types: enterocytes, goblet cells and enteroendocrine cells (6, 23). Enterocytes are the absorptive cells of the intestinal epithelium, composing 90% of the cell population in the mucosa (6, 23, 24). Goblet cells secrete mucins such as Muc2 that form the protective mucus barrier in the intestine (6, 23). They compose 8-10% of the mucosal cells (23, 24). Enteroendocrine cells compose <1% of the mucosal cells and secrete several digestive hormones including serotonin, secretin, glucagon-like peptides 1 and 2 and incretin (6, 23-25). The crypts are populated by Paneth cells and stem cells (6, 23). Paneth cells secrete antimicrobial proteins such as lysozyme and cryptdins that protect the mucosa against harmful bacteria (23, 26). Stem cells in the crypts periodically renew the mucosal layer (23, 27-29).

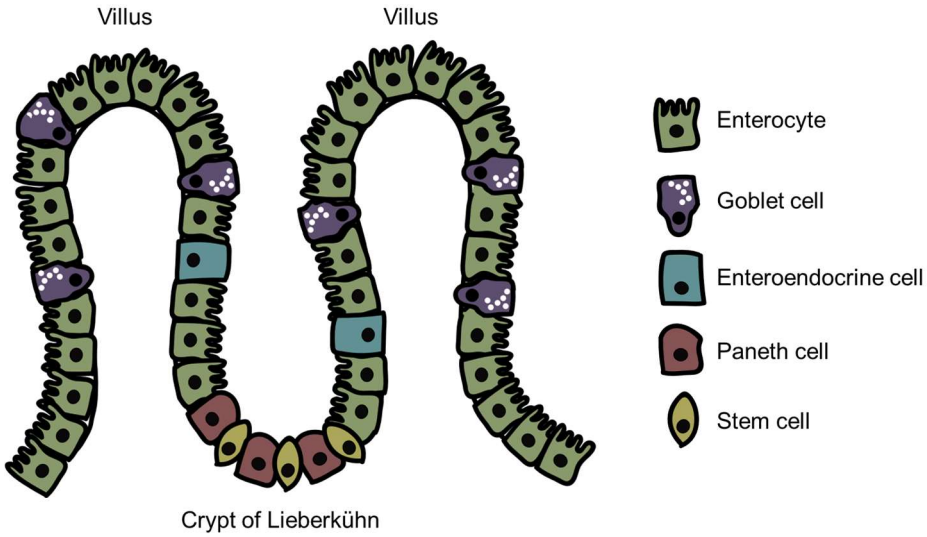

Figure 1.4: Schematic showing the different cell types of the intestinal mucosa. Enterocytes, goblet cells and enteroendocrine cells are arranged along finger-like projections called the villi. Paneth cells and stem cells are located in the invaginations between villi, known as the crypts of Lieberkühn.

1.1.4 *In vitro* models to study the intestine

A number of *in vitro* intestinal models have been developed to study development, metabolism and toxicity (30-32). Some of the commonly used models have been described below.

1.1.4.1 Immortalized Cell Lines

Immortalized or cancerous cell lines are commonly used to model the intestine *in vitro* (33-37). Cell lines such as Caco-2 have been widely used to model enterocytes, while HT-29 cells have been used to model goblet cells (36, 37). Both Caco-2 and HT-29 cells are derived from human colon carcinoma (33, 38, 39). While such cell lines are easy to work with, they lack crucial physiologic similarities (33, 35, 40). For example, Caco-2 monolayers exhibit over 100-fold lower permeability than the human small intestine *in vivo* (35, 41). Moreover, the expression levels of several phase I and phase II enzymes in these cell lines are much lower than *in vivo* levels (33, 35, 41). Co-culture models of Caco-2 and HT-29 cells have been studied to more accurately mimic the *in vivo* physiology with presence of both enterocytes and goblet cells and a mucus layer (34, 37). However, these models still lack several of the other important cell types of the intestinal epithelium.

1.1.4.2 Intestinal Organoids

Recently, organoids developed from intestinal stem cells or crypts cultured in Matrigel™ or similar matrices have gained widespread attention primarily because all cell types of the intestinal epithelium can be achieved in culture (42-51). Intestinal organoids have been used for several applications such as studying and designing treatments for cystic fibrosis, cancers and infections of the GI tract (45, 46, 52-54). However, since the organoids lack an epithelial monolayer for exposure, they cannot be used for studies on transport and absorption of drugs (40, 55). Moreover, intestinal organoid cultures involve complex and time - and cost - intensive protocols to develop mature epithelial cells, posing another challenge (40, 55).

1.1.4.3 Explants and Everted gut sacs

Intestinal tissue explants have been used as another model of *in vitro* culture of the intestine. Traditionally, everted intestinal sacs have been used for short term studies on transport,

absorption and metabolism of drugs and nutrients (56-58). In this system, a segment of the intestine is inverted inside out such that the mucosal layer is exposed to the outside environment (56, 59). Transport studies are then conducted by filling the segment with a buffer and tying it at the ends (56-58).

Compared to everted sacs, traditional explants have been cultured for longer periods of time (60-63). For example, reported culture times of explants from the small and large intestines vary between a few days to several weeks (60-64). These explants have either been isolated as full thickness explants (mucosa to serosa) (64), mucosal layers (65, 66) or biopsies (60, 61, 67, 68).

Precision cut intestinal slices (PCIS) constitute another type of explants that are 300-400 μm thick intestinal tissue slices (69-72). The slices are obtained by sectioning intestinal tissues filled with and embedded in agarose (73). PCIS have been used to study drug metabolism and toxicity, as well as diseases such as intestinal fibrosis (69-72, 74).

Explant-based cultures contain all cell types and layers of the intestine, which makes the investigation of the functions of different cell types possible (75, 76). Moreover, the epithelial layer can be used to investigate drug metabolism in the intestine. The disadvantage to this culture technique is that the explants are not viable for long culture times (75, 77). For example, adult rat jejunum explants are difficult to culture after 24h (62). Moreover, explant cultures of the intestine can be inconsistent, which can prove difficult for *in vitro* studies (76, 77). A potential reason for this variability in culture could be the location-dependent variations in functional markers of the small intestine (78). The second research aim discussed in this document later attempts to address this issue.

1.2 The Liver

1.2.1 Physiology

The liver is the largest solid organ in the body and is involved in several crucial physiological functions (2, 79). It plays a crucial role in metabolism of carbohydrates, lipids and vitamins, synthesis of proteins, cholesterol and bile, and biotransformation of xenobiotics (2, 79, 80). The biotransformation of xenobiotics takes place through phase I and phase II enzymes (80, 81). Phase I reactions such as oxidation and reduction primarily involve cytochrome P450 (CYP) enzymes (80-82). Phase II reactions are conjugation reactions that primarily involve glucuronidation, sulfation, acetylation or methylation of the xenobiotics (80, 82).

1.2.2 Cell types of the liver

The liver is composed of hepatocytes that are the parenchymal cells, and non-parenchymal cells (NPCs) that include the liver sinusoidal endothelial cells (LSECs), hepatic stellate cells (HSCs) and Kupffer cells (KCs) (79, 82-84). Hepatocytes are involved in most of the liver functions and are organized along blood capillaries known as sinusoids (79, 81, 83-86). Hepatocytes and the liver NPCs are separated from each other by a proteinaceous interface called the Space of Disse (79, 87, 88). This interface primarily contains fibronectin and collagen types I and III and helps in transport of nutrients between the sinusoids and the hepatocytes (79, 82, 84).

LSECs are permeable endothelial cells that form the lining of the sinusoid that help in transfer of nutrients from the blood to the hepatocytes (2). KCs are the resident liver macrophages that are located in the sinusoids (79, 81-84, 86). HSCs, found in the Space of Disse, are involved in storage of vitamin A and lipids in a healthy liver (79, 84).

1.2.3 *In vitro* models to study the liver

Several 2D and 3D *in vitro* models have been developed to study the liver. Many liver studies incorporate immortalized and cancerous cell lines such as HepG2, HepaRG and Huh7 cells (83, 84). The following sections focus on some of the primary cultures used to model the liver.

1.2.3.1 2D Models of the Liver

Hepatocytes have been cultured as monolayers on substrates such as collagen (**Figure 1.5A**) (89, 90). However, these monolayers lose hepatocyte phenotype within 24-72h of seeding (89, 91). Reduction in levels of biotransformation enzymes such as CYPs makes these monolayers less sensitive to xenobiotics compared to *in vivo* (92-95). Collagen sandwich (CS) models (**Figure 1.5B**) are formed by culturing hepatocytes between two layers of collagen. These culture models help in inducing polarity in hepatocytes and have been shown to maintain expression of CYP enzymes (96-103). However, CS models also lack heterotypic cell interactions due to presence of only one cell type of the liver. To overcome this limitation, 2D models incorporating secondary cell types such as NPCs, fibroblasts or other cell types with hepatocytes have been developed (104-106).

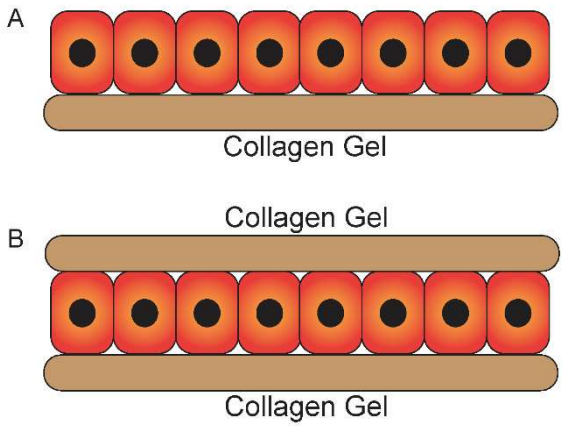

Figure 1.5: Some commonly used 2D *in vitro* models of the liver. (A) Hepatocyte monolayer, and (B) Collagen sandwich cultures. Hepatocyte monolayers are typically cultured on a layer of collagen gel, while hepatocytes in collagen sandwich cultures are seeded on a layer of collagen and allowed to adhere, after which another collagen gel is cast on the top.

1.2.3.2 3D Models of the Liver

3D *in vitro* models of the liver attempt to recapitulate its complex microarchitecture and multiple cell types. Such models maintain both hepatocyte phenotype and the expression levels of biotransformation enzymes (83, 84). In addition to maintaining hepatocyte tight junctions and

polarity, these models also attempt to emulate the extracellular matrix composition and dynamic flow that is observed *in vivo* (79-86, 104, 107).

1.3 The Intestine-Liver Axis

1.3.1 Holistic understanding of the intestine-liver axis

The intestine and the liver together regulate several physiological functions including bile acid homeostasis, nitrogen cycling through the urea cycle, glucose homeostasis, inflammation and drug metabolism (108-111). The intestine-liver crosstalk in drug metabolism has been described below to highlight the importance of studying these two organs together.

The intestine and the liver are the primary organs responsible for metabolism of orally administered drugs and chemicals (23, 112). In the body, the first line of defense against orally ingested chemicals is the intestine, where they are first metabolized and absorbed (23, 113). If the chemicals and/or their metabolites are toxic to the intestine, signs of damage will be seen in the layers of the GI tract (113-115). Substances absorbed by the small intestine are absorbed into the blood stream and transported to the liver through the portal vein (**Figure 1.6**) (2, 108). In the liver, phase I and II biotransformation enzymes involved in nutrient and xenobiotic metabolism process these substances further (108, 116). After metabolism by the liver, chemicals and their metabolites can be excreted through the kidneys and a fraction of these metabolites is sent back to the intestine through the bile duct (108, 117). This process is known as enterohepatic circulation (**Figure 1.6**) (118, 119).

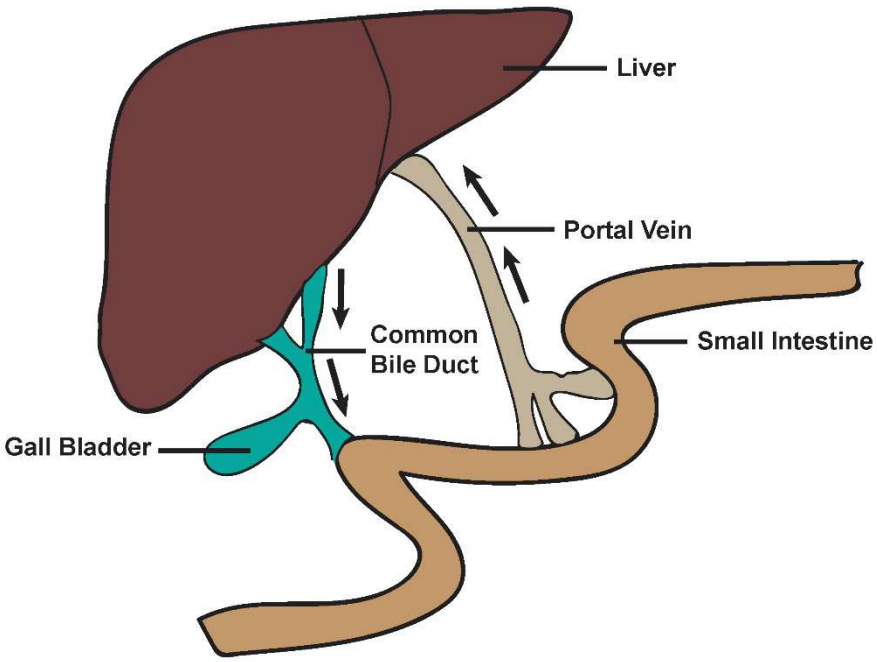

Figure 1.6: Enterohepatic circulation. Nutrients and metabolites absorbed by the small intestine are transported to the liver through the portal vein. The liver metabolizes the absorbed substances further and a fraction of the metabolites is sent back to the small intestine through the common bile duct.

1.3.2 Integrated *in vitro* gut-liver models

Given the host of functions that these two organs regulate together in the body, it is important to study their interaction and communication. *In vitro* models provide the opportunity to isolate this connection and study interorgan effects. Some of the models that have been developed to this end have been described below.

1.3.2.1 Integrated models with cell lines

One of the first integrated *in vitro* models of the gut and the liver utilized HepG2 cells to model hepatocytes in the liver, and Caco-2 cells as intestinal enterocytes (120). In this static model, Caco-2 cells were cultured on the apical side of a Transwell® membrane, while HepG2 cells were cultured in the basal chamber. The system was used to study toxicity of benzo[α]pyrene (a

carcinogen that has been detected in food products) and showed increased sensitivity to the toxicant.

Numerous microfluidic gut-liver on a chip models have also been established to mimic the gut-liver axis (63, 120-126). These models incorporate dynamic flow to mimic the *in vivo* environment. Co-culture models of both the intestine and the liver have also been used in a microfluidic gut-liver on a chip system. For example, Mahler *et al* incorporated a co-culture of Caco-2/HT29-MTX cells to model the intestine and HepG2/C3A cells to model the liver in a microfluidic chip (125). Such static and microfluidic culture systems have been used to investigate drug absorption, metabolism and toxicity (122, 127).

1.3.2.2 Integrated model with primary tissues

Despite the presence of these few *in vitro* models of the gut-liver axis, there is only one study so far that has described the use of primary gut and primary liver tissues to emulate their interorgan communication (128). This study utilized precision-cut liver slices (PCLS) and PCIS from rats and connected them in a microfluidic environment/chamber (128). Culture medium was transferred from the PCIS chamber to the PCLS chamber to mimic *in vivo* physiology. The time points explored in this study were limited to 3-7 h after integration to investigate changes in morphology, induction of phase I and phase II enzymes, and bile acid homeostasis. **Chapter 4** of this document presents a new primary integrated model of the gut and the liver and explores its application in studying ethanol toxicity *in vitro*.

1.4 Ethanol Toxicity

Ethanol-induced toxicity is responsible for 1 in 3 liver transplants in the US alone (129). Moreover, ethanol is responsible for over 48% of all liver disease related deaths (130). Alcohol toxicity is implicated in several liver and gut diseases (131, 132). In the intestine, ethanol can lead to a leaky gut barrier, bacterial overgrowth and translocation of bacteria and their metabolites to the liver

(131, 133-135). In the liver, ethanol can cause alcoholic hepatitis, fatty liver and alcoholic cirrhosis (132, 136, 137).

Ethanol metabolism primarily takes place through three different oxidative pathways in the body, all of which lead to formation of the toxic carcinogenic metabolite acetaldehyde (**Figure 1.7**) (138-143). Around 90% of ethanol is metabolized through the alcohol dehydrogenase pathway (144, 145). The microsomal ethanol-metabolizing system that involves CYP2E1-mediated reaction accounts for less than 10% of ethanol metabolism under normal conditions, but this pathway gets activated under high concentrations of ethanol (144, 145). Metabolism through the catalase pathway occurs in peroxisomes (142, 145). It is a minor contributor under normal conditions but becomes important in starved conditions (143, 145). The product of metabolism of ethanol through these pathways is the toxic compound acetaldehyde, which can be metabolized further to acetic acid through aldehyde dehydrogenase (ALDH) (144, 145). Acetaldehyde can bind to proteins and form adducts, leading to cell damage (146-148). Acetate, on the other hand, is rapidly converted to carbon dioxide and water by incorporation into the Krebs cycle through acetyl-CoA formation (144, 145).

Even though the liver is the primary site of ethanol metabolism in the body, ethanol metabolizing enzymes are expressed in the intestine as well (149, 150). In the intestine, the damaging effects of ethanol due to availability in the lumen after consumption are most expected in the duodenum and the jejunum due to its rapid absorption along the length of the GI tract (150). Effects of acute ethanol consumption on the intestine include inhibition of transport of nutrients across the mucosa, lesions in the mucosa and damage to villi (142, 150-153). Such observations make ethanol an apt toxicant to investigate toxicity in an integrated gut-liver model.

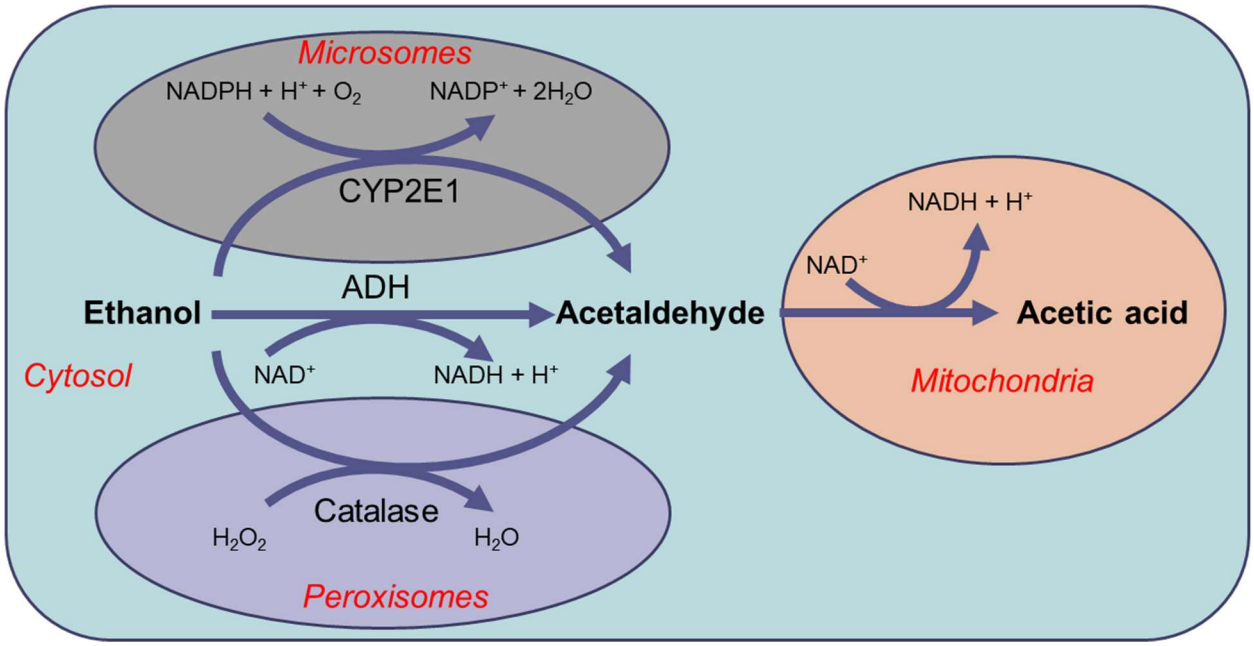

Figure 1.7: Primary pathways involved in ethanol metabolism. The ADH pathway contributes to more than 90% of ethanol metabolism under normal conditions while the CYP2E1 and catalase pathways metabolize the remaining 10% EtOH. In the cells, the ADH, CYP2E1 and catalase pathways are localized in the cytosol, the microsomes and the peroxisomes, respectively. All three pathways lead to formation of the toxic metabolite acetaldehyde, which can be further metabolized into acetic acid by ALDH in the mitochondria (138-143).

1.5 Liquid Chromatography – Mass Spectrometry (LCMS)

Mass spectrometric (MS) techniques have been extensively used for investigating the metabolites secreted by various cells and tissues (154-156). LCMS analyses have been utilized to investigate a wide range of physiological phenomena including disease pathologies as well as drug metabolism by the liver, intestine, and the intestinal microbiota (155, 157-163). In the investigations of the small intestine, LCMS has been also been widely used to study the metabolism of amino acids and lipids including bile acids and fatty acids (164-166).

Most of the *in vivo* studies on intestinal metabolites have focused on the gut microbiome (162, 167, 168). Chen *et al* (162) and Vernocchi *et al* (167) described the importance of metabolomics

studies in understanding host-microbiota interactions in the intestine. *In vivo* gut metabolomics studies have commonly been conducted on fecal samples or intestinal contents, intestinal tissues or urine or blood samples from animals in both targeted and untargeted manner (165, 168-170). Targeted analyses are performed when a known set of compounds is being investigated, while untargeted analyses are used when it is not known which metabolites are going to affected in an experiment (171). Mass spectrometric analyses of metabolites in *in vitro* intestinal cultures have focused on identification of metabolites of a drug or toxicant administered to Caco-2 cells (172, 173). Similar studies on intestinal drug metabolism using LCMS have been conducted using other *in vitro* systems such as primary enterocytes or intestinal contents (174).

Intestinal lipidomics is a growing field of interest due to the diverse roles of lipid biomarkers in investigating the intestine in health and disease (175-177). Lipid composition of the intestine is affected by several factors such as location, number and species of bacteria present and pathological conditions (178-180). Several techniques have been developed to study biological lipids (181, 182). These include gas chromatography (GC), nuclear magnetic resonance (NMR), enzyme-linked immunosorbent assays (ELISAs) and MS (181, 182). GC requires additional processing of samples to improve the volatility of the samples being analyzed as well as higher amounts of the analytes, while NMR has 10-100-fold lower sensitivity compared to MS (181, 182). While ELISAs are less expensive and time-consuming, they have lower sensitivity (20-200-fold) and require prior knowledge of lipid identity before the analysis can be conducted (181, 183-185). Therefore, the technique that has gained the most importance in the field of lipid analysis is MS (181). The reasons for increased reliance on this method are its high sensitivity and sensitivity coupled with high accuracy and the possibility of high throughput analyses of the lipidome (181, 182, 186). In **Chapter 5** of this dissertation, LCMS has been applied to investigate lipophilic metabolites such as bile acids, lysophosphatidylcholines (LPCs) and fatty acids (FAs) secreted or metabolized by the intestinal explants and hepatocytes *in vitro*.

1.6 Gut Microbiome

The human body is home to numerous commensal bacteria. The number of bacteria hosted by the human body has been estimated in different ways in the past few decades (187-189). Most recently, the ratio of number of bacteria to number of human cells in an average human has been recently approximated to be 1.3 (188). The GI lower tract, particularly the colon, houses most of these bacteria. The gut bacteria are increasingly being considered as an 'organ' because of the host of functions they perform in the mammalian body such as nutrient metabolism, vitamin synthesis, bile acid homeostasis and even drug metabolism (190-193). On the other hand, changes in the gut microbiota are also linked to pathologies such as inflammatory bowel diseases, irritable bowel syndrome, colon cancer, non-alcoholic steatohepatitis and liver fibrosis (194-196).

The number and diversity of gut bacteria changes along the length of the GI tract owing to vast differences in the physicochemical conditions in different regions, such as pH, oxygen concentration, immune response and intestinal flow rate (197, 198). For example, gut bacterial diversity changes from aerobic to facultatively anaerobic to obligatorily anaerobic along the length of the rat GI tract due to an oxygen gradient (198). In gut microbial diversity assessed using rat feces, it was found that 65% of the bacteria were gram positive and 35% were gram negative (199). However, the diversity of gut microbiota also increases along the length of the intestine *in vivo* (198). Lactate producing bacteria such as *Lactobacillus* and *Turicibacter* are predominant in the upper GI tract of rats (198-201). The gut microbiota affects intestinal properties in numerous ways. For example, in germ-free mice, as compared with conventionally raised mice, villi in the distal small intestine are longer and thinner, the crypt depth is lower with fewer proliferating stem cells and goblet cells are fewer in number (202, 203).

The effects of antibiotics on the gut microbial diversity have been studied *in vivo*. Treatment of rats with a broad-spectrum antibiotic cocktail containing vancomycin and imipenem led to

significant loss in *Firmicutes* and *Bacteroidetes*, while *Proteobacteria* and *Tenericutes* increased significantly due to loss of competition from the other two groups (201). Ethanol is also known to cause changes in the gut microbiome (131, 204). In human jejunum, ethanol consumption was reported to lead to an increase in the number of gram negative bacteria (205).

1.7 The Enteric Nervous System

The small intestine is also characterized by the presence of the enteric nervous system (ENS), which forms the largest part of the peripheral nervous system in the body (206). The ENS communicates with the central nervous system and controls gut motility and transit of food along the GI tract through its actions on the muscles of the muscularis externa (207). Cells of the enteric nervous system are present in the submucosa (submucosal plexus) as well as between the longitudinal and circular smooth muscle layers in the muscularis externa (myenteric plexus) (207, 208).

The ENS cell types include both enteric neurons and glial cells (206, 208). The neurons of the ENS express numerous stimuli-responsive receptors (208). The stimuli include luminal properties such as nutrient concentrations and pH, as well as mechanical properties of the intestinal mucosa (207, 208). Moreover, enteric neurons express receptors such as the Toll-like receptors which are capable of responding to bacterial metabolites directly (206). Myenteric neurons have also been shown to respond to ethanol toxicity in a location-dependent manner in the intestine (209). Neurotransmitters such as nitric oxide, dopamine, serotonin, acetylcholine and epinephrine are known to be important in maintaining gut homeostasis (210). For example, acetycholine-mediated activation of the acetylcholine receptor can lead to release of mucins and antimicrobial peptides from goblet cells and Paneth cells, respectively (208, 211). In addition to neurons, the enteric glial cells are also responsive to inflammatory stimuli in the intestine and their growth can be regulated by the gut microbiota (206).

1.8 Research Aims

The scientific objectives of my doctoral research are:

Research objective 1: Develop an explant culture protocol to enable investigations of the intestine both alone and in conjunction with hepatocytes.

Research objective 2: Study the variation in properties along the length of the jejunum *in vitro.*

Research objective 3: Investigate the effects of ethanol toxicity in an integrated jejunum-liver model *in vitro.*

Research objective 4: Investigate differences in intestinal metabolites in rat jejunum alone and integrated cultures as a function of location and time.

Chapter 2: Isolating Rat Intestinal Explants for *In Vitro* Cultures

NOTE: This chapter was published in the journal *Current Protocols in Toxicology* (Wiley) in May 2019: ***Kothari, A., & Rajagopalan, P. (2019). Isolating Rat Intestinal Explants for In Vitro Cultures. Current protocols in toxicology, e79, doi: 10.1002/cptx.79***.

2.1 Abstract

The small intestine is an important organ primarily involved in digestion of food and absorption of nutrients. *In vitro* intestinal models are being developed to study this organ in health and disease. Intestinal explants can be used in such investigations since they contain all the major intestinal cell types. We report a detailed procedure to isolate intestinal explants from the rat jejunum. We also report a protocol for culturing them *in vitro* for up to 24h.

Keywords

Small intestine, Explant culture, *In vitro*, Inverted

Significance Statement

The protocol described here enables the inversion of intestinal explants prior to culture. By inverting the intestinal explant the mucosal regions are exposed to the culture medium and any drugs or chemicals that may be tested. The method to culture explants described in this report has potential applications in toxicology and drug metabolism studies.

2.2 Introduction

The small intestine is involved in several functions including digestion, absorption, secretion and biotransformation (2, 6-8). Longitudinally, it is segregated into the duodenum, the jejunum and the ileum (2, 4, 212). Radially, it is organized into four different tissue layers: mucosa, submucosa, muscularis externa and serosa/adventitia (2, 22, 212, 213). The mucosa is the most important layer for absorption, secretion and defense against orally ingested xenobiotics as it is exposed to food and other substances in the intestinal lumen (1, 212, 213).

Small intestinal physiology has been modelled *in vitro* following various approaches. While immortalized cell lines such as Caco-2 cells have been in use as the gold standard, organoids developed from stem cells are being explored for research in intestinal development and disease (33-36, 42-48, 50-54, 214, 215).

Intestinal explants are used to model different sections of the small intestine (60-62, 67, 68). Full thickness explants include all four layers of the intestine, thus closely mimicking the *in vivo* physiology of the intestine (76, 216) (62). We report a detailed procedure to isolate intestinal explants from the rat jejunum. We also report a protocol for culturing them *in vitro*.

2.3 Basic Protocol 1: Isolation of jejunum explants from a rat small intestine

This protocol describes the surgical excision of the small intestine from adult rats, followed by isolation of intestinal explants.

2.3.1 Materials

Oxygenated intestinal medium (see Reagents and Solutions)
Small intestine excised from a rat
Silk sutures (Covidien Sofsilk™; Thermo Fisher Scientific Cat. No. 50-676-26)

Surgical scissors (Thermo Fisher Scientific Cat. No. 08-940)
Tweezers (Thermo Fisher Scientific Cat. No. 13-812-36)
Hemostat (Thermo Fisher Scientific Cat. No. 13-812-8)
Petri dishes (Thermo Fisher Scientific Cat. No. FB0875713)
Tape measure / ruler
Stainless steel rod (custom-prepared), 25 cm in length and 3.3 mm in diameter. At 6.4 mm from one end of the rod, a groove of diameter 1.5 mm and length 6.4 mm should be machined at the university/department machine shop.

Polydimethylsiloxane (PDMS)-coated tweezers. These can be prepared by following the PDMS curing protocol in **Support Protocol 1**.

Millicell® hanging cell culture inserts (EMD Millipore Cat. No. MCSP12H48) with two diametrically opposite holes of diameter 4 mm drilled at a height of 5 mm above the polyethylene terephthalate (PET) membrane of the inserts.

37°C water bath
37°C, 10 % sterile incubator

NOTE: Please ensure that all animal protocols are approved by an Institutional Animal Care and Use Committee (IACUC).

NOTE: Store the intestine excised from the rat in ~ 40mL ice-cold oxygenated intestinal medium (see recipe) supplemented with 50 µg/mL gentamicin in a 50 mL centrifuge tube. Place the centrifuge tube with the intestine on ice.

NOTE: Steps of explant isolation should be performed as promptly as possible to ensure tissue viability and function.

2.3.2 Identifying and separating different segments of the intestine

1. Transfer the small intestine and media from the centrifuge tube to a dish placed in ice in a biosafety cabinet.
2. Separate the duodenum from the rest of the intestine at the ligament of Treitz (**Figure 2.1A-B**).
3. Remove the first 2 cm length of the remaining intestinal segment to prevent working with explants obtained from the duodenum-jejunum transitional region.
4. Find the transition region between the jejunum and the ileum and cut the intestine appropriately at a location where there is a clear increase in diameter and the amount of mesenchyme around the intestinal serosa (**Figure 2.1A**).
5. Remove 2 cm length of the intestine after this to avoid excising explants from the transition region between the jejunum and ileum (**Figure 2.1A**).
6. Measure and record the lengths of the duodenum, jejunum and ileum (**Figure 2.1A**).

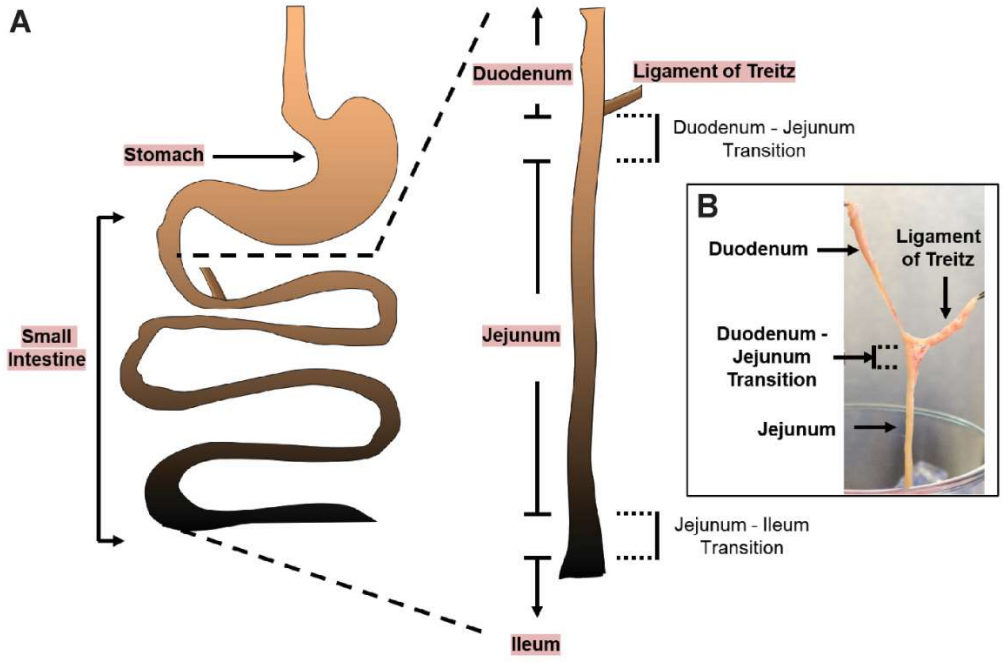

Figure 2.1: (A) A schematic representation of the small intestine. The small intestine is divided into three segments: the duodenum, the jejunum and the ileum. The duodenum ends at the

ligament of Treitz. The beginning of the ileum is determined through an increase in the diameter of the intestine. (B) An image of the ligament of Treitz in a rat intestine, showing the separation between the duodenum and the jejunum.

2.3.3 Inverting the intestinal segments

7. Pull the intestinal segment up on the grooved metallic rod and tie it at the groove with a suture (**Figure 2.2A - B**).

   The purpose of the groove is to help tie the suture and prevent slippage of the intestine during the inversion process.

   If using the intestinal segment is filled with chyme, it is advisable to rinse the chyme out using antibiotic-containing media before step 7.
8. Rinse the intestinal segment 3 times with 5 mL gentamicin-supplemented intestinal medium.
9. Invert the intestinal segment carefully using a pair of PDMS-coated tweezers by slowly coaxing the intestinal segment downwards along the metal rod (**Figure 2.2C - D**).

   Coating the tweezers with PDMS provides a material softer than metal for inverting the intestine and prevents damage to the segment.
10. Rinse the inverted intestinal segment 3 times with 5 mL gentamicin-supplemented intestinal medium.
11. Cut the inverted intestinal segment at the end of the metallic rod and store it in ice-cold intestinal medium in a petri dish on ice until the next step.

    It is crucial that the proximal and distal ends of the inverted segment be identified as such when placing it in the petri dish.

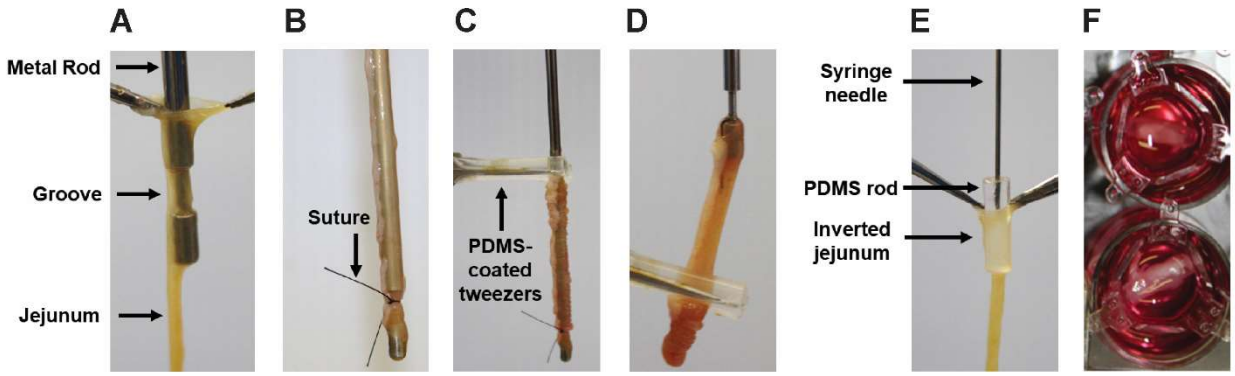

Figure 2.2: Procedure for obtaining and culturing explants from a rat jejunum. (A) The intestinal segment is pulled up on a grooved metallic rod and (B) tied at the groove with a suture. (C - D) The intestinal segment is inverted using a pair of PDMS-coated tweezers by coaxing the intestinal segment in the downward direction. (E) The inverted jejunum is pulled up on a PDMS rod and cut to obtain explants of length ~10mm. (F) The PDMS rod with the explant is transferred and fit into two diametrically opposite holes drilled through a cell culture insert.

2.3.4 Culturing jejunum explants

12. Place a 1.4 cm long Matrigel™ coated PDMS rod on a 10mL syringe needle (**Figure 2.2E**).
13. Pull the inverted intestinal tube on the PDMS rod and snip it off at a length of ~10mm (**Figure 2.2E**).

    NOTE: Before this step, it is advisable to remove the first ~ 5 mm length of the tissue since this is the most prone to damage during the inversion process.

    NOTE: Be careful not to cause the explant to slip off the PDMS rod when cutting the intestinal segment.
14. Adjust the position of the explant to the middle of the PDMS rod and gently slide the PDMS rod through the two diametrically opposite holes in the Millicell® hanging cell culture inserts.
15. Transfer the cell culture inserts to a 12-well plate pre-coated with collagen gels (see **Support Protocol 2**).

16. Add 3 mL oxygenated intestinal medium to cover the whole surface of the explant in the well (**Figure 2F**).

    NOTE: Check for any signs of degradation of the isolated explants such as shedding of visible cell sheets.

17. Once all the explants are isolated, incubate the plate at 37°C in a humidified incubator with 10 % CO_2.

    NOTE: Culture medium may be changed once around 3-4h after isolation to ensure that any proteins/cells leaking from the explant-associated vasculature are removed. Any subsequent media changes will depend on the timeline of the experiments being conducted.

    NOTE: The explants can be cultured for at least 24h after isolation.

    NOTE: Explants should be used immediately after isolation and not frozen for later use.

2.4 Support Protocol 1: Preparation of Matrigel™ – coated PDMS rods

This protocol describes preparation of PDMS rods required to culture the intestinal explants in the basic protocol.

2.4.1 Materials

Sylgard 184 Silicone Elastomer Kit (Thermo Fisher Scientific Cat. No. NC9285739)
Polypropylene straws (4 mm inner diameter)
Vacuum oven (Isotemp Model 281A, Thermo Fisher Scientific Cat. No. 13-262-51)
Matrigel™ (Corning Cat. No. 354234)

2.4.2 Protocol

1. Mix 10 parts by weight of PDMS solution (base) with 1 part by weight of hardening solution (curing agent). Mix manually.

   NOTE: 15 g total solution is enough for 4 straws (each of inner diameter 4 mm, length 15 cm).

2. Incubate the PDMS filled straws in the vacuum oven for 30 min under -12.5 inch Hg vacuum pressure.

   NOTE: This step is necessary to get rid of any air bubbles trapped in the PDMS solution after the manual mixing step.

3. After 30 min, purge the vacuum and turn on the heat (100°C) and let the straws incubate for 2 h to cure the PDMS.
4. Take the straws out of the vacuum oven and cut open the straws carefully along the length using a razor blade, trying not to cut through the PDMS.
5. Cut the PDMS rod into smaller 1.4 cm long segments.

   NOTE: Typically, ~25-30 such tubes can be obtained from 4 straws of 15 cm length.

6. Rinse the PDMS rods in deionized water to remove any debris.
7. Sterilize the PDMS rods in UV light for at least an hour.
8. These rods should be coated with Matrigel™ and hydrated in intestinal medium overnight a day before rat surgery.
9. Place 1 mL of the Matrigel™ solution in a sterile 1.5 mL tube.
10. Dip the sterile PDMS rods into the Matrigel™ solution in the 1.5 mL microcentrifuge tube one at a time.

    NOTE: Maintain the Matrigel™ in ice throughout the coating process to avoid its gelation.

11. Place the Matrigel™ coated rods in the drilled Millicell® hanging culture inserts.

    NOTE: Cell culture inserts must be washed with deionized water to remove any debris from the drilling process and then UV-sterilized for at least an hour, prior to this step.

12. Transfer the inserts to a 12-well plate coated with collagen (See **Support Protocol 2**) and incubate at 37°C (sterile incubator) for 30 min.
13. Hydrate the PDMS rods and cell culture inserts in intestinal media overnight.

2.5 Support Protocol 2: Preparation of Collagen Gels

This protocol describes the coating of 12-well plates with collagen gels before explant culture.

NOTE: Collagen gels should be made the day prior to the rat surgery for explant isolation and culture.

2.5.1 Materials

10X DMEM (see Recipe)
Collagen type I solution – concentration ≤ 3.5 mg/mL, pH ~ 3.1
Can be extracted from rat tail tendons or purchased from a commercial source
1 mM hydrochloric acid (HCl) (diluted from 6M HCl, Thermo Fisher Scientific Cat. No. SA56)

2.5.2 Protocol

1. Add 1-part (by volume) 10x DMEM to 9 parts (by volume) 1.1 mg/mL collagen to prepare the collagen gels. Adjust the pH of the solution to ~7.0-7.3 using 1 mM HCl.
2. Place 0.5 mL of this collagen gel into each well of a 12-well plate to ensure full coverage of the surface.
3. Incubate the plate(s) at 37°C for at least 45 min.
4. Hydrate collagen gels with 1 mL intestinal media overnight.
5. Place the plate(s) back in the incubator until explant isolation.

2.6 Reagents and Solutions

Culture medium for intestinal explants

Materials

Dulbecco's Modified Eagle Medium 10X powder (DMEM) (Gibco Cat. No. 12100046)
Sodium Bicarbonate ($NaHCO_3$) (Thermo Fisher Scientific Cat. No. AC424270010)
Fetal Bovine Serum (FBS) (Gibco Cat. No. 16000044)
Penicillin-Streptomycin (Gibco Cat. No. 15140-122)
Porcine Insulin (MP Biomedicals Cat. No. 0215504450)

Epidermal Growth Factor (EGF) (Thermo Fisher Scientific Cat. No. 354001)
Glucagon (Sigma Aldrich Cat. No. G3157)
Hydrocortisone (hydrocortisone 21-hemisuccinate sodium) (Sigma Aldrich Cat. No. H4881)
0.22 µm filters (VWR Cat. No. 73520998)

Preparation of Intestinal Media

1. Add 1 packet of powdered DMEM and $NaHCO_3$ (3.7 g/L) to 1 L deionized water.

   NOTE: Liquid DMEM may be used as an alternative.

2. Bubble the media with oxygen gas at 45 min per liter of media.

   NOTE: Intestinal media must be freshly oxygenated during culture. Perform the oxygenation before adding any supplements to the culture to prevent foaming.

3. Adjust the pH of the culture media to 7.2 – 7.3.
4. Add supplements to media in the appropriate concentration as listed in **Table 1**.
5. Mix thoroughly and filter through 0.22 µm filter to sterilize the culture media.

   Store at 4°C until further use. Prepare freshly oxygenated media every 24h.

Table 2.1: Intestinal media supplements

Name	Final Concentration
DMEM solution	-
$NaHCO_3$	0.37 % (w/v)
FBS (Heat Inactivated)	10 % (v/v)
Penicillin (Pen)- Streptomycin (Strep)	200 U/mL Pen 200 µg/mL Strep
Gentamicin	50 µg/mL
Insulin	0.5 U/mL
Epidermal Growth Factor (EGF)	20 ng/mL
Glucagon	14.28 ng/mL
Hydrocortisone	1.65 µg/mL

DMEM (10X) solution for collagen gels

1. Add 100 mL of deionized water to a beaker or a glass bottle.
2. Pour 1 pack of powdered DMEM powder to the water and stir using a stir bar on a stir plate.
3. Add 3.7 g of sodium bicarbonate to the DMEM solution prepared in step 2.
4. Keep stirring the solution on the plate for at least 20 min.
5. Adjust the pH to ~7.0-7.1.
6. Filter through a 0.22 µm filter to sterilize the solution and store at 4°C until further use.

   Store for 1 week at 4°C. It is important to check that the DMEM (10X) has not precipitated in the bottle before each use.

2.7 Commentary

2.7.1 Background information

Wilson *et al* (59) first described the method of everting an intestinal segment to overcome the problem of insufficient oxygenation of the mucosal surface. The eversion method involved inserting a glass rod into one end of the intestinal lumen and tying a silk suture around the end. This was followed by pushing the glass rod further into the lumen until the intestine was turned inside out. The everted intestinal segment was filled with a buffer and tied at both ends. Fluid-filled everted sacs were then used to study absorption and transport of methionine, glucose and oxygen from the mucosal side to the serosal side of the explant in 1h.

Nik *et al* (217) described a method to turn the intestine inside out which was slightly different from the ‘eversion’ technique used to obtain gut sacs. They called the method ‘inversion’ of the intestine. In this method, plastic or a stainless steel rod with a hook/groove was inserted into the lumen of 4-5 cm long intestinal segments. A suture was tied around the groove, and the rod was pulled upward until the segment was inverted. The inversion method described in our protocol is an adaptation of this method. In the study by Nik *et al* (217), inverted segments were inflated and

deflated with BD Cell Recovery Solution to dissolve the basement membrane. Epithelial sheets with intact crypts and villi were released as a result of this process. However, these sheets were further dissociated to obtain primary cells of the intestinal epithelium and not cultured intact.

The primary advantage of explant-based cultures is the presence of all cell types as well as layers of the intestine (76, 216). Moreover, the epithelial layer is available for drug metabolism and transport studies. However, explants cultured in this manner are not viable for a long time (77, 216).

We have reported a protocol for isolation and culture of inverted rat intestinal explants for up to 24h. The jejunum explants isolated and cultured in this manner may be used up to 24h or even longer for *in vitro* investigations. The protocol described here enables the inversion of intestinal explants prior to culture. By inverting the intestinal explant, the mucosal regions are exposed to the culture medium and any drugs or chemicals that may be tested. The method to culture explants described in this report has potential applications in toxicology and drug metabolism studies.

While the inversion of the intestinal segments promotes oxygen availability to the mucosal regions, hypoxia-induced damage may still occur to other regions of the explant. In the future, the design of custom bioreactors with oxygen flow may alleviate such problems.

2.7.2 Critical Parameters and Troubleshooting

2.7.2.1 Preparation of PDMS rods and collagen gels

When coating PDMS rods, Matrigel™ must be kept on ice to prevent it from solidifying. Similarly, when making collagen gels, all solutions must be kept on ice until the collagen solution is pipetted into the well plates. This is also to prevent the gel from solidifying.

2.7.2.2 Inversion of intestinal segments

The inversion process is a critical step in the protocol. It is important to be careful during the inversion process as excessive pressure can damage the intestine and may even lead to snipping of the intestinal segment during the inversion process. If this happens, the identification of the location of segments may be difficult and the intestine may start degrading rapidly. Degradation will be visible through shedding of large numbers of sheets into the media. To prevent this, it is recommended that only segments ~10-12 cm long be inverted at a time. Longer segments may lead to difficulties in inversion and may cause damage to the intestine.

After inversion, the first ~5 mm length of the tissue should be removed since this is the region most likely to get damaged while inverting. The rinsing steps before and after inversion to get rid of stool particles and associated gut bacteria are also crucial to the culture.

2.7.2.3 Shedding of cell sheets

Shedding of sheets of cells from the mucosal layer can occur if the explants are damaged during the isolation. The damage could be caused by application of large amount of pressure or accidental scraping of the surface when putting the PDMS rod (with the explant) into the holes in the Millicell® hanging cell culture insert. Lack of oxygenation of media could also lead to degradation of the explants. If attempting to culture for longer time periods, it is recommended that media be prepared fresh every day with oxygenation. It is advisable to take regular notes on any observations of sheet shedding from the explants during the culture period.

2.7.2.4 Extending the protocol to other species

The procedure to obtain and culture intestinal explants described here may be extended to any species where entire sections of the explant may be excised. Although it is difficult to obtain human intestinal sections, it is possible to obtain such tissues from hospitals and clinics with appropriate institutional approvals. If the diameter of intestinal segments is larger than what is described in this protocol, then custom-designed bioreactors will be required.

2.7.2.5 Time considerations

The explants described in this protocol may be cultured up to 24h. Longer studies may be undertaken if required.

2.7.2.6 Effect of the age of the donor

While this protocol has been developed using the adult rat small intestine, it may be extended to small intestine obtained from donor animals of different ages.

2.7.3 Anticipated Results

Intestinal explants can be excised and cultured on PDMS rods in cell culture inserts for up to 24h. A researcher with sufficient experience in the presented method will be able to reproducibly obtain viable explants of ~1 cm length from different regions of the intestine.

Chapter 3: The Assembly of Integrated Rat Intestinal-Hepatocyte Cultures

NOTE: This chapter was accepted to be published in the journal Bioengineering and Translational Medicine (Wiley) in October 2019: ***Kothari, A., & Rajagopalan, P. (2019). The Assembly of Integrated Rat Intestinal-Hepatocyte Cultures. Bioengineering and translational medicine, doi: 10.1002/btm2.10146*.** The article is copyrighted by John Wiley & Sons, Inc (© 2019 John Wiley & Sons, Inc.). It has been reproduced here with permission from John Wiley & Sons, Inc.

3.1 Abstract

The jejunum is the segment of the small intestine responsible for several metabolism and biotransformation functions. In this report, we have cultured rat jejunum explants *in vitro* and integrated them with hepatocyte cultures. We have also investigated the changes in jejunum function at different locations since spatial variations in intestinal functions have been reported previously. We divided the length of the rat jejunum into three distinct regions of approximately 9 cm each. We defined the regions as proximal (adjacent to the duodenum), medial and distal (adjacent to the ileum). Spatiotemporal variations in functions were observed between these regions within the jejunum. Alkaline phosphatase (ALP) activity (a marker of enterocyte function), decreased 2-fold between the proximal and distal regions at 4h. Lysozyme activity (a marker of Paneth cell function) increased from the proximal to the distal jejunum by 40% at 24h. Mucin-covered areas, a marker of goblet cell function, increased by 2-fold between the proximal and distal segments of the jejunum at 24h. When hepatocytes were integrated with proximal jejunum explants, statistically higher urea (~ 2.4-fold) and mucin (57%) production were observed in the jejunum explants. The integrated intestine-liver cultures can be used as a platform for future investigations.

3.2 Introduction

The small intestine is a complex organ that conducts a wide range of functions including the digestion of food, absorption of nutrients and metabolism of drugs and toxicants (1, 6, 218). It is divided into three distinct segments, namely the duodenum, the jejunum and the ileum, each of which is responsible for different specialized functions (1, 23). The intestine is also divided into different layers radially, namely the mucosa, the submucosa, the muscularis externa, and the serosa/adventitia (1, 23). The mucosa forms the intestinal lumen where it absorbs nutrients and secretes proteins (1, 23). The epithelial layer of the intestinal mucosa is composed of five primary cell types: enterocytes (> 90% of the epithelial cell population), goblet cells (~8-10%), enteroendocrine cells (< 1%), Paneth cells and stem cells (6, 23). The first three of these cell types are arranged along finger-like projections known as villi (1, 6). Enterocytes are the primary absorptive cells that also express biotransformation enzymes such as cytochrome P450s (such as CYP2E1) and alcohol dehydrogenase (ADH) (1, 218, 219). Goblet cells are involved in the secretion of glycoproteins called mucins that constitute the mucus barrier in the intestine, while enteroendocrine cells are responsible for the secretion of hormones such as secretin and serotonin (1, 6). The villi are accompanied by corresponding invaginations in the mucosa called the Crypts of Lieberkühn (1, 6). These are populated by Paneth cells that secrete antimicrobial proteins including lysozyme and defensins, and stem cells that renew the mucosal epithelium (1, 6).

The small intestine and the liver work together to modulate several physiological functions such as, bile acid homeostasis, urea cycle, and absorption and metabolism of orally administered drugs and toxicants (23, 220). Disruption of the small intestine-liver axis is implicated in diseases such as alcoholic liver disease and hepatic encephalopathy (221). The interactions between these two organs highlight the need to study them together.

In vitro culture of the small intestine has been conducted through several means such as explants, primary epithelial cells, immortalized cell lines, and more recently, organoids (23, 62, 216). Intestinal explants are comprised of all cell types in the epithelium as well as the underlying layers such as the submucosal mesenchyme (216, 222). These explants have been used to investigate a wide range of intestinal phenomena (23, 62, 77). The adult small intestine has only been cultured for shorter time periods typically ranging from 4h to 5 days (23, 62, 77). Explants from the adult rat jejunum have been shown to degrade after 24h in culture (62).

In vitro studies on integrating the intestine and the liver have focused on using cell lines such as Caco-2 cells with either primary hepatocytes or hepatocyte cell lines such as HepG2 cells (23). So far, there has only been one study where primary models of the intestine and liver were integrated (78). Van Midwoud *et al* (78) integrated rat precision-cut intestinal slices (PCIS) and precision-cut liver slices (PCLS) to investigate the induction of phase I and phase II enzymes and maintenance of bile acid homeostasis over a 7h period (78). This study did not investigate the effects of location or integration on individual functions of the PCIS and PCLS.

Between the duodenum, jejunum and ileum, the jejunum is critical for the digestion of food as well as the absorption of nutrients such as sugars, fats and amino acids (1, 4). The jejunum has the highest surface area for absorption among the three segments (223, 224). It is primarily responsible for the absorption of bile salts transported from the liver into the intestine (225, 226). In addition, the jejunum has the highest abundance of several phase I and phase II drug-metabolizing enzymes in the small intestine (218). Therefore, we have focused our investigations on the jejunum.

In vivo and *ex vivo* studies on the intestine have revealed several spatial trends in its properties (219, 227, 228). For example, activities of enzymes such as ALP and ADH decrease (219, 227), while lysozyme activity and the thickness of the mucus barrier increase along the length of the small intestine (227, 228). However, investigations of location-dependent trends have been

reported primarily through *in vivo* or *ex vivo* studies (219, 227, 228). Moreover, these reports have focused on the differences between the duodenum, the jejunum and the ileum. There are a few *ex vivo* reports where the entire length of the small intestine was divided into small sections to study spatial variations (229, 230). To the best of our knowledge, there are no studies that have reported changes within the jejunum.

Since the location of intestinal cells plays a crucial role in determining their function (219, 227, 228), investigating the jejunum as a whole does not allow for the delineation of these spatial effects. Hence isolating the effects of location on the functions of the jejunum *in vitro* necessitates its division into short segments obtained from different locations. We report the culture of rat jejunum explants to investigate location-dependent variations in biochemical markers of enterocytes, Paneth and goblet cells. In this report, we have divided the length of the rat jejunum into three regions; proximal (adjacent to the duodenum, ~ 9 cm), medial (~ 9 cm) and distal (adjacent to the ileum, ~ 9 cm). Jejunum explants were integrated with primary rat hepatocytes in collagen sandwich (CS) cultures. The effects of integration were evaluated through monitoring changes in intestinal cells and hepatocytes.

3.3 Materials and Methods

Alcian blue, calcium chloride, collagenase type IV, gentamicin sulfate, glucagon, glutaraldehyde, 4-(2-hydroxyethyl)-piperazine-1-ethanesulfonic acid (HEPES), hydrocortisone, periodic acid, protease inhibitor cocktail and Schiff's reagent were purchased from Sigma-Aldrich (St. Louis, MO). All other chemicals were purchased from Thermo Fisher Scientific (Waltham, MA) unless otherwise stated.

3.3.1 Collagen extraction

Type I collagen was extracted from rat tails as described previously (231, 232). Briefly, rat tail tendons were dissolved in acetic acid. The resulting solution was centrifuged at 13,000 x g,

following which collagen was precipitated with 30% (w/v) sodium chloride. Precipitated collagen was centrifuged at 8,500 x g and the pellets were resuspended in 0.6% acetic acid. The resulting suspension was dialyzed against 1 mN hydrochloric acid. Collagen concentration was measured by measuring absorbance at 280 nm and used at a pH of 3.1. Collagen was sterilized with chloroform prior to cell culture. Collagen gels were cast at a concentration of 1.1 mg/mL in 12-well plates (250 µL per well for hepatocyte seeding and 500 µL per well for jejunum explant cultures).

3.3.2 Isolation and culture of primary rat hepatocytes

Primary hepatocytes were isolated from female Lewis rats weighing 180-210 g (Envigo, Indianapolis, IN) using an *in situ* two-step collagenase method as previously described before (231, 233). Animal care and excision protocols were approved by and conducted in accordance with the Virginia Tech Institutional Animal Care and Use Committee. Total isolated hepatocyte counts typically lay in the range of 100-150 million hepatocytes with ≥ 97% viability, as determined by trypan blue exclusion. Hepatocytes were seeded on collagen gels at a cell density of 5 x 105 cells/well in a 12-well plate. A second collagen gel layer (1.1 mg/mL) was deposited on top of the hepatocyte monolayer approximately 3h post-hepatocyte seeding, to assemble CS hepatocyte cultures. Hepatocyte culture medium was added 4h post-seeding. Hepatocyte culture medium was composed of Dulbecco's modified Eagle medium (DMEM), with 0.37% sodium bicarbonate, 10% (v/v) heat-inactivated fetal bovine serum, 200 U/mL penicillin, 200 µg/mL streptomycin, 0.5 U/mL insulin (MP Biomedicals, Santa Ana, CA), 20 ng/mL Epidermal Growth Factor (EGF), 14.28 ng/mL glucagon, and 7.65 µg/mL hydrocortisone. Cultures were maintained at 37°C in a humidified incubator with 10% carbon dioxide.

3.3.3 Isolation and culture of rat jejunum explants

The small intestine was excised from female Lewis rats from which the liver was excised. The duodenum was removed at the ligament of Treitz (**Figure 3.1A**). The jejunum was separated from

the ileum at the zone where there was an increase in the diameter and amount of mesenchyme (**Figure 3.1C**). A detailed procedure on the excision of jejunum explants has been previously reported (222). Briefly, an inverted jejunum segment (approximately 1 cm in length) was pulled on Matrigel®-coated polydimethylsiloxane (PDMS) rods, placed in a Millicell® insert (**Figure 3.1D and E**) and transferred to 12-well plates containing collagen gels. Oxygenated gentamicin-containing medium (3 mL) was added to each well. Each jejunum segment resulted in approximately 18 explants, with an average length of 9.9 ± 0.4 mm (n = 84 explants from 7 rats) (**Figure 3.1D**). The top six sections were identified as proximal, the middle six as medial and the bottom six as distal (**Figure 3.1B**). Explant cultures were maintained at 37°C in a humidified incubator with 10% CO2. The media was removed and replenished at 3h and 4h. At 4h, the explants were transferred to new collagen-coated wells to be maintained as jejunum cultures, or to well-plates that contained hepatocyte cultures to assemble integrated jejunum-hepatocyte cultures. All cultures (CS alone, jejunum, or integrated) were supplemented with 3 mL of hepatocyte medium.

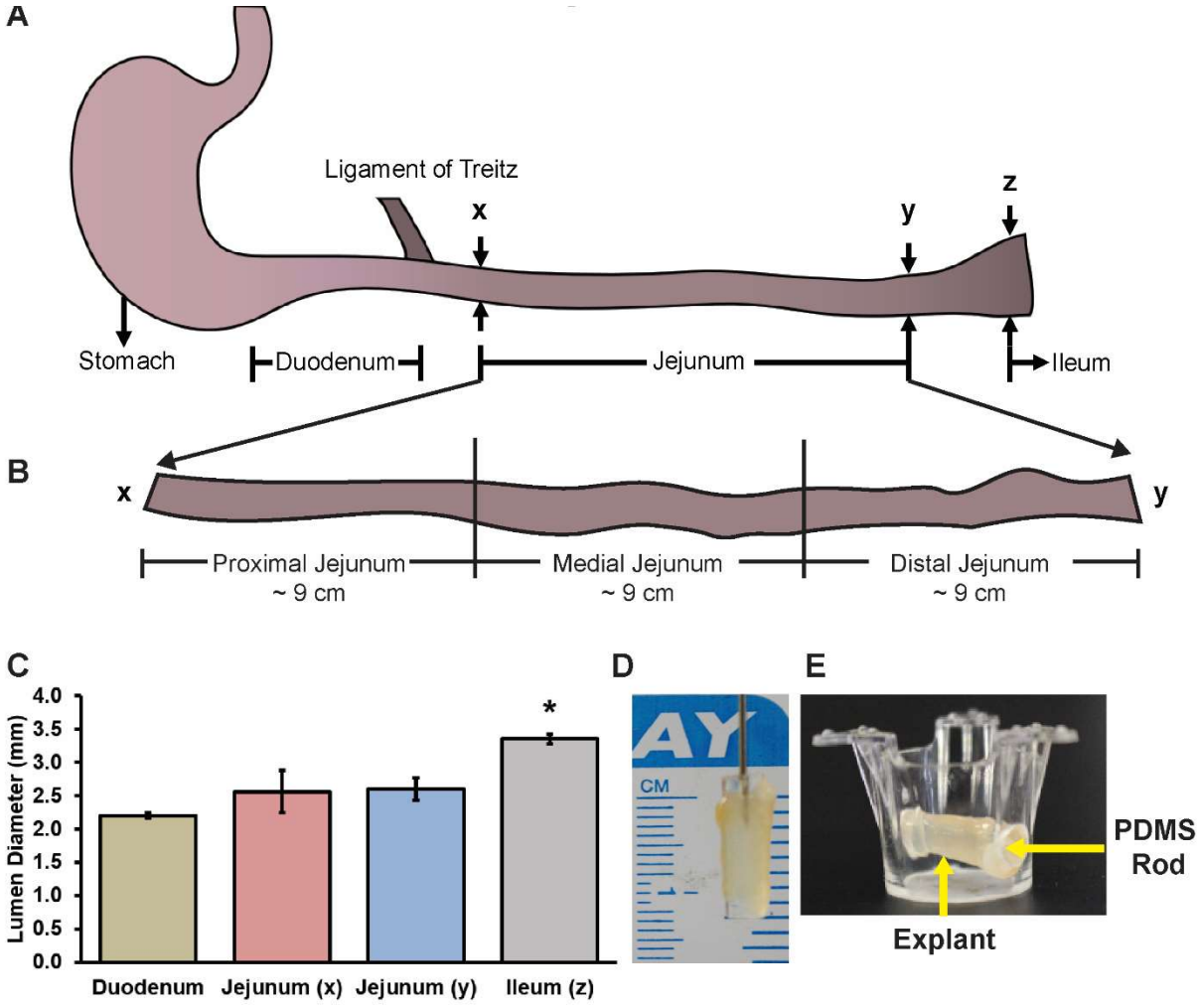

Figure 3.1: (A) Schematic of the small intestine showing its longitudinal segments. The duodenum ends at the ligament of Treitz. 'x' and 'y' denote the start and the end of the jejunum, respectively. 'z' denotes the start of the ileum. (B) The jejunum was divided into three segments, namely, proximal, medial and distal jejunum. (C) The jejunum-ileum transition is marked by an increase in diameter of the intestine. (D) To excise explants, the jejunum was inverted, pulled up on a PDMS rod and cut at a length of ~10 mm. (E) The PDMS rod was suspended in a Transwell® insert with two diametrically opposite holes drilled through it. * denotes $p < 0.05$ relative to duodenum, jejunum (x) and jejunum (y).

3.3.4 Protein measurements in hepatocyte cultures and jejunum explants

All CS cultures were ended through collagenase IV-mediated digestion of the collagen gels. This was followed by the lysis of hepatocyte protein in the presence of a protease inhibitor cocktail. The protease inhibitor cocktail consisted of 4-(2-aminoethyl) benzenesulfonyl fluoride hydrochloride, aprotinin, bestatin, E-64, leupeptin, and pepstatin A as described before (231). Jejunum explants were homogenized using a TissueRuptor® homogenizer (Qiagen, Hilden, Germany) at a speed setting of 8 for 2 min per sample. Homogenization was performed in 0.5 mL lysis buffer in presence of the protease inhibitor cocktail to isolate protein. Homogenates were centrifuged at 10,000x g for 5 min and the supernatant was collected and frozen until further use. Protein concentrations in cell or tissue lysates were determined through the Bradford assay using a commercially available kit (Coomassie (Bradford) Protein Assay Kit; Thermo Fisher Scientific) as previously described (231).

3.3.5 Measurement of alkaline phosphatase (ALP) activity

ALP activity was measured using a commercially obtained assay kit (Abcam, Cambridge, UK) following the manufacturer's instructions. Briefly, jejunum explant lysates and hepatocyte lysates were incubated with para-nitrophenyl phosphate (pNPP) substrate for 1h at 25 °C, following which the absorbance was measured at 405 nm to quantify the para-nitrophenol (pNP) produced through ALP-mediated dephosphorylation. A standard curve was generated using the pNPP substrate and ALP enzyme provided by the manufacturer.

$$ALP\ Activity\ \left(\frac{U}{mL}\right) = \frac{\frac{A}{V}}{T},$$

where A = concentration of pNP generated in samples (µmol), V = volume of sample (mL), T = reaction time (min). ALP activity values were normalized to the protein content of each sample.

3.3.6 Measurement of alanine aminotransferase (ALT) activity

Alanine aminotransferase (ALT) activity was measured using a commercially obtained kit (ALT (SGPT) Reagent, Colorimetric, Endpoint Method; Teco Diagnostics, Anaheim, CA) following the manufacturer's protocol (231). The absorbance was measured at 505 nm. Absorbance values were converted to enzyme concentrations using a calibrator of known ALT activity provided by the manufacturer.

3.3.7 Measurement of lysozyme activity

Lysozyme activity in spent culture media was measured using a commercially available assay kit (EnzChek™ Lysozyme Assay Kit, Thermo Fisher Scientific) following the manufacturer's protocol. Briefly, spent culture media was incubated with fluorescein-conjugated *Micrococcus lysodeikticus* cell walls that acted as a lysozyme substrate. Fluorescence was measured after 2h of incubation at 37°C at excitation and emission wavelengths of 485 nm and 538 nm, respectively. Lysozyme activity values were calculated through a standard curve and normalized to protein content.

3.3.8 Urea secretion

Urea secretion was measured as described previously (234, 235) through a colorimetric, diacetyl monoxime based assay using a commercially available Blood Urea Nitrogen (BUN) assay kit (Stanbio Laboratory, Boerne, TX). Absorbance was measured at 520 nm and a standard curve was generated using urea diluted in culture medium.

3.3.9 Cryosectioning of jejunum explants

Explants were cut lengthwise and fixed with 2 mL of glutaraldehyde (3% w/v) at 4°C for 7h. Fixed samples were washed with PBS (1X), followed by a 5 min incubation in 15% (w/v) sucrose, and a 15 min incubation in 30% (w/v) sucrose solutions. Thereafter, samples were equilibrated in Tissue-Tek Optimal Cutting Temperature (OCT) compound (Electron Microscopy Sciences, Hatfield, PA) for 15 min. Samples were frozen in OCT compound in cryomolds using an isopentane solution partially frozen with liquid nitrogen (236). The embedded samples were then

cryosectioned transversely at a thickness of 10 μm per section to visualize the intestine. Sections were stored at -80°C until used. Prior to histochemical or immunofluorescence staining, cryosections were fixed with 3% (w/v) glutaraldehyde (in PBS (1X)) for 20 min at room temperature.

3.3.10 Hematoxylin and Eosin staining of jejunum explants

Jejunum cryosections were stained with Mayer's Hematoxylin and Eosin according to the manufacturer's instructions (237). Briefly, cryosections were stained with Mayer's hematoxylin solution, and rinsed in warm water (pH = 8.2-8.4). Thereafter, sections were dehydrated in 95% ethanol and stained with Eosin Y solution (0.5% (w/v), in 95% (v/v) ethanol alcoholic solution, pH = 4.2 - 4.3). Stained sections were decolorized in 95% ethanol until streaking of the eosin stain ceased. Finally, samples were serially dehydrated for 2 min each in 95% (v/v) ethanol and absolute ethanol and mounted on glass slides with Cytoseal™ 60.

3.3.11 Alcian blue (AB)/Periodic acid-Schiff's base (PAS) staining of jejunum explants

Jejunum cryosections were stained with Alcian blue/PAS staining to visualize acidic and neutral mucins. Staining procedures were adapted from a previous report (238). Briefly, samples were equilibrated with 3% (v/v) acetic acid and incubated with the Alcian blue dye (1% (w/v) in 3% (v/v) acetic acid, pH = 2.5) for 2.5h. Non-specific stain was removed with 3% (v/v) acetic acid. Thereafter, samples were incubated in 0.1% (w/v) periodic acid, followed by incubation with Schiff's reagent. Stained samples were washed in running tap water for 10 min, rinsed in deionized water, and serially dehydrated for 2 min each in 95% (v/v) ethanol and absolute ethanol. Finally, the samples were mounted on glass slides with Cytoseal™ 60.

3.3.12 Morphometric analyses

Villus area was measured using FIJI (ImageJ software, NIH) (239) for n = 20 villi per condition. The fraction of each cryosection stained with Alcian Blue was measured using FIJI (n = 3 cryosections per condition). Images of complete cryosections were thresholded using the hue, saturation and brightness (HSB) color model. The image hue and saturation parameters were adjusted to isolate blue-colored areas stained by AB in the samples. The blue colored area was then divided by total area of the cryosection to calculate the 'mucin-covered area fraction'.

3.3.13 Immunofluorescence staining for ZO-1

Fixed samples were treated with 0.1% (w/v) sodium borohydride, followed by a 5 min incubation in 0.05% (v/v) TritonX-100. The samples were rinsed with warm PBS and blocked with 1% (w/v) BSA in PBS (1X) supplemented with rabbit serum (15μL/mL) at 37°C for 1h. Samples were incubated at 4°C overnight with primary monoclonal anti-rat ZO-1 antibody (Developmental Studies Hybridoma Bank, University of Iowa; 1:5 dilution). A FITC-conjugated rabbit anti-rat IgG secondary antibody was then used to visualize ZO-1 expression. Nuclei were stained with Hoechst 33258 dye. Samples were imaged using a Zeiss LSM confocal microscope (Oberkochen, Germany). Immunofluorescence was quantified through ImageJ as corrected total fluorescence intensity using n = 10 images as described previously (232). Corrected total fluorescence intensity = [Integrated fluorescent intensity] – [fluorescent area x mean background fluorescence]. The mean background fluorescence was measured as the mean of fluorescence intensities at 10 locations per image not corresponding to the villi.

3.3.14 Statistical Analyses

Statistical significance was determined using p-values determined by one-tailed student's t-tests, assuming unequal variance when sample sizes were unequal, and equal variance when sample sizes were equal between the groups being compared. The Bonferroni correction (multiple

hypothesis testing) was applied with α = 0.05. All data are reported as mean ± standard deviation, and n denotes sample size.

3.4 Results

3.4.1 Identification of different segments of the rat small intestine

The total length of the small intestine excised from the rats was found to be 92.7 ± 3.8 cm (n = 7 intestines). The duodenum, jejunum and ileum were identified and segregated based on their morphological differences (**Figure 3.1A**). The lengths of the duodenum, jejunum and ileum were found to be 9.6 ± 0.6 cm (n = 7 intestines), 26.0 ± 1.2 cm (n = 7 intestines) and 34.4 ± 1.7 cm (n = 5 intestines) respectively. These lengths are in agreement with previous reports (240). The jejunum was divided into 3 segments of equal length (~ 9 cm), denoted as proximal, medial and distal jejunum (**Figure 3.1B**). The inner diameters of the intestinal segments were measured at the end of the duodenum, the beginning and end of the jejunum, and the beginning of the ileum (n = 3 intestines for each location) (**Figure 3.1C**). The diameter at the end of the duodenum was 2.21 ± 0.04 mm, which was statistically similar to the diameters at the start (2.56 ± 0.31 mm) and end (2.60 ± 0.17 mm) of the jejunum. The diameter at the start of the ileum was 3.36 ± 0.07 mm, which was statistically higher (29%) than the diameter at end of the jejunum ($p \leq 0.05$). Jejunum explants approximately 1 cm in length were excised and subsequently cultured in Transwell® inserts in 12-well plates (**Figure 3.1D and E**).

3.4.2 Spatial differences in enterocyte markers

Explants isolated from the jejunum were used to evaluate the spatial variation in enterocyte markers in the three jejunum locations (proximal, medial and distal; n = 3 explants per location). ALP and ALT activities were measured after 4h and 24h of culture. At 4h, explants from the distal jejunum exhibited a ~2-fold lower ALP activity ($p \leq 0.05$) compared to values obtained from the proximal or medial sections. The ALP activities of the proximal and the medial sections were

statistically similar ($p > 0.05$) (**Figure 3.2A**). The decrease in ALP activity is consistent with reported *in vivo* observations in rats (227, 230). ALT is expressed in intestinal enterocytes and is involved in glutamine and glutamate metabolism (241). At 4h, the ALT activity in culture media from the distal jejunum was 1.8-fold higher than in proximal and medial sections ($p \leq 0.05$ for both proximal and medial comparisons) (**Figure 3.2B**). However, at 24h, no significant differences were observed in the activities of the two enzymes as a function of location (**Figures 3.2D-E**). To evaluate enterocyte function at longer time points, ALP activity was measured after 72h in culture. Compared to the 24h time point, ALP activities of the proximal and medial jejunum decreased significantly at 72h (38% and 42%, respectively; $p \leq 0.05$) **(Figure 3.3A)**. ALP activity in the distal segment decreased by 29% ($p > 0.05$).

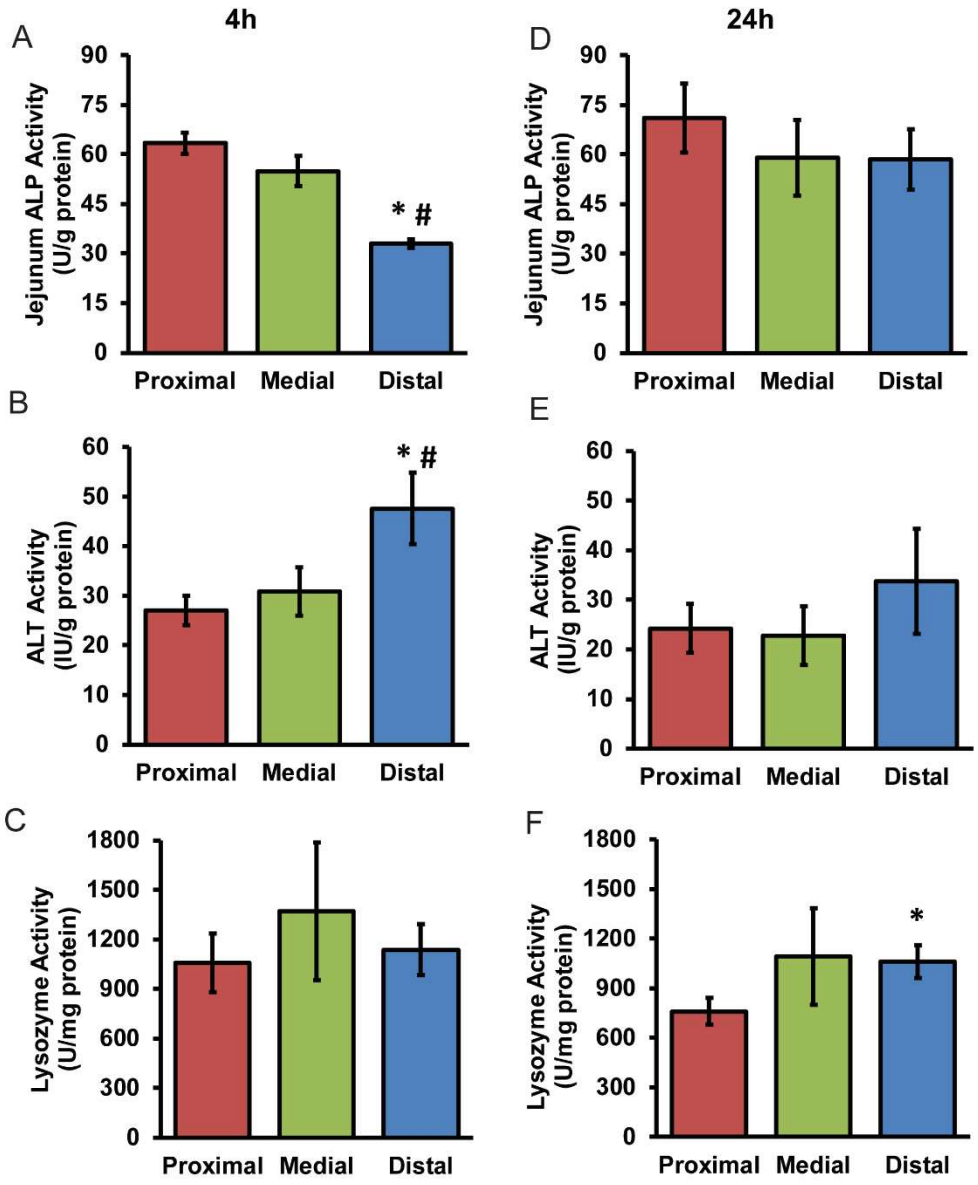

Figure 3.2: Jejunum ALP activity (A, D), ALT activity (B, E), and lysozyme activity (C, F) activity measured after 4h and 24h of explant culture. * and # denote $p \leq 0.05$ relative to proximal and medial jejunal segments respectively.

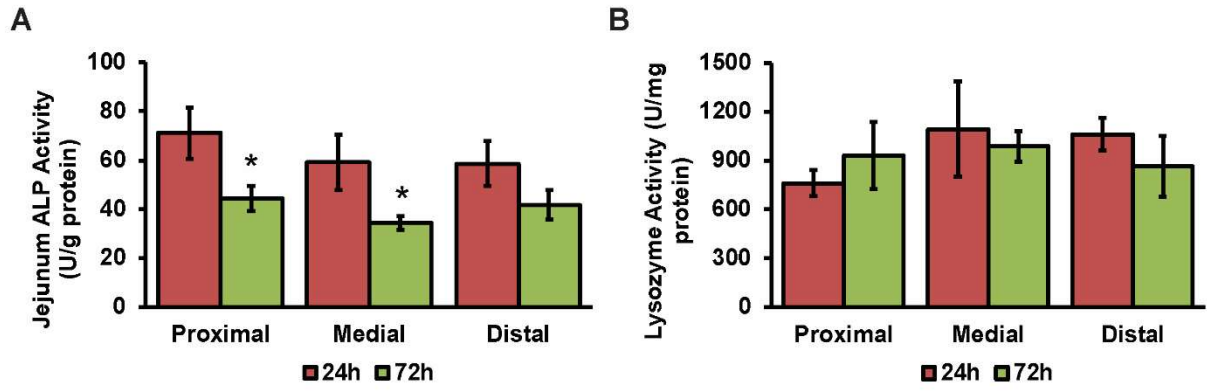

Figure 3.3: (A) Jejunum ALP activity and (B) lysozyme activity at 24h and 72h after culture (* denotes $p \leq 0.05$ relative to 24h time-point).

3.4.3 Variations in Paneth cell function

Lysozyme activity was measured at 4h and 24h to assess Paneth cell function (n = 3 explants per jejunum location). The enzyme activity measured at 4h did not exhibit variation (**Figure 3.2C**). In contrast, a spatial trend was observed at 24h. Lysozyme activity increased significantly (40%) from proximal to distal jejunum ($p \leq 0.05$) (**Figure 3.2F**). Lysozyme activity in the medial jejunum was 43% higher than proximal, but this difference was not statistically significant ($p > 0.05$). Laval *et al* (227) reported an increase of approximately 2.5-fold from proximal to distal jejunum in rats *in vivo* (0h), which is qualitatively similar to what is reported in the present study. Lysozyme activity was measured at 72h to evaluate Paneth cell function at longer time points. Lysozyme activity did not vary significantly ($p > 0.05$) compared to the activity at 24h for proximal, medial or distal jejunum explants **(Figure 3.3B)**.

3.4.4 Changes in epithelial cells and villi morphology

H&E staining and villus area measurements were performed to investigate changes in morphology (**Figures 3.4A-L**). Explants from all three locations of the jejunum showed the crypt-villus morphology at 0h, 4h and 24h after culture as visualized through H&E staining (**Figures 3.4A-C, E-G and I-K**). The number of epithelial cells appeared to decrease with culture time with

distal explants exhibiting the greatest decrease (**Figures 3.4A-C, E-G and I-K**). Villus area did not differ significantly between the proximal, medial and distal regions of the jejunum at the 0h, 4h and 24h timepoints (n = 20 villi per condition) (**Figures 3.4D, H and L**). Villus surface area has been reported to be similar between the duodenum, jejunum and ileum in rats *in vivo* (242). Villus morphology appeared to be degraded in the distal jejunum after 72h in culture compared to the proximal and medial segments (**Figures 3.5A-C**). The villus area in the distal explants at 72h was significantly lower than the proximal or medial jejunum (42% and 38% lower, respectively; n = 20 villi per condition; $p \leq 0.05$ for both) (**Figure 3.5D**).

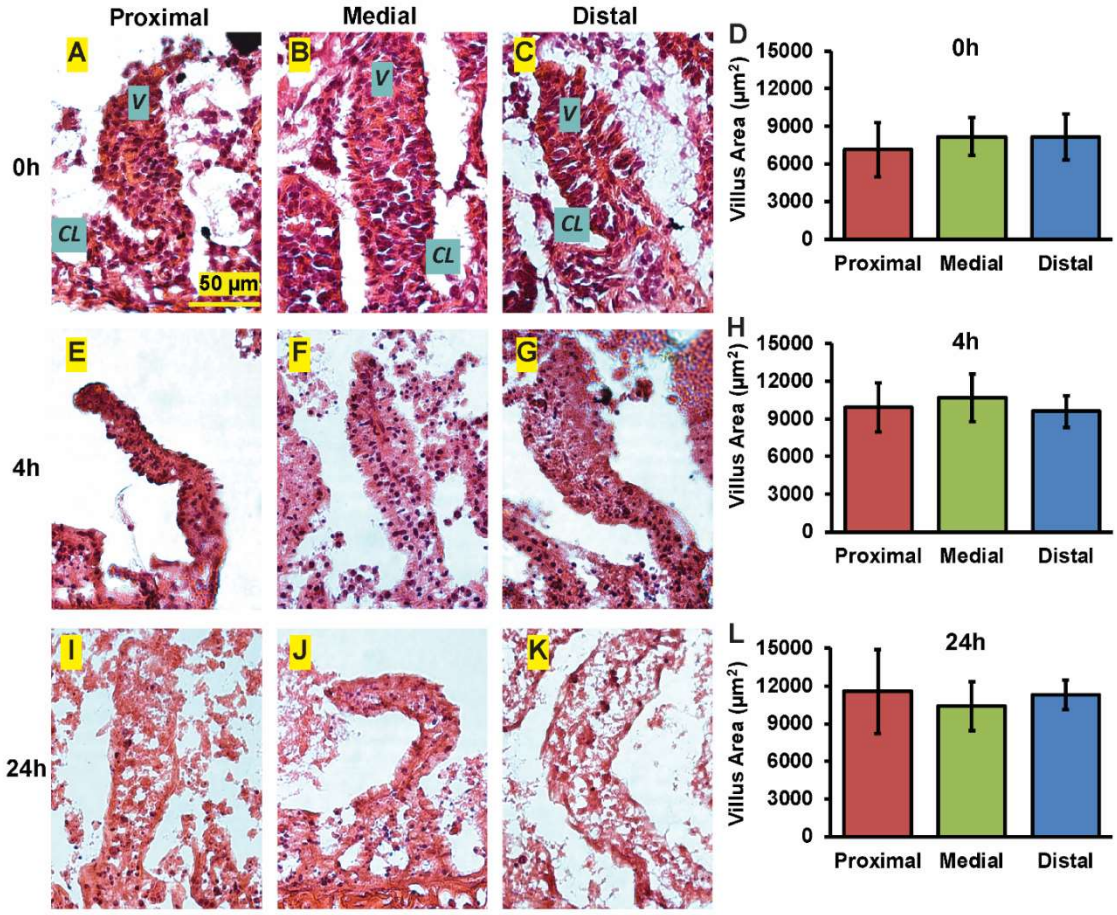

Figure 3.4: H&E staining of the proximal, medial and distal jejunum after (A - C) 0h, (E - G) 4h and (I - K) 24h in culture. V = villi, CL = crypts of Lieberkühn. Morphometric analysis of villus area across locations at (D) 0h, (H) 4h and (L) 24h.

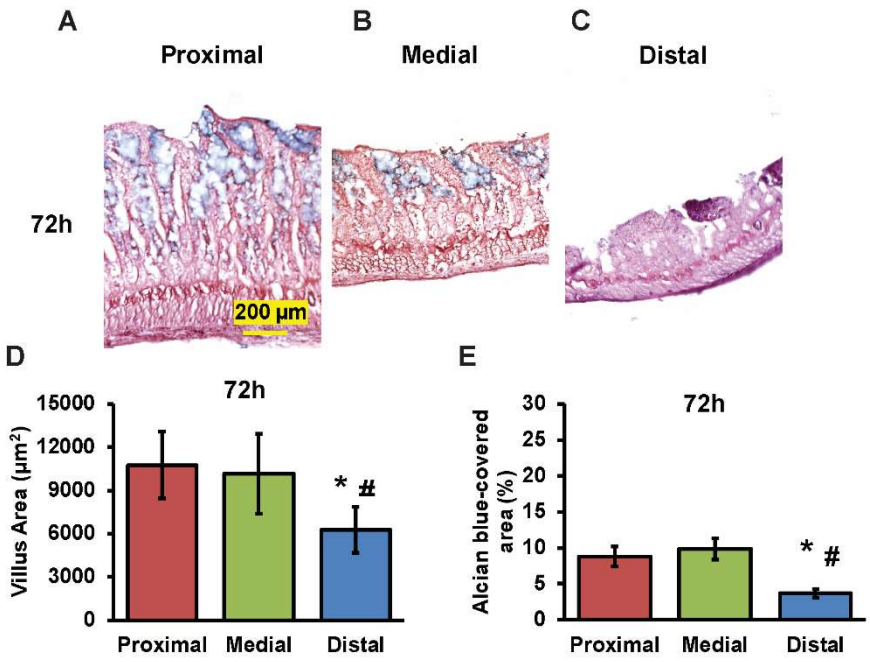

Figure 3.5: Alcian blue/PAS staining for mucins in the (A) proximal, (B) medial and (C) distal jejunum after 72h in culture. (D) Villus areas and (E) alcian blue-covered area fractions across locations at 72h (* and # denote $p \leq 0.05$ relative to proximal and medial jejunal segments, respectively).

The expression of ZO-1, a tight junction protein in the intestinal epithelium, was investigated by immunofluorescence staining. Corrected total fluorescence intensity of ZO-1 expression in villi was measured using n = 10 images per condition. Differences were investigated across the three locations at the 0h, 4h and 24h time-points (spatial), and from one time-point to the other within a location on the jejunum (temporal). Spatially, ZO-1 immunofluorescence did not change significantly across locations at 0h ($p > 0.05$) (**Figures 3.6A-D)**. This is consistent with ZO-1 trends reported in mice *in vivo* (0h) where the expression of ZO-1 was unchanged across the length of the small intestine (243). However, at 4h, ZO-1 immunofluorescence was 29% higher ($p \leq 0.05$) in the distal jejunum compared to the proximal jejunum (**Figures 3.6E-H**). At 24h, the ZO-1 immunofluorescence decreased by 14% ($p \leq 0.05$) in the distal jejunum relative to the proximal jejunum (**Figures 3.6I-L**).

Temporal effects were also observed in ZO-1 immunofluorescence. At 4h, ZO-1 immunofluorescence decreased significantly in proximal jejunum (34%) compared to 0h ($p \leq 0.05$ for both), while no significant change was observed in the medial and distal sections ($p > 0.05$). The decrease could be a result of loss of epithelial cells from the villi at later time points as observed by H&E staining. ZO-1 immunofluorescence in explants from all three locations did not change significantly between 0h and 24h ($p > 0.05$). From 4h to 24h, the ZO-1 intensity increased in proximal jejunum by 35% ($p \leq 0.05$). However, no significant change in ZO-1 immunofluorescence was observed in medial and distal explants between 4h and 24h ($p > 0.05$).

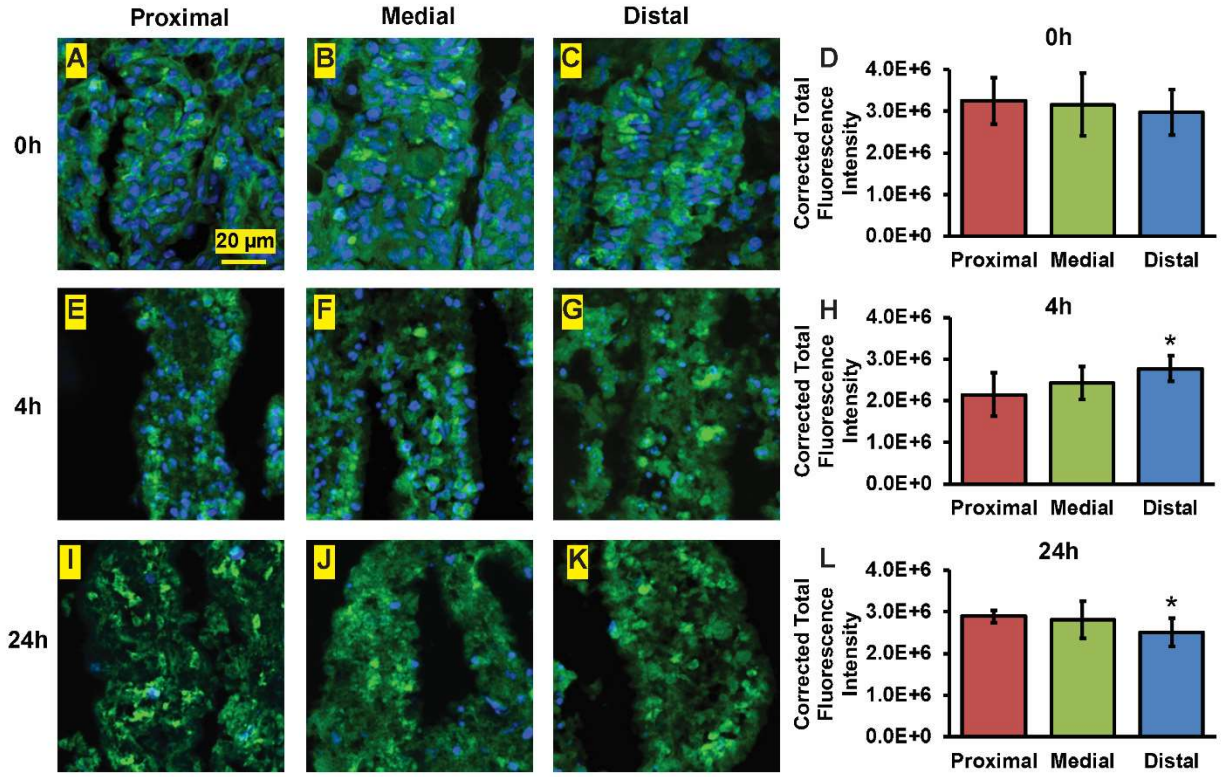

Figure 3.6: ZO-1 immunofluorescence staining of the proximal, medial and distal jejunum after (A - C) 0h, (E - G) 4h and (I - K) 24h in culture. Green = ZO-1 immunofluorescence, Blue = Nuclei. Corrected total fluorescence intensity measurements at (D) 0h, (H) 4h and (L) 24h. * denotes $p \leq 0.05$ relative to respective proximal groups.

3.4.5 Goblet cell function

Goblet cell function was evaluated through AB/PAS staining of the explant samples (244). The area of an explant covered by mucin was measured as a function of location as well as time. Spatial and temporal variations are discussed individually. At 0h, mucins in the explants from all three locations covered only 3-4% of the cryosection area (**Figures 3.7A-D**). However, at 4h and 24h, the area of mucin-covered regions increased for all three locations of the jejunum (**Figures 3.7E-L**). At 4h, the mucin-covered area increased approximately 2-fold from the proximal to the distal jejunum, but this increase was not statistically significant ($p > 0.05$) (**Figure 3.7H**). A ~1.5-fold increase in the mucin-covered area fraction was measured from the medial to the distal jejunum ($p > 0.05$). At 24h, the areas of mucin-covered regions for the proximal and medial jejunum were similar ($p > 0.05$) (**Figure 3.7L**). The distal jejunum exhibited ~2-fold higher mucin-covered regions than proximal or medial explants ($p > 0.05$ for both) (**Figures 3.7L**). In the rat intestine, an approximate 30-50% increase in the mucin volume from proximal to distal regions has been reported *in vivo* (0h) (228). Although, our data may not be statistically significant, we do observe increases in the area of an explant covered by mucins.

Temporal variations were also observed within each location on the jejunum. In the proximal jejunum, the mucin-covered area fractions at 0h, 4h and 24h were 3.9 ± 0.4%, 4.2 ± 0.8% and 7.8 ± 1.7%, respectively (n = 3 cryosections at each timepoint) (**Figures 3.7D, H and L**). In the medial jejunum, the mucin-covered area fractions at 0h, 4h and 24h were 3.2 ± 0.8%, 6.0 ± 0.6% and 9.8 ± 1.0%, respectively (n = 3 cryosections at each timepoint) (**Figures 3.7D, H and L**). In the distal jejunum, the mucin-covered area fractions at 0h, 4h and 24h were 3.2 ± 0.5%, 8.9 ± 1.3% and 19.5 ± 4.7%, respectively (n = 3 cryosections at each timepoint) (**Figures 3.7D, H and L**).

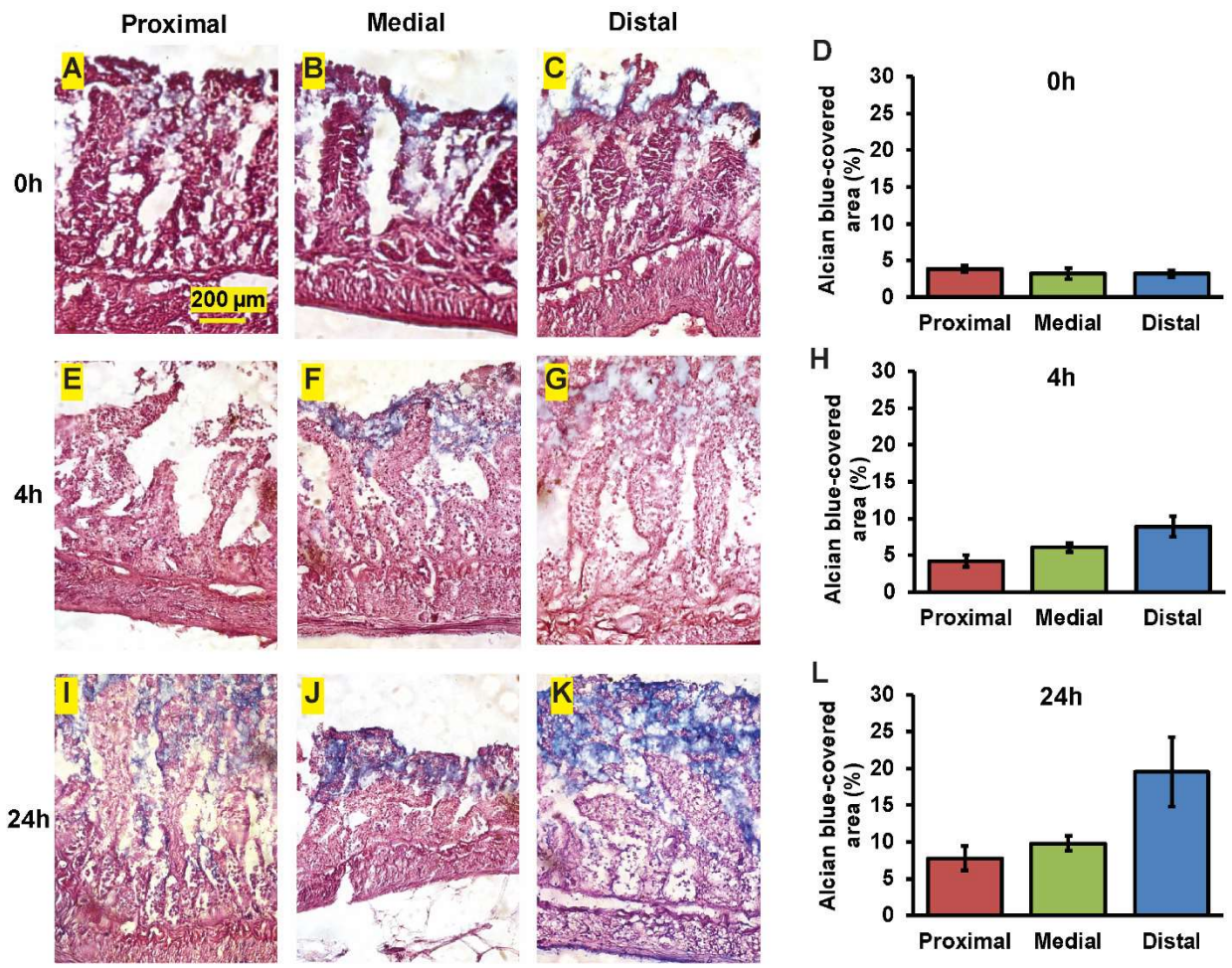

Figure 3.7: Alcian blue/PAS staining for mucins in the proximal, medial and distal jejunum after (A - C) 0h, (E - G) 4h and (I - K) 24h in culture. Alcian blue-covered area fractions across locations at (D) 0h, (H) 4h and (L) 24h.

In the proximal jejunum, the mucin-covered area fraction at 24h was 2-fold higher than at 0h ($p > 0.05$). No significant change was observed in the mucin-covered area at 72h compared to 24h ($p > 0.05$) (**Figures 3.5A and E**). In the medial explants, the mucin-covered area fractions increased significantly by 3-fold from 0h to 24h ($p \leq 0.05$). At 72h, the mucin-covered area fraction (9.8 ± 1.5%, n = 3) was similar to that at the 24h time-point ($p > 0.05$) (**Figures 3.5B and E**). In the distal explants, mucin-covered area fractions increased significantly by 2.8-fold from 0h to 4h and by 6-fold from 0h to 24h ($p \leq 0.05$ for both comparisons) (**Figures 3.7D, H and L**). However, a 5.3-fold

decrease in mucin-covered area was observed after 72h compared to 24h in culture ($p \leq 0.05$) (**Figures 3.5C and E)**.

3.4.6 Integration of hepatocyte cultures and jejunum explants

Jejunum explants were integrated with CS cultures of primary rat hepatocytes to understand how the two systems modulated each other's function. Both the jejunum and the hepatocytes were obtained from the same rat for the assembly of integrated intestinal-hepatocyte cultures (**Figure 3.8**). Proximal, medial and distal jejunum explants were integrated with hepatocytes and functions were evaluated 20h post-integration (**Figure 3.9**). Integrated cultures with proximal, medial and distal jejunum explants are henceforth referred to as 'proximal integrated', 'medial integrated' and 'distal integrated' cultures, respectively.

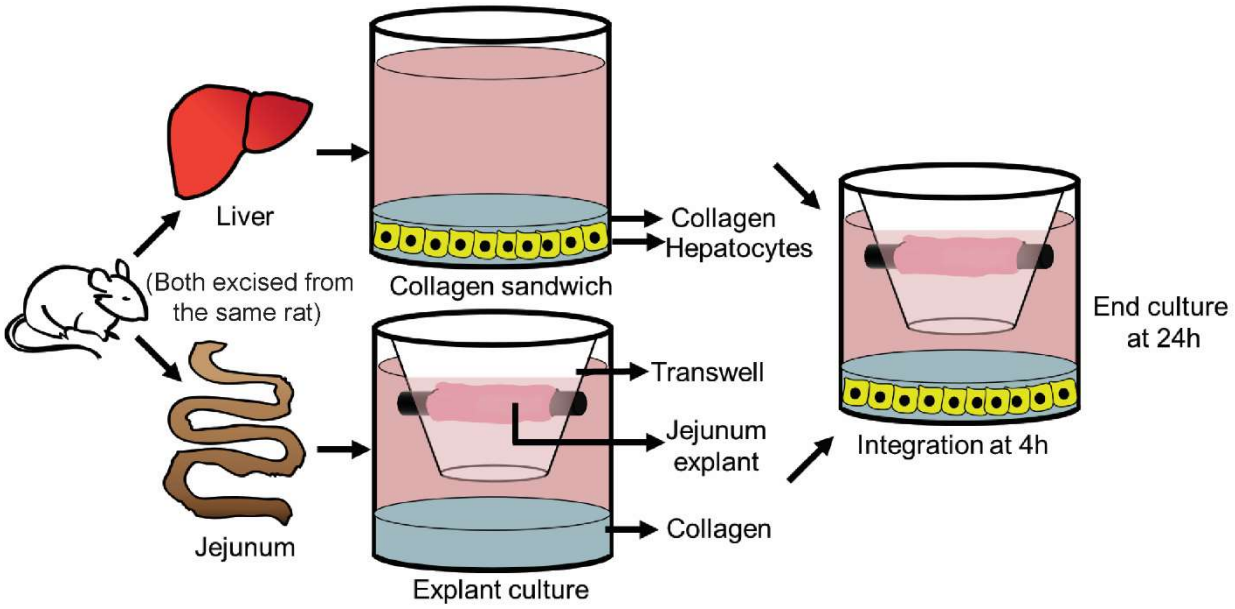

Figure 3.8: Schematic depicting the timeline for culture and integration of jejunum explants with hepatocyte collagen sandwich (CS) cultures. Jejunum explants and hepatocytes isolated from the same rat were integrated 4h post-isolation and ended at the 24h timepoint.

Phase contrast images (**Figures 3.9A and B)** and H&E staining (**Figure 3.10**) of hepatocytes in CS cultures exhibited binucleated cells with polygonal morphologies. The protein content of

hepatocyte CS cultures did not change as a function of integration (**Figure 3.9C**) indicating that the jejunum did not cause an adverse effect on protein expression in hepatocytes. In proximal integrated cultures, urea secretion was ~2.4-fold higher ($p \leq 0.05$) than by hepatocytes cultured alone (**Figure 3.9D**). Medial and distal integrated cultures did not exhibit a statistically significant change ($p > 0.05$) (**Figure 3.9D**). Hepatocytes in proximal integrated cultures did not exhibit a statistically significant change in ALP activity compared to CS alone controls ($p > 0.05$) (**Figure 3.9E**). However, hepatocyte ALP activity increased significantly in medial (62%) and distal (58%) integrated cultures compared to CS alone controls ($p \leq 0.05$ for both) (**Figure 3.9E**). These trends indicate that integration with proximal jejunum explants may have improved hepatocyte function, while medial and distal jejunum explants may have a negative effect on hepatocytes.

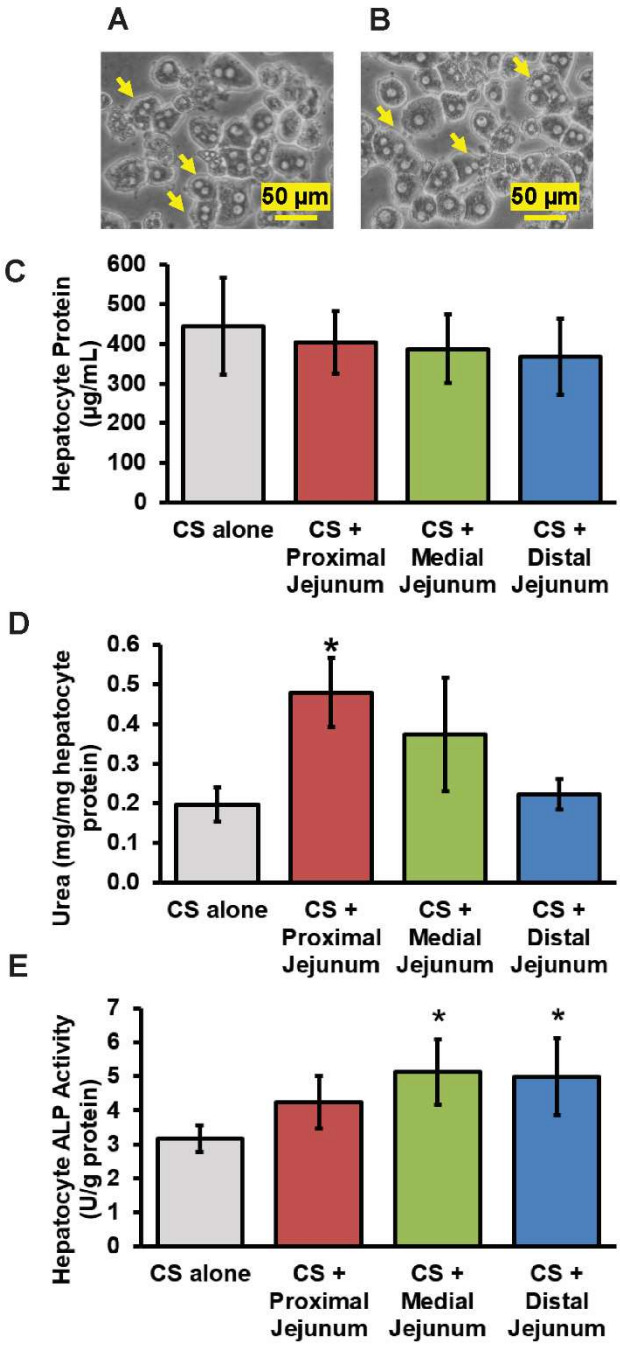

Figure 3.9: (A and B) Phase contrast images of hepatocytes in collagen sandwich cultures at the 24h time-point. Arrows indicate binucleated hepatocytes. Effect of integration on hepatocytes. (C) Hepatocyte protein, (D) urea production and (E) ALP activity in CS alone and integrated cultures (CS + proximal jejunum, CS + medial jejunum and CS + distal jejunum). * denotes $p \leq 0.05$ relative to CS alone cultures.

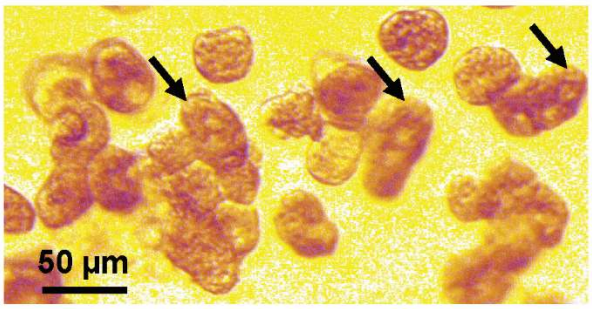

Figure 3.10: Hematoxylin and Eosin staining of hepatocytes in CS cultures. Arrows indicate binucleated hepatocytes.

ALP and lysozyme activities in jejunum explants did not change significantly in proximal, medial or distal integrated cultures, suggesting that there were no deleterious effects as a result of integration (**Figures 3.11A-F**).

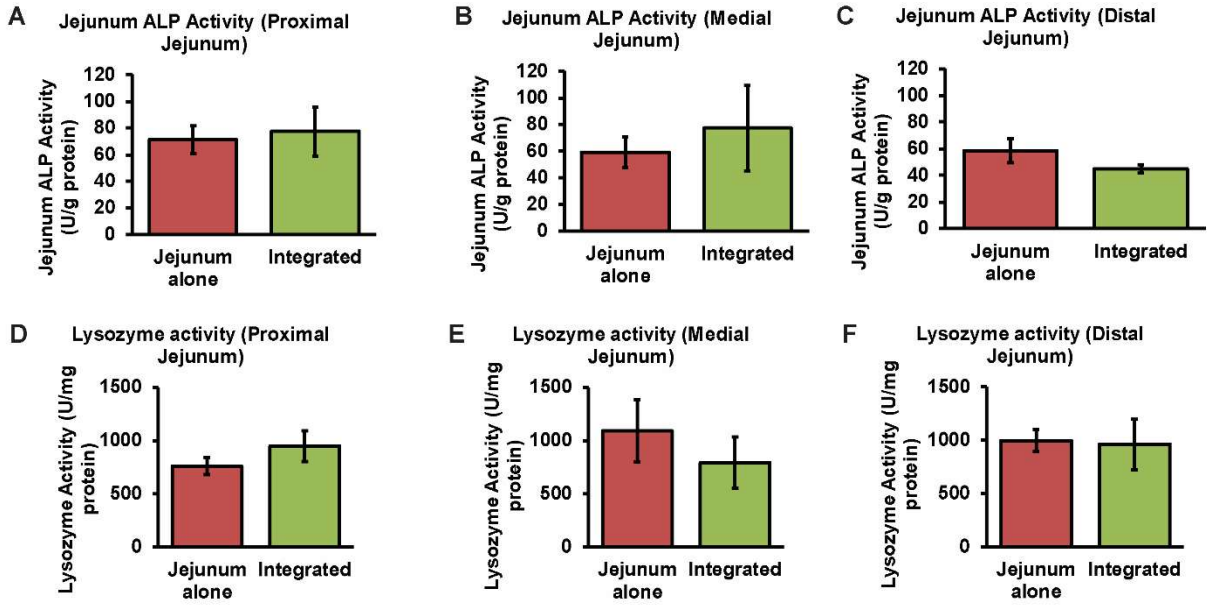

Figure 3.11: Effects of integration on (A - C) enterocyte and (D – F) Paneth cell markers.

Changes in villus area upon integration were not statistically significant for proximal, medial or distal jejunum ($p > 0.05$) (**Figures 3.12A-C**). AB/PAS staining was performed to investigate the

effect of integration of jejunum explants with hepatocytes on the mucus barrier (**Figures 3.12D-I**). AB/PAS staining revealed that the fraction of mucin-covered cryosection area was significantly higher (57%) in proximal integrated cultures than the corresponding jejunum alone controls ($p \leq 0.05$) (**Figures 3.12D, E and J**). This result suggests an effect of hepatocytes on the proximal jejunum explants. This was not true for explants from the medial or distal jejunum (**Figures 3.12F-I, K and L**).

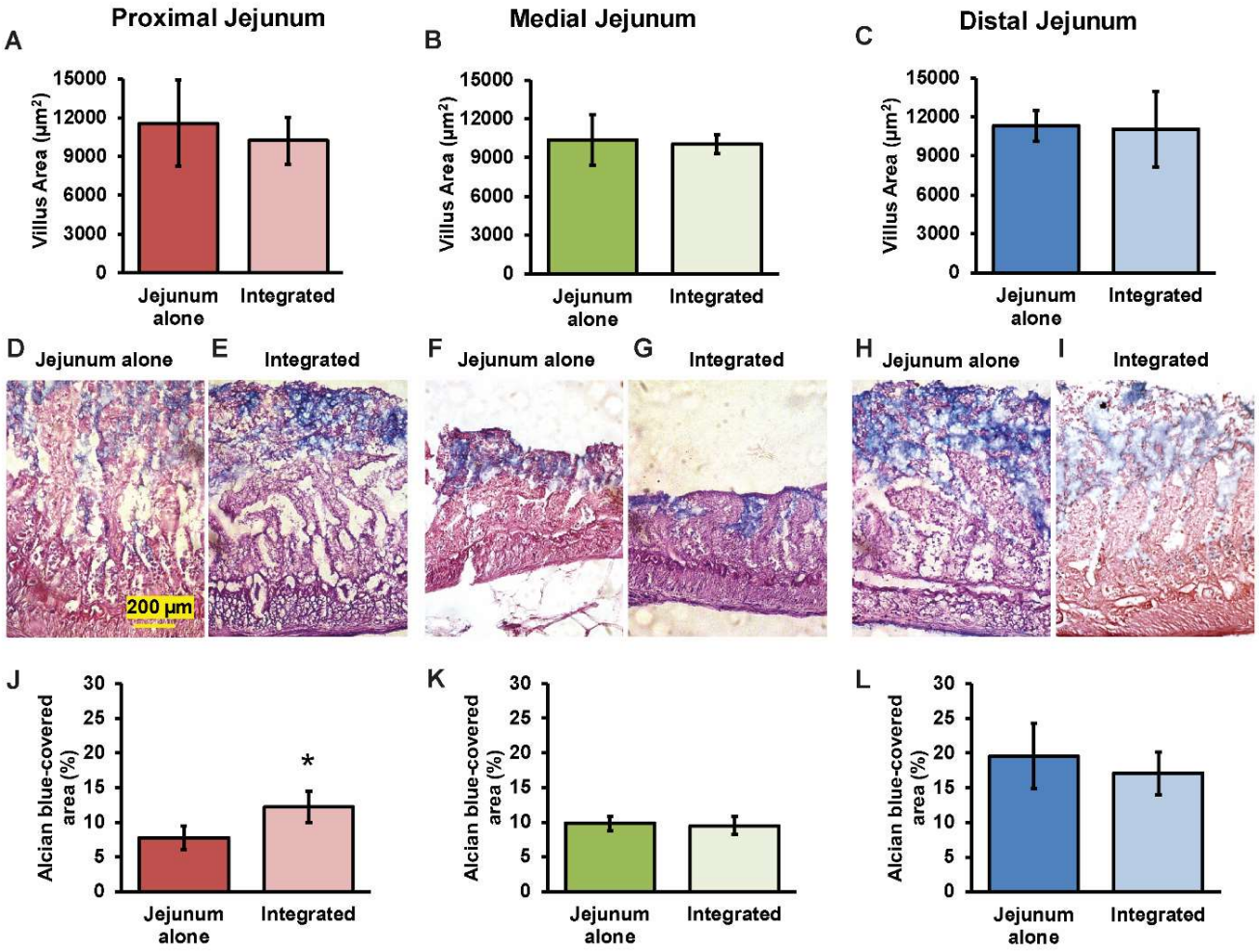

Figure 3.12: Effect of integration on jejunum explants. (A - C) Villus area and (D - I) alcian blue/PAS staining of proximal, medial and distal explants cultured alone or with hepatocyte CS cultures. (J - L) Mucin-covered area fractions in proximal, medial and distal segments respectively. * denotes *p* ≤ 0.05 relative to corresponding jejunum alone cultures.

3.5 Discussion and Conclusions

The small intestine exhibits variations in its absorptive, secretory and metabolic functions based on location (219, 227, 228). To understand these spatial effects on intestinal function in culture, it is necessary to divide the intestine into small segments and separately investigate these sections *in vitro*. Most studies on the small intestine only report location-dependent trends between the duodenum, the jejunum and the ileum *in vivo* (219, 227, 228). For these reasons, we investigated the properties in different regions within the rat jejunum prior to integrating with hepatocytes.

Explants from the proximal, medial and distal regions of the jejunum were cultured and functional and morphological differences between these regions were evaluated. ALP activity decreased from proximal to distal jejunum at 4h. Similar trends have been reported in the small intestine of rats (227, 230) . Within the jejunum, one study reported that the ALP activity in the proximal end of the rat jejunum at 0h (*in vivo*) is approximately 1.6-fold higher than that of the distal jejunum (230). At 24h, no significant differences were observed between the ALP activity among the three regions. This could be due to the presence of bacterial endotoxins such as lipopolysaccharides (245). Since intestinal bacteria increase from the proximal to the distal regions of the intestine (244), it may explain increased lysozyme secretion in the distal jejunum explants by 24h. Future studies will focus on identifying the specific endotoxins that can cause increased ALP activity and changes in bacterial growth as a function of jejunum location.

ALT activity in rat intestinal homogenates has been shown to increase from the stomach to the duodenum to the jejunum, followed by a decrease from jejunum to ileum (246). This suggests that ALT activity could increase along the length of the jejunum, as reported in the present study. ALT activity did not change significantly across the jejunum at 24h. One possible reason for this observation could be that enterocytes are continually shed from the tips of the villi (247) and it is likely that at later time points, cell shedding affected the activity of this enzyme.

Further spatiotemporal trends were revealed upon analyzing the area covered by the mucus barrier. Mucus deposition occurs over time and can take up to approximately 4.5h for its renewal (248). At 0h, the inversion process may have caused damage to the mucin layer, which may explain the location-based differences starting after 4h in culture. It has been shown *in vivo* that the number of goblet cells increases along the length of the intestine from the duodenum to the distal ileum (249, 250). There were significant increases in mucin-covered areas between 0h and 24h in explants obtained from the medial or distal jejunum sections. While the increase in the area covered by mucins from proximal to medial to distal jejunum in the present study was similar to *in vivo* observations (228), these spatial trends were not statistically significant. Taken together, our measurements and observations demonstrate that the mucin barrier, an important intestinal characteristic is maintained up to 72 h in culture in the proximal and medial regions of the jejunum, although, degradation was observed in the distal sections.

Temporal trends were observed in ZO-1 expression in proximal jejunum explants. ZO-1 immunofluorescence increased from 4h to 24h in proximal jejunum explants in culture. In the future, additional measurements such as western blots or ELISA assays will provide more comprehensive information.

We measured the functional markers for enterocyte, goblet and Paneth cells in jejunum explants after 72h in culture to investigate the extent to which explants can be cultured *in vitro*. The change in ALP activity between 24h and 72h of culture in the proximal and medial jejunum suggests decreased enterocyte function. These results support previously reported observations of degradation of adult rat jejunum explants after 24h in culture (62). The trends in mucin-covered area fractions between 24h and 72h could have resulted from decreased goblet cell function or the release of mucin proteins from the adherent mucus barrier into the cell culture media. Future investigations into specific mechanisms will provide information on which process causes such changes.

The second part of the study aimed to understand how individual cell functions could change when jejunum explants were integrated with hepatocyte CS cultures. To the best of our knowledge, only one study so far has described the integration of the intestine and the liver using primary cells and tissues (78). However, the focus of van Midwoud *et. al.* was to investigate changes in phase I and phase II metabolism. Moreover, the two tissue slices were only integrated for 3-7h.

Since our data showed that the proximal, medial and distal sections of the jejunum behaved differently from each other in culture, we maintained the distinction between these regions of the jejunum for our investigations with integrated jejunum-hepatocyte cultures as well. The integration of hepatocyte CS cultures with explants from the proximal, medial and distal jejunum did not affect hepatocyte viability, or enterocyte and Paneth cells functions significantly. However, an effect of explant location was observed in urea secretion and hepatocyte ALP activity. Urea secretion was significantly higher in hepatocytes integrated with proximal jejunum explants. *In vivo*, the small intestine produces ammonia which is detoxified by conversion to urea in the liver (220). Future studies will focus upon measuring changes in ammonia to correlate to variations in urea concentration (220). Hepatocyte ALP activity was significantly increased in medial and distal integrated cultures. Since bacterial endotoxins may have been the reason for this trend, our future studies will focus upon identifying specific toxins that may have played a role.

The spatiotemporal trends obtained in jejunum explants suggest that cellular and morphological markers change even within this region of the intestine. The trends reported demonstrate the importance of knowing which region of the jejunum is used when conducting future investigations into metabolism or biotransformation. The intestine-hepatocyte models described and evaluated in this study will be very useful for studies on understanding the crosstalk between these organs, specifically in the areas of drug discovery, validation and in their biotransformation.

Chapter 4: Investigating Ethanol Toxicity in an *In Vitro* Integrated Jejunum-Liver Model

4.1 Abstract

The small intestine and the liver together regulate many physiological functions such as glucose homeostasis, bile acid homeostasis and response to toxic xenobiotics. Toxicants such as ethanol (EtOH) affect both the intestine and the liver. EtOH-induced toxicity is responsible for over 48% of all liver disease related deaths. Moreover, EtOH is responsible for 1 in 3 liver transplants in the US alone. There is a lack of studies where primary cell or tissues have been utilized to investigate EtOH toxicity to the intestine *in vitro*. Further, spatial variations in the response of the jejunum to EtOH toxicity have not been explored. Additionally, to the best of our knowledge, there are no studies that investigate EtOH toxicity in an integrated intestine-liver model. We were thus motivated to develop an *in vitro* model to recapitulate the response of an integrated intestine - liver system to investigate EtOH toxicity. In this study, hepatocytes in collagen sandwich (CS) cultures and jejunum explants from three different locations (proximal, medial and distal jejunum) were integrated and treated with 100 mM and 200 mM EtOH (LC_{50}/2 and LC_{50} for rats) for 20 h. Activities of enzymes such as alkaline phosphatase (ALP), lysozyme and alcohol dehydrogenase (ADH) were found to be significantly increased with EtOH treatment in a dose- and location-dependent manner. On the other hand, villus area and area covered by acidic mucins were found to be decreased upon EtOH treatment. Differential responses were also observed based on whether the jejunum or hepatocytes were cultured alone or together. Integration of hepatocyte CS cultures with explants from the proximal jejunum increased the sensitivity of these cultures to EtOH. The results of this study suggest the importance of gut-liver integration in investigating EtOH toxicity *in vitro*. Overall, we were able to recapitulate the effects of EtOH on the intestine and the intestine-liver axis *in vitro*.

4.2 Introduction

The small intestine and the liver are the primary organs responsible for metabolism of orally administered drugs and chemicals (23, 112). The small intestine is a crucial part of the first line of defense against these chemicals, and this is where they are first metabolized and absorbed (23, 113). Damage caused by toxic chemicals and/or their metabolites is manifested in the different layers of the small intestine (113-115). Substances absorbed by the small intestine are absorbed into the blood stream and transported to the liver through the portal vein (2, 108). In the liver, phase I and II biotransformation enzymes involved in nutrient and xenobiotic metabolism further process these substances (108, 116). After metabolism by the liver, a fraction of these metabolites is sent back to the intestine through the bile duct (108, 117). This process is known as enterohepatic circulation (118, 119).

Toxicants such as EtOH are known to affect both the intestine and the liver (131-137). EtOH-induced toxicity is responsible for over 48% of all liver disease related deaths (130). Moreover, EtOH is responsible for 1 in 3 liver transplants in the US alone (129). EtOH overuse can lead to a leaky gut barrier, gut bacterial overgrowth and translocation of bacteria and their metabolites to the liver (131, 133-135). EtOH is also implicated in liver diseases such as alcoholic hepatitis, fatty liver and alcoholic cirrhosis (132, 136, 137).

EtOH metabolism primarily takes place through three different oxidative pathways in the body (138-143). Around 90% of EtOH is metabolized through the ADH pathway, while the CYP2E1 pathway accounts for less than 10% of EtOH metabolism under normal conditions (144, 145). The catalase pathway is a minor contributor under normal conditions (142, 145). The product of metabolism of EtOH through these pathways is the toxic compound acetaldehyde, which can be metabolized further to acetic acid through aldehyde dehydrogenase (ALDH) (144, 145).

Acetaldehyde causes cell damage by binding to proteins and forming adducts, while acetate is safely incorporated into the Krebs cycle through acetyl-CoA formation (144-148).

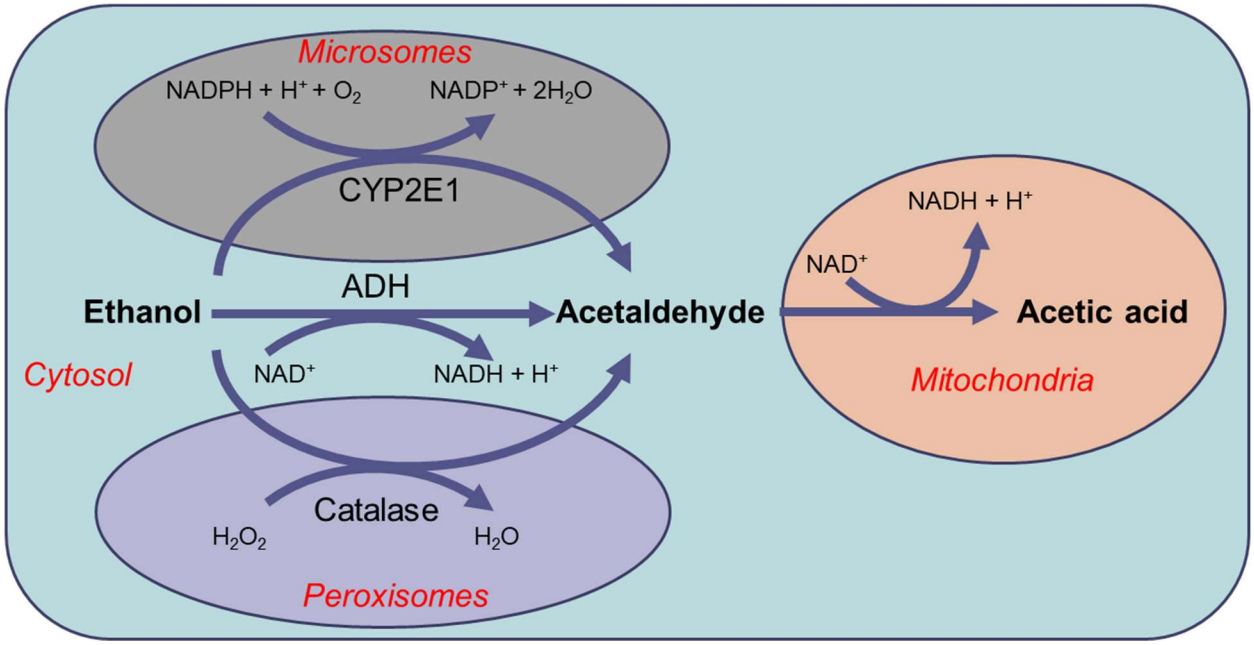

Figure 4.1: Pathways of EtOH metabolism. The ADH pathway contributes to more than 90% of ethanol metabolism under normal conditions while the CYP2E1 and catalase pathways metabolize the remaining 10% EtOH. In the cells, the ADH, CYP2E1 and catalase pathways are localized in the cytosol, the microsomes and the peroxisomes, respectively. All three pathways lead to formation of the toxic metabolite acetaldehyde, which can be further metabolized into acetic acid by ALDH in the mitochondria.

The liver is the primary site of EtOH metabolism in the body, but enzymes that metabolize this toxicant are also expressed in the intestine (149, 150). The harmful effects of EtOH are mostly manifested in the duodenum and the jejunum due to its rapid absorption along the length of the gastrointestinal (GI) tract (150). Acute EtOH consumption can lead to inhibition of transport of nutrients and formation of lesions in the mucosa, damage to villi and increased permeability (142, 150-153, 251). These effects of EtOH observed *in vivo* make it a relevant toxicant to evaluate an integrated gut-liver model.

However, *in vitro* studies on EtOH toxicity on the small intestine have focused on using Caco-2 cells (252, 253). There are very few studies where primary cell or tissues have been used (254). Such studies have explored effects of EtOH on tight junction integrity, cell glycosylation and calcium homeostasis (252-254). *In vitro* studies on EtOH toxicity to the liver have also used both cell lines such as HepG2 and SK-Hep-1 cells (255-257) and primary cells or tissues (258-260). To the best of our knowledge, there are no studies that investigate EtOH toxicity in an integrated gut-liver model.

Intestinal explants are appropriate for GI toxicity studies because they facilitate the evaluation of chemical toxicity in not just the epithelial layer of the gut mucosa, but also in the underlying layers such as the lamina propria and muscularis (75, 76). For example, toxicity of EtOH to the gut is manifested not only in the epithelial layer, but also in the myofibroblasts in the lamina propria, or the muscularis layer (261).

We hypothesized that integrated *in vitro* jejunum-hepatocyte cultures would recapitulate the response of these tissues to ethanol toxicity *in vivo*. In the present study, we integrated full thickness jejunum explants from the rat with primary hepatocyte collagen sandwich (CS) cultures to evaluate the response of these *in vitro* culture models to EtOH.

4.3 Materials and Methods

Alcian blue solution, calcium chloride, chloroform, collagenase type IV, absolute EtOH (200-proof), gentamicin sulfate, glucagon, glutaraldehyde, 4-(2-hydroxyethyl)-piperazine-1-ethanesulfonic acid (HEPES), hydrocortisone, periodic acid, protease inhibitor cocktail, Schiff's reagent and sodium dodecyl sulfate were purchased from Sigma-Aldrich (St. Louis, MO). Unless stated otherwise, all other chemicals were purchased from Thermo Fisher Scientific (Waltham, MA). Absorbance and fluorescence readings were taken using SpectraMax ME2 spectrophotometer (Molecular Devices, San Jose, CA).

4.3.1 Collagen extraction

Type I collagen was extracted from rat tail tendons as previously described (231). Briefly, the tendons were dissolved in 3 % (v/v) acetic acid and centrifuged at 13,000 x *g*. Collagen was subsequently precipitated from the supernatant with 30 % (w/v) sodium chloride. The suspension of precipitated collagen was further centrifuged at 8,500 x *g* and the pellets were resuspended in 0.6 % acetic acid. The resulting solution was then dialyzed in 1 mN hydrochloric acid. The concentration of collagen in the solution was determined through its absorbance at 280 nm. The pH of the solution was maintained at 3.1. Finally, the collagen solution was sterilized with chloroform before its use cell culture.

4.3.2 Isolation and culture of primary rat hepatocytes

Primary hepatocytes were obtained from the livers of female Lewis rats weighing 180-210 g (Envigo, Indianapolis, IN). Rat liver perfusion was performed using an *in situ* two-step collagenase perfusion protocol as described previously (231) (234). All animal care and surgical procedures were approved by and conducted in accordance with the Virginia Tech Institutional Animal Care and Use Committee. Hepatocyte counts ranged between 60-160 million hepatocytes. The viability of isolated hepatocytes, as calculated through trypan blue exclusion assay, was ≥ 97%. Hepatocytes were seeded in 12-well plates on 1.1 mg/mL collagen gels (0.25 mL per well) at a density of 500,000 cells per well. To prepare CS hepatocyte cultures, a second layer of collagen (1.1 mg/mL) was deposited over the hepatocyte monolayer 3h after hepatocyte seeding. Hepatocyte culture medium was added 1h later (3mL per well). The hepatocyte culture medium was composed of Dulbecco's modified Eagle medium (DMEM), supplemented with 0.37 % (w/v) sodium bicarbonate, 10 % (v/v) heat-inactivated fetal bovine serum, 200 U/mL penicillin, 200 µg/mL streptomycin, 0.5 U/mL insulin (MP Biomedical, Santa Ana, CA), 20 ng/mL Epidermal Growth Factor (EGF), 14.28 ng/mL glucagon, and 7.65 µg/mL hydrocortisone. Cultures were incubated at 37°C in a humidified incubator in an atmosphere of 10% carbon dioxide.

4.3.3 Isolation and culture of rat jejunum explants

The small intestine was obtained from female Lewis rats in which the liver was perfused and isolated earlier. The intestine was stored in ice-cold hepatocyte culture medium supplemented with 50 µg/mL gentamicin sulfate until explant isolation. The duodenum was dissected from the remaining length of the small intestine at the ligament of Treitz as described previously (222). The jejunum-ileum transition was identified by observing increases in the diameter of the intestine and the amount of mesenchyme. To expose the mucosa outward, the jejunum was inverted as described before (222). Approximately 1 cm-long sections of the inverted jejunum were pulled on Matrigel® - coated PDMS rods and transferred to Millicell® inserts. Thereafter, the inserts were placed in 12-well plates coated with 0.5 mL of 1.1 mg/mL collagen gel. Hepatocyte culture medium supplemented with gentamicin (50 µg/mL) was added to each well to cover the intestinal segment in the Millicell® insert (3 mL per well). Eighteen explants (~ 1 cm in length) were isolated from the entire jejunum. The top six sections (obtained from the region next to the duodenum) were identified as '***proximal***', the middle 6 as '***medial***' and the bottom 6 (from the region right before the ileum) as '***distal***'. All explants were cultured in a humidified incubator maintained at 37°C in an atmosphere of 10% CO_2. The media was changed at T = 3h and T = 4h after their isolation (T = 0h). The hepatocyte culture medium (3mL per well) added to the explants at 0h and 3h was additionally supplemented with 50 ug/mL gentamicin. At T = 4h, the explants were transferred to either new collagen-coated wells with or without hepatocytes to be maintained as integrated/jejunum alone cultures, respectively. All cultures (CS alone, jejunum, or integrated) were supplemented with 3mL per well of common culture medium.

4.3.4 Administration of EtOH

EtOH was administered to all cultures at $LC_{50}/2$ and LC_{50} at T = 4h after isolation/seeding. For rats, the LC_{50} of EtOH is 200mM, where LC_{50} is the concentration that results in 50% cell death

(235, 262). Thus, three conditions were used for all cultures: 0mM, 100mM and 200mM EtOH added to the culture medium.

4.3.5 Extraction and measurement of protein

To extract hepatocyte protein, the collagen gels in CS cultures were digested with collagenase IV (231). Hepatocytes thus detached and separated were lysed in the presence of a protease inhibitor cocktail (4-(2-aminoethyl) benzenesulfonyl fluoride hydrochloride, aprotinin, bestatin, E-64, leupeptin, and pepstatin A) (231).

To extract jejunum protein, explants were homogenized using a TissueRuptor® homogenizer (Qiagen, Hilden, Germany) at setting 8 (2 min per sample). Explant homogenization was performed in 0.5 mL lysis buffer supplemented with the protease inhibitor cocktail. Explant homogenates were centrifuged at 10,000 x *g* for 5 min to collect the supernatant. All protein samples were aliquoted and frozen at -80°C until further use. The concentrations of protein in cell or tissue lysates were subsequently measured using the Bradford assay (Coomassie (Bradford) Protein Assay Kit; Thermo Fisher Scientific) as previously described (231).

4.3.6 Measurement of ALP activity

ALP activity was measured using a commercially sourced kit (Abcam, Cambridge, UK) as per the manufacturer's protocol (263, 264). Briefly, jejunum and hepatocyte lysates were incubated with para-nitrophenyl phosphate (pNPP) substrate for 1h at 25 °C to quantify the extent of the dephosphorylation reaction. The colorimetric reaction was ended, and the absorbance was measured at 405 nm to quantify the chromogen para-nitrophenol (pNP). A standard curve was generated using the ALP enzyme and pNPP substrate supplied by the manufacturer. ALP activity was calculated as defined by the manufacturer

$$ALP\ Activity\ \left(\frac{U}{mL}\right) = \frac{\frac{A}{V}}{T},$$

where A = concentration of pNP generated in samples (µmol), V = volume of sample (mL), T = reaction time (min). ALP activity was normalized to the total protein measured in each sample.

4.3.7 Measurement of lysozyme activity

Lysozyme activity was measured using a commercially available fluorometric assay kit (EnzChek™ Lysozyme Assay Kit, Thermo Fisher Scientific) (265). Spent culture media was used to conduct the assay following the manufacturer's protocol. Briefly, spent culture media was incubated with lysozyme substrate provided by the manufacturer (fluorescein-conjugated *Micrococcus lysodeikticus* cell walls). After a 2h incubation at 37°C, fluorescence was measured at the excitation and emission wavelengths of 485 nm and 538 nm, respectively. A standard curve was utilized to determine the lysozyme activity values. Activity was normalized to protein content.

4.3.8 Measurement of alcohol dehydrogenase ADH activity

ADH activity was measured using a commercially sourced assay kit (BioVision, Inc.) as per the manufacturer's instructions (266, 267). Briefly, jejunum explant lysates and hepatocyte lysates were incubated with an isopropanol substrate and reduced nicotinamide adenine dinucleotide (NADH) at 37 °C, and the absorbance was measured at 450 nm at 3 min and 30 min to quantify the conversion of oxidized nicotinamide adenine dinucleotide (NAD^+) to the reduced form NADH by ADH-mediated metabolism of the isopropanol substrate. A standard curve was generated using NADH provided by the manufacturer. Activity was calculated as defined by the manufacturer

$$ADH\ activity\ \left(\frac{mU}{mL}\right) = \frac{\frac{A}{V}}{T},$$

where A = amount of NADH generated in the reaction (in nmol), V = volume of sample used in mL, T = time difference between the first and the last absorbance measurements = 30 min – 3 min = 27 min.

4.3.9 TNF-α measurements

Concentration of TNF-α in the jejunum lysates was quantified using a commercially available ELISA kit (R&D Biosciences) following the manufacturer's protocols (231, 268). Absorbance was measured at a wavelength of 450 nm and used to determine concentrations using a standard curve. TNF-α measurements were normalized to protein concentrations.

4.3.10 Cryosectioning of jejunum explants

Explants were fixed with 3% (w/v) glutaraldehyde at 4°C for 7h as described previously (265). Fixed explants were washed with PBS (1X). Thereafter, the explants were sequentially incubated in a 15% (w/v) sucrose solution for 5 min and 30% (w/v) sucrose solution for 15 min. Samples were then incubated in Tissue-Tek Optimal Cutting Temperature (OCT) compound (Electron Microscopy Sciences, Hatfield, PA) for 15 min to equilibrate. Samples were then embedded in OCT compound in cryomolds using isopentane partially frozen with liquid nitrogen as described previously (236, 265). Cryosections of thickness 10 µm were obtained from the embedded samples to visualize the different radial layers of the intestine. All samples were stored at -80°C until further use. Before any staining procedure, all cryosections were fixed at room temperature for 20 min with 3% (w/v) glutaraldehyde (in PBS (1X)).

4.3.11 Hematoxylin and Eosin (H&E) staining of jejunum explants and hepatocytes

Jejunum sections and hepatocytes were stained with Mayer's H&E using a protocol described before (237). Briefly, fixed cryosections and hepatocyte CS cultures were incubated with Mayer's hematoxylin solution, followed by rinsing in warm water pH adjusted to 8.2-8.4). Hematoxylin-stained sections and CS cultures were then equilibrated in 95% (v/v) EtOH and stained further with Eosin Y solution (0.5% (w/v), in 95% (v/v) EtOH alcoholic solution, pH = 4.2 - 4.3). Eosin-stained cryosections and CS cultures were decolorized using 95% (v/v) EtOH until the eosin stain stopped streaking. Stained samples were dehydrated for 2 min in 95% (v/v) EtOH, followed by a

2 min incubation in absolute EtOH (100% v/v) before mounting with Cytoseal™ 60 (Thermo Fisher Scientific).

4.3.12 Alcian blue (AB)/Periodic acid-Schiff's base (PAS) staining of jejunum explants and hepatocytes

Cryosections from jejunum explants were stained with AB/PAS for intestinal mucins. Hepatocytes in CS alone cultures were also stained as controls. AB/PAS staining was performed as described before, using protocols adapted from previously described procedures (238, 269). Briefly, samples were incubated for 2.5 h with Alcian blue dye (1% (w/v) in 3% (v/v) acetic acid, pH = 2.5) after equilibration with 3% (v/v) acetic acid. Stained samples were rinsed briefly in 3% (v/v) acetic acid to remove non-specific stain. Stained samples were then sequentially incubated in 0.1% (w/v) periodic acid and Schiff's reagent. Subsequently, the samples were washed in tap water for 10 min and rinsed in deionized water. Finally, all samples were serially dehydrated in 95% (v/v) EtOH and absolute EtOH for 2 min each before mounting with Cytoseal™ 60.

4.3.13 Morphometric analyses

Villus area was determined using FIJI (ImageJ software, NIH) (239) by outlining individual villi as visualized through the H&E staining (n = 20 villi per condition). The extent of Alcian blue staining was quantified by calculating the fraction of each cryosection stained with the dye. This was performed in FIJI (n = 3 cryosections per condition) by thresholding complete images of cryosections using the hue, saturation and brightness (HSB) color model under the color threshold plugin. Blue areas were isolated in the AB/PAS images by adjusting the hue and saturation parameters. Mucin-covered area fraction was subsequently calculated by dividing the area of blue regions by the total area of the cryosection.

4.3.14 Statistical analyses

Statistical significance was determined by obtaining *p*-values through one-tailed student's t-tests. Unequal/equal variance was assumed when the sample sizes were unequal/equal respectively between the groups being compared. All *p*-values were corrected for multiple hypotheses testing using Bonferroni correction. For all tests of statistical significance, $\alpha = 0.05$. Data have been reported as mean ± standard deviation, with n denoting the sample size.

4.4 Results

4.4.1 Integration of hepatocytes and jejunum explants

Explants obtained from the ***proximal***, ***medial*** and ***distal*** regions of the jejunum were integrated with collagen sandwich models of primary rat hepatocytes. Integrated cultures were treated with EtOH at concentrations of 100mM ($LC_{50}/2$) and 200mM (LC_{50}) (235, 262). Millicell® inserts with jejunum explants were placed above collagen sandwich cultures of rat hepatocytes approximately 4h after isolation of the explants (**Figure 4.2**). Integrated cultures with proximal, medial and distal jejunum explants have been called '***proximal integrated'***, '***medial integrated***' and '***distal integrated***' cultures respectively.

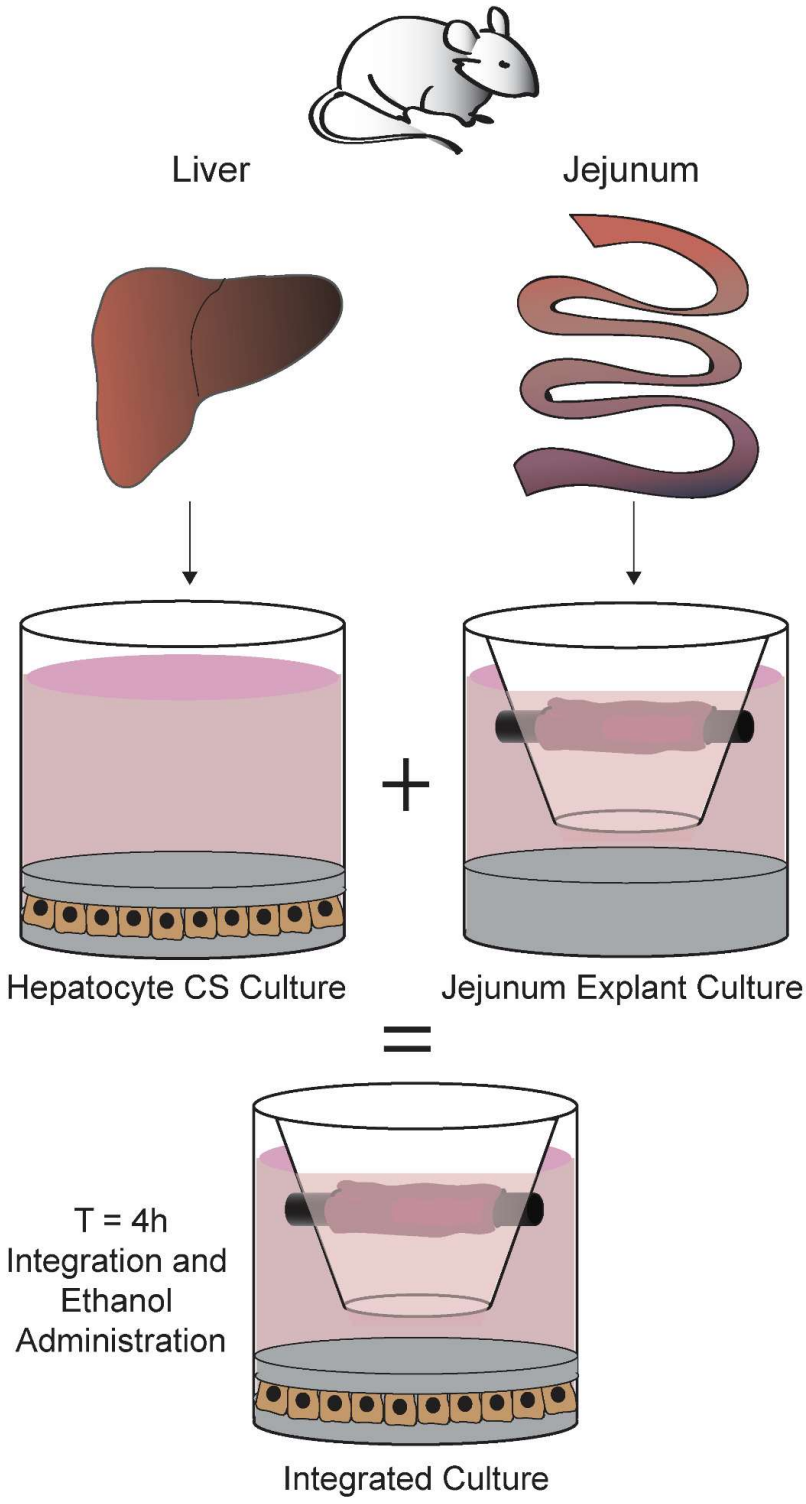

Figure 4.2: Schematic depicting the timeline for culture and EtOH treatment of jejunum explants with/without hepatocyte collagen sandwich (CS) cultures.

4.4.2 Effect of EtOH on explant protein

Changes in jejunum protein were calculated to evaluate the effect of EtOH on explant viability (**Figures 4.3A-C**). Jejunum protein decreased by 31% ($p \leq 0.05$) in ***proximal*** jejunum explants cultured alone and treated with 200mM EtOH compared to untreated controls. The decrease at 100mM was not significant (17%, $p > 0.05$). Similarly, jejunum protein in ***proximal integrated*** cultures decreased by 23% and 32% ($p \leq 0.05$ for both) with 100mM and 200mM EtOH respectively. However, no significant changes in explant protein were observed in ***medial*** and ***distal jejunum alone*** or ***integrated*** cultures. These trends show the toxic effects of EtOH to the proximal jejunum in culture at both $LC_{50}/2$ and LC_{50}. ***Proximal integrated*** cultures showed increased sensitivity as a significant decrease in protein was observed even at 100mM.

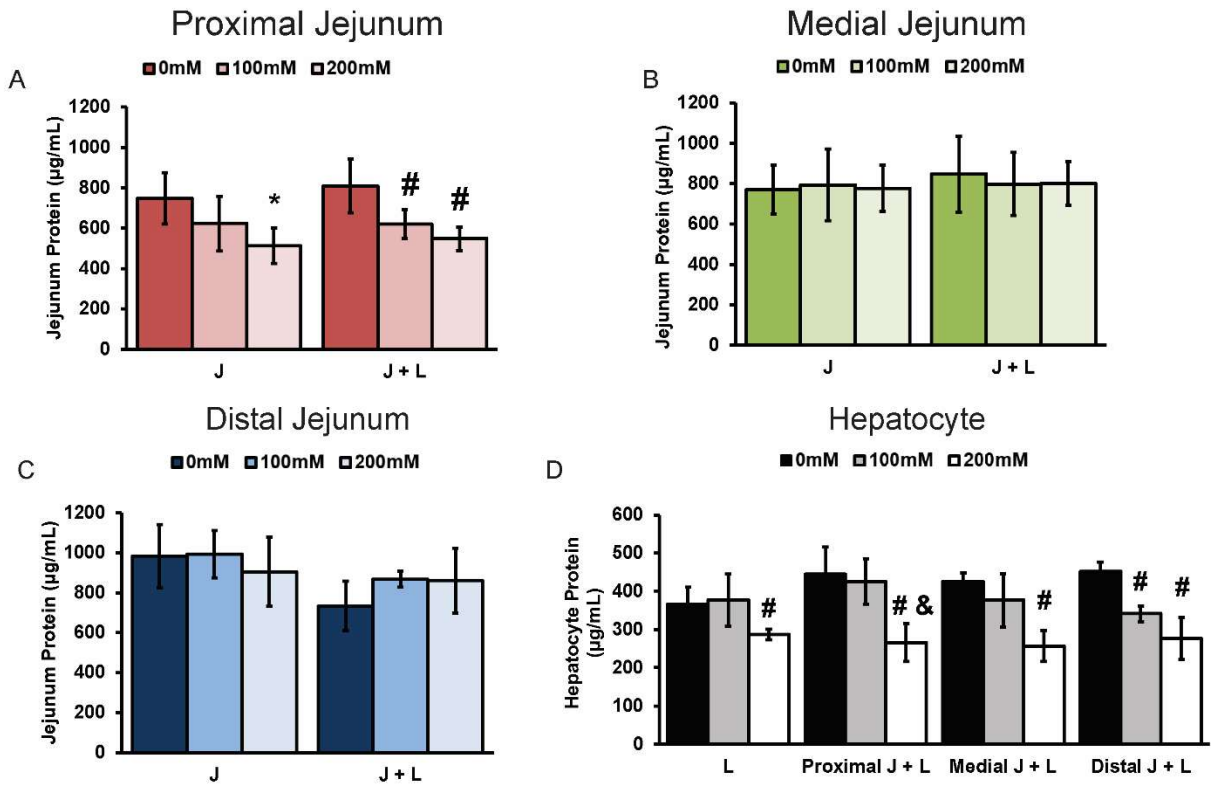

Figure 4.3: Effects of EtOH on (A-C) proximal, medial and distal jejunum protein and (D) hepatocyte protein with 0, 100 and 200mM EtOH. (A-C) * and # denote $p \leq 0.05$ relative to untreated

jejunum alone and integrated groups, respectively; (D) # and & denote $p \leq 0.05$ relative to 0mM and 100mM groups, respectively.

4.4.3 Effect of EtOH on hepatocyte protein

Hepatocytes in CS alone as well as integrated cultures from all 3 jejunum locations exhibited a significant protein decrease in protein at 200 mM EtOH (**Figure 4.3D**). Hepatocyte protein decreased by 30% ($p \leq 0.05$) in CS alone cultures treated with 200mM EtOH. In both ***proximal*** and ***medial integrated*** cultures, hepatocyte protein content decreased by ~40% at 200mM EtOH ($p \leq 0.05$). Hepatocytes in ***distal integrated*** cultures showed a significant decrease in protein content at both 100mM and 200mM EtOH (24% and 34%, respectively; $p \leq 0.05$ for both). These results show the toxic effects of EtOH to hepatocytes cultured alone or with jejunum explants.

4.4.4 Effect of EtOH on ALP activity in jejunum and hepatocytes

ALP activity was measured in lysates from jejunum explants as well as hepatocytes as a marker of toxicity. In ***proximal jejunum alone***, ALP activity increased by 54% and 67% ($p \leq 0.05$ for both) when treated with 100 mM and 200 mM EtOH respectively (**Figure 4.4A**). In ***proximal integrated*** cultures, greater increases of 2.3- and 1.8-fold in jejunum ALP activity were observed at 100 mM and 200 mM EtOH, respectively ($p \leq 0.05$ for both). The trends in ***medial jejunum*** cultures were different from those observed in the ***proximal jejunum***. In ***medial jejunum alone*** cultures, the jejunum ALP activity increased significantly by 79% with 100 mM EtOH, but only by 47% with 200 mM EtOH ($p \leq 0.05$ for both) (**Figure 4.4B**). Interestingly, jejunum ALP activity in ***medial integrated*** cultures did not change significantly at 100 mM EtOH ($p > 0.05$). However, at 200 mM EtOH, the ALP activity increased significantly by 2.8-fold ($p \leq 0.05$). The ***distal jejunum alone*** cultures were not sensitive to EtOH-induced changes in ALP activity. In ***distal jejunum alone*** cultures, the jejunum ALP activity did not change significantly with 100 mM or 200 mM EtOH (**Figure 4.4C**). However, in ***distal integrated*** cultures, the ALP activity increased by 1.8-

fold at 200 mM EtOH ($p \leq 0.05$). Taken together, effects of both integration and location of jejunum explants were observed on EtOH toxicity to these cultures.

ALP activity was also measured in hepatocyte lysates. In CS alone cultures, hepatocyte ALP activity did not change significantly when treated with EtOH (**Figure 4.4D**). However, significant changes in hepatocyte ALP activity were observed in the integrated cultures (**Figure 4.4D**). In ***proximal integrated*** cultures, the hepatocyte ALP activity increased by 70% with 100 mM and 66% with 200 mM EtOH ($p \leq 0.05$ for both) compared to untreated controls. In ***medial integrated*** cultures, hepatocyte ALP activity increased by 38% ($p > 0.05$) at 100 mM and by 75% ($p \leq 0.05$) at 200 mM EtOH compared to untreated controls. The hepatocytes in ***distal integrated*** cultures behaved differently at the two concentrations of EtOH and did not follow the same trends as the integrated cultures with explants from the other two jejunum locations. At 100 mM EtOH, a 75% increase in hepatocyte ALP activity was observed, but this increase was not significant ($p > 0.05$). However, at 200 mM, no significant changes in ALP activity were observed ($p > 0.05$).

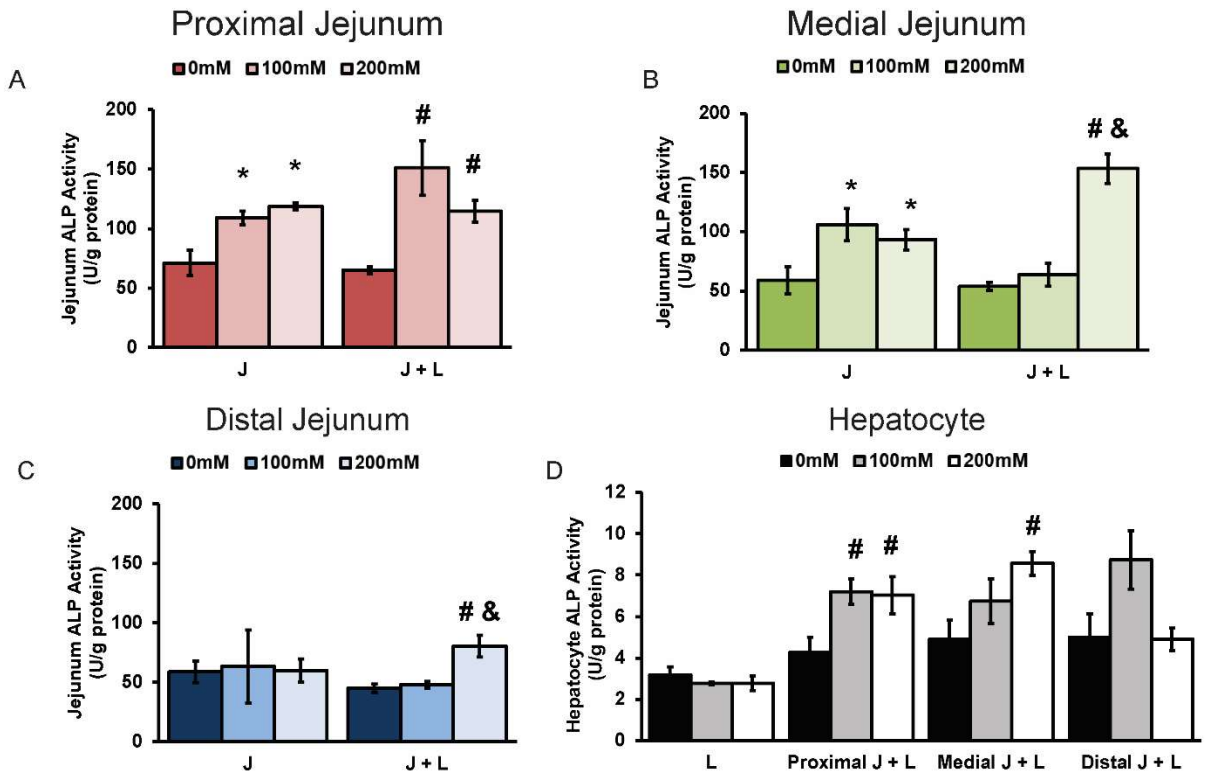

Figure 4.4: Effects of EtOH on (A-C) proximal, medial and distal jejunum ALP activity and (D) hepatocyte ALP activity with 0, 100 and 200mM EtOH. (A-C) * and # denote $p \leq 0.05$ relative to untreated jejunum alone and integrated groups, respectively and & denotes $p \leq 0.05$ relative to integrated 100mM group; (D) # denotes $p \leq 0.05$ relative to 0mM group.

4.4.5 Effect of EtOH on lysozyme activity

Effect of EtOH on Paneth cell function in the jejunum was evaluated through the measurement of lysozyme activity (227). Upon treatment with 200 mM EtOH, lysozyme activity in the spent culture media increased by 2.3-fold and 2-fold in ***alone*** and ***integrated*** cultures of the ***proximal jejunum*** respectively ($p \leq 0.05$ for both) (**Figure 4.5A**). At the $LC_{50}/2$ of 100 mM, lysozyme activity in ***proximal integrated*** cultures increased by 45%, but this increase was not significant ($p > 0.05$). In the ***medial jejunum***, lysozyme activity changed significantly only in ***integrated*** cultures at 200 mM EtOH. The activity increased by 50% at 100 mM ($p > 0.05$) and by 1.8-fold at 200 mM EtOH

($p \leq 0.05$) (**Figure 4.5B**). Interestingly, in the distal jejunum, lysozyme activity changed significantly only in jejunum alone cultures (**Figure 4.5C**). In ***distal jejunum alone***, lysozyme activity increased significantly by 52% and 69% at 100 mM and 200 mM EtOH, respectively ($p \leq 0.05$ for both). Similar changes were observed in ***distal integrated*** cultures where the lysozyme activity increased by 50% ($p > 0.05$) at 100 mM and 69% ($p > 0.05$) at 200 mM EtOH.

Lysozyme activity in hepatocyte only cultures was similar to basal concentration detected in the fresh media (**Figure 4.5D**). Further, no changes in lysozyme activity were observed in hepatocyte only cultures treated with EtOH (**Figure 4.5D**). This was expected because hepatocytes are not known to secrete lysozyme.

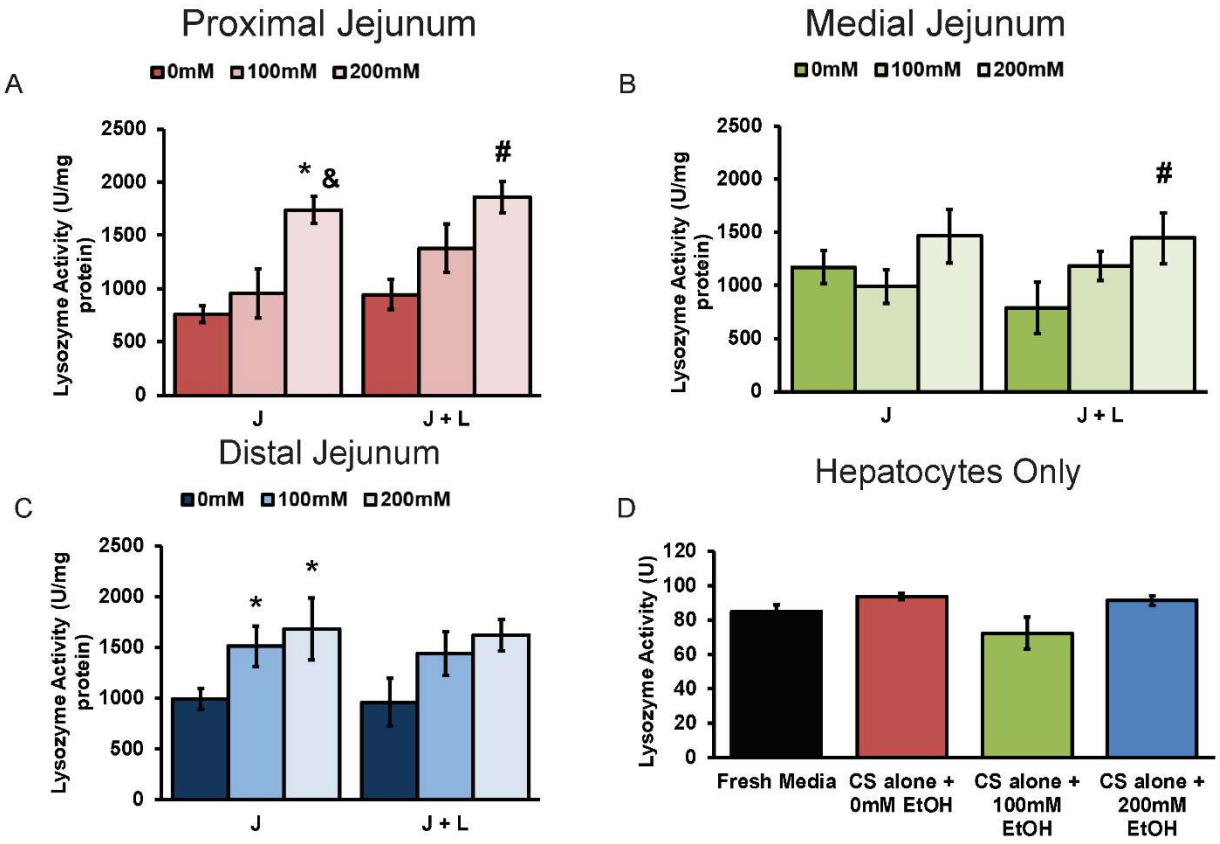

Figure 4.5: Effects of EtOH on (A-C) proximal, medial and distal jejunum lysozyme activity and (D) hepatocyte lysozyme activity with 0, 100 and 200mM EtOH. (A-C) * and # denote $p \leq 0.05$ relative to

untreated jejunum alone and integrated groups, respectively and & denotes $p \leq 0.05$ relative to alone 100mM group.

4.4.6 Effect of EtOH on ADH activity in jejunum and hepatocytes

ADH activity was measured to investigate if EtOH induced the activity of this enzyme upon treatment. Jejunum ADH activity in ***proximal jejunum alone*** cultures did not change significantly with EtOH treatment (**Figure 4.6A**). However, in ***proximal integrated*** cultures, ADH activity increased by 2-fold with 100 mM and 2.7-fold with 200 mM EtOH ($p \leq 0.05$ for both). In ***medial jejunum*** cultures, an induction of ADH activity was observed in both alone and integrated cultures only at 200 mM EtOH (**Figure 4.6B**). In ***medial alone*** cultures, ADH activity increased by 67% ($p \leq 0.05$) whereas in ***medial integrated*** cultures, the increase was 3.2-fold ($p \leq 0.05$). Jejunum ADH activity increased by ~3.5-fold in ***distal jejunum alone*** cultures treated with 100 mM or 200 mM EtOH ($p \leq 0.05$ for both) (**Figure 4.6C**). In ***distal integrated*** cultures, the jejunum ADH activity increased by 2.8-fold when treated with 100 mM ($p > 0.05$) and by 3.2-fold at 200 mM EtOH ($p \leq 0.05$). Compared to ***proximal alone*** and ***medial alone*** cultures, ***integrated*** cultures again exhibited increased sensitivity to EtOH treatment.

ADH activity was also measured in hepatocyte lysates. In the hepatocyte homogenates obtained from CS alone cultures, no significant changes in ADH activity were detected when treated with 100 mM or 200 mM EtOH (**Figure 4.6D**). An induction in hepatocyte ADH activity was observed at 200 mM EtOH in both ***proximal*** and ***medial integrated*** cultures. At 200 mM EtOH, hepatocyte ADH activity increased by 2-fold ($p \leq 0.05$) in ***proximal integrated*** cultures, and only by 36% ($p \leq 0.05$) in ***medial integrated*** cultures. Interestingly, in ***medial integrated*** cultures treated with 100 mM EtOH, the hepatocyte ADH activity decreased by 37% compared to untreated controls ($p \leq 0.05$). Decreases in ADH activity were also observed in ***proximal*** and ***distal integrated*** cultures at 100 mM (31% and 14%, respectively), but these changes were not statistically

significant ($p > 0.05$). No significant changes were observed in hepatocyte ADH activity in ***distal integrated*** cultures at either EtOH concentration.

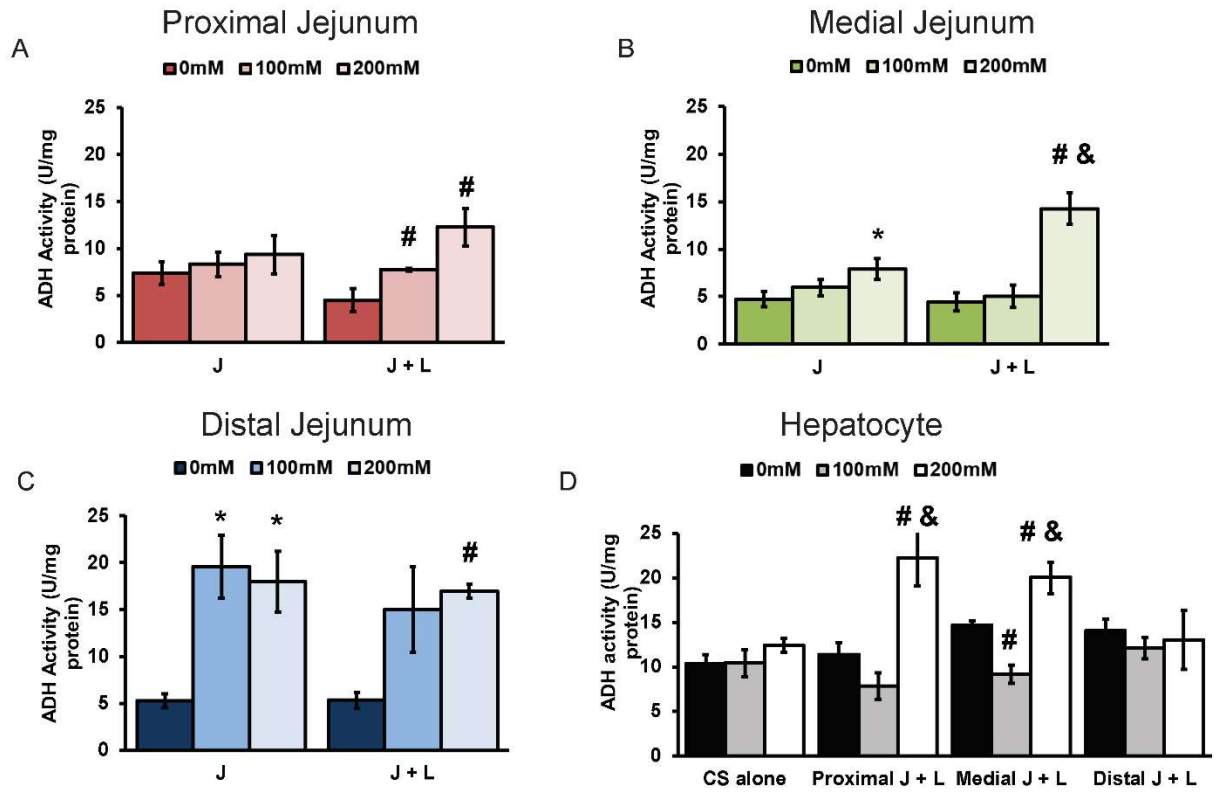

Figure 4.6: Effect of EtOH on ADH activity in (A) proximal, (B) medial and (C) distal jejunum and (D) hepatocytes. (A-C) * and # denote $p \leq 0.05$ relative to untreated jejunum alone and integrated groups, respectively and & denotes $p \leq 0.05$ relative to integrated 100mM group; (D) # and & denote $p \leq 0.05$ relative to 0mM and 100mM groups, respectively.

4.4.7 Effect of EtOH on TNF-α

Levels of the pro-inflammatory cytokine TNF-α were measured in the jejunum. Paneth cells are the primary source of TNF-α in these cultures. In ***proximal jejunum alone*** and ***integrated*** cultures treated with 200 mM EtOH, TNF-α in the jejunum was significantly increased by ~1.9-fold and 1.7-fold, respectively ($p \leq 0.05$) (**Figure 4.7A**). However, no significant changes in TNF-

α levels were observed in ***medial*** or ***distal jejunum*** cultures with EtOH treatment ($p > 0.05$) (**Figure 4.7B and C**).

TNF-α levels were also measured in hepatocyte only cultures. The TNF-α concentrations in hepatocyte only cultures also did not vary with EtOH treatment (**Figure 4.7D**).

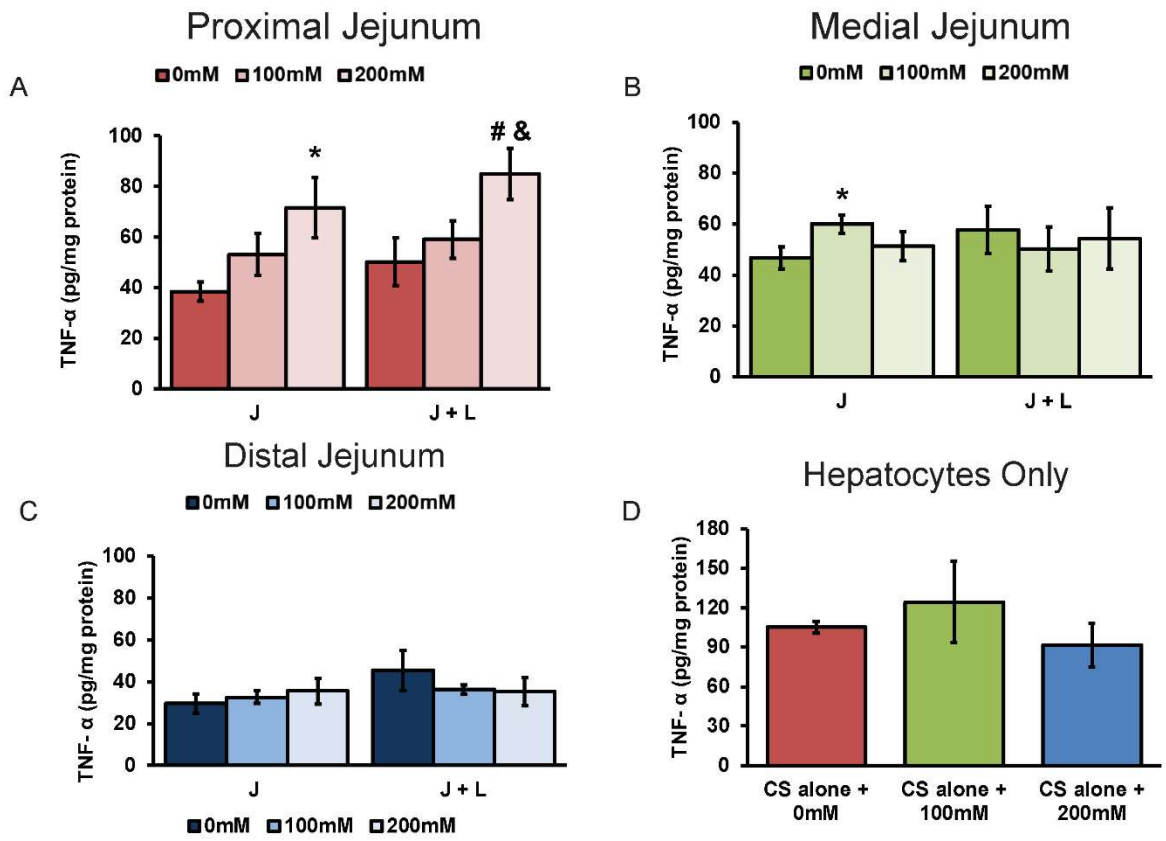

Figure 4.7: Changes in TNF-α concentrations in (A) proximal, (B) medial and (C) distal jejunum and (D) hepatocytes in CS alone cultures with EtOH treatment. * and # denote $p \leq 0.05$ compared to jejunum alone and integrated untreated controls respectively and & denotes $p \leq 0.05$ relative to integrated 100mM group.

4.4.8 Effect of EtOH on villus morphology

Villus morphology was visualized using H&E staining. Damage incurred to the villus architecture in explants treated with EtOH was observed in all cultures (**Figures 4.8A-M, 4.9A-M and 4.10A-**

M). Morphometric analysis was performed on H&E stained sections to compare villus area between untreated and treated samples. Significant decreases in villus area were observed in both jejunum alone and integrated cultures at all 3 locations and both EtOH concentrations. Villus area decreased by 29% and 32% in ***proximal explants cultured alone*** when treated with 100 mM and 200 mM EtOH, respectively ($p \leq 0.05$ for both) (**Figure 4.8M**). In ***proximal integrated*** cultures, villus area decreased by 20% and 29% with 100 mM and 200 mM, respectively ($p \leq 0.05$ for both). Similarly, villus area decreased by 40% and 32% in ***medial alone*** cultures at 100 mM and 200 mM EtOH, respectively ($p \leq 0.05$ for both) (**Figure 4.9M**). In ***medial integrated*** cultures, villus area decreased significantly by 29% at both 100 mM and 200 mM EtOH ($p \leq 0.05$ for both). In ***distal jejunum alone*** cultures, villus area decreased by 21% and 32% at 100 mM and 200 mM EtOH, respectively ($p \leq 0.05$ for both) (**Figure 4.10M**). In ***distal integrated*** cultures, villus area decreased by 28% and 27% at 100 mM and 200 mM EtOH, respectively ($p \leq 0.05$ for both).

H&E staining was also performed on rat hepatocytes in CS alone cultures treated with EtOH at $LC_{50}/2$ and LC_{50} to understand direct effects of EtOH on hepatocyte morphology (**Figure 4.11A-C**). As observed through H&E staining, the hepatocyte morphology did not change significantly when the CS alone cultures were treated with EtOH for 20 h (**Figure 4.11A-C**).

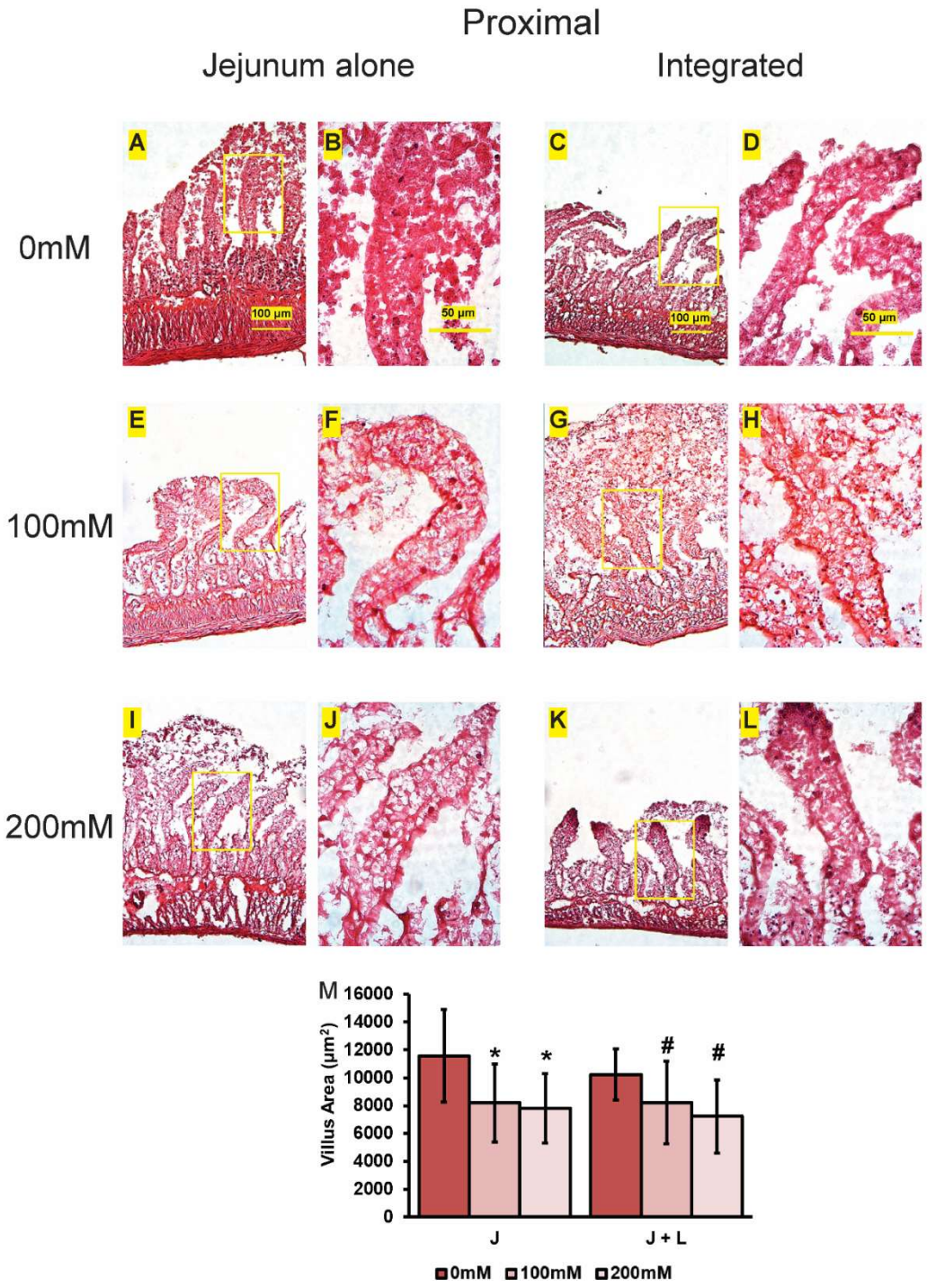

Figure 4.8: (A-L) Effects of EtOH on proximal jejunum villus morphology and (M) villus area determined through H&E staining. B, D, F, H, J and L are higher magnification images of the areas bordered by the yellow rectangles in A, C, E, G, I, and K, respectively. * and # denote $p \leq 0.05$ relative to untreated jejunum alone and integrated groups, respectively, n = 20 villi for villus area.

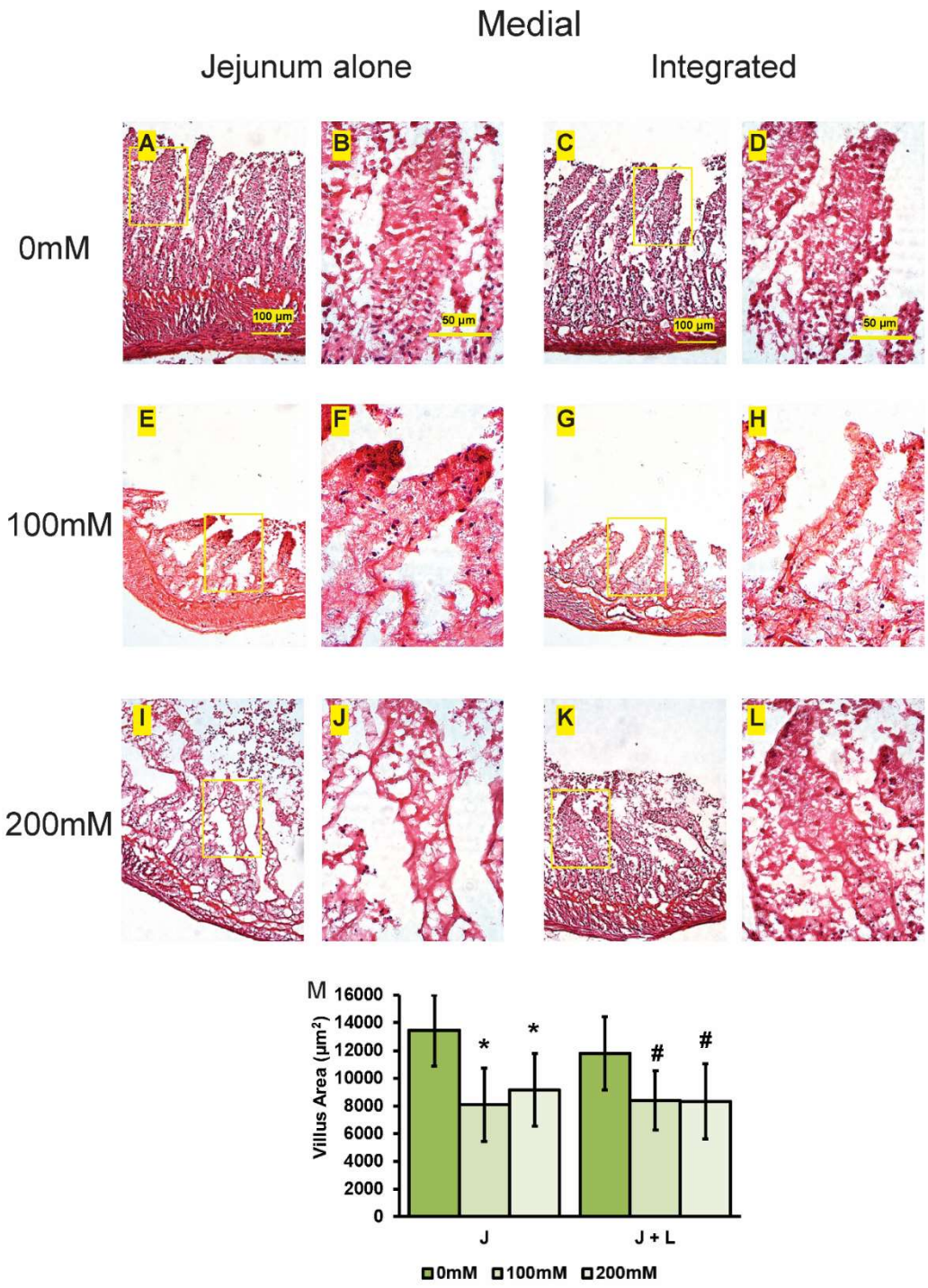

Figure 4.9: (A-L) Effects of EtOH on medial jejunum villus morphology and (M) villus area determined through H&E staining. B, D, F, H, J and L are higher magnification images of the areas bordered by the yellow rectangles in A, C, E, G, I, and K, respectively. * and # denote $p \leq 0.05$ relative to untreated jejunum alone and integrated groups, respectively, n = 20 villi for villus area.

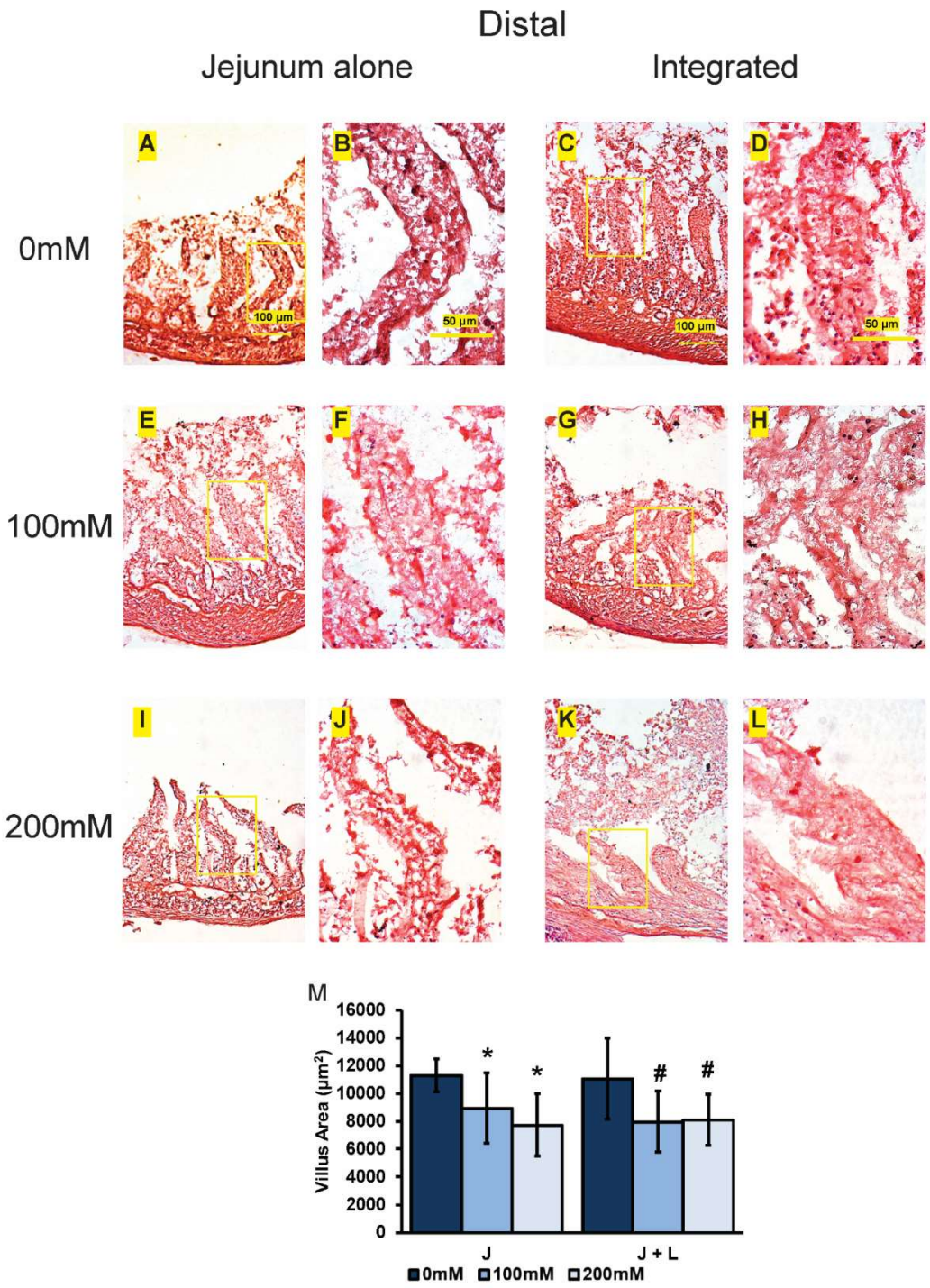

Figure 4.10: (A-L) Effects of EtOH on distal jejunum villus morphology and (M) villus area determined through H&E staining. B, D, F, H, J and L are higher magnification images of the areas bordered by the yellow rectangles in A, C, E, G, I, and K, respectively. * and # denote $p \leq 0.05$ relative to untreated jejunum alone and integrated groups, respectively, n = 20 villi for villus area.

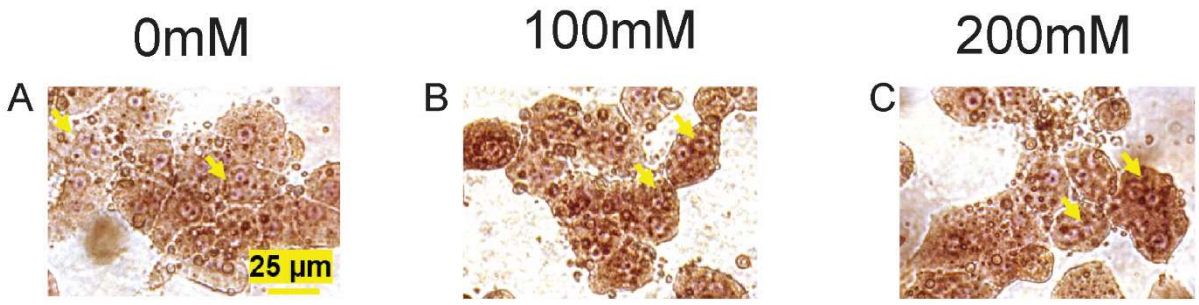

Figure 4.11: H&E staining on CS alone controls. (A) 0 mM, (B) 100 mM and (C) 200 mM EtOH.

4.4.9 Effect of EtOH on acidic mucins

As visualized through AB/PAS staining, there was a clear difference in the area covered by mucins in the jejunum explants after treatment with 100 mM and 200 mM EtOH for 20h (**Figures 4.12A-G, 4.13A-G and 4.14A-G**). Mucin area in ***proximal jejunum alone*** cultures decreased by 1.7-fold ($p > 0.05$) and 2.3-fold ($p \leq 0.05$) after treatment with 100 mM and 200 mM EtOH, respectively (**Figure 4.12G**). Mucin area in ***proximal integrated*** decreased by 1.9-fold and 2.7-fold at 100 mM and 200 mM EtOH, respectively ($p \leq 0.05$ for both) (**Figure 4.12G**). Medial jejunum cultures responded differently to 100 mM and 200 mM EtOH. While the mucin-covered area fraction decreased by 2.1-fold at 100 mM EtOH in ***medial jejunum alone***, the decrease was only 1.4-fold at 200 mM EtOH ($p \leq 0.05$ for both) (**Figure 4.13G**). Similarly, in ***medial integrated*** cultures, mucin-covered area decreased by 2.1-fold at 100 mM EtOH ($p \leq 0.05$), but no significant change was observed at 200 mM EtOH ($p > 0.05$). In ***distal jejunum alone***, a significant decrease in mucin area was observed only at 200 mM EtOH (3.6-fold; $p \leq 0.05$) (**Figure 4.14G**). No significant changes in mucin area were observed in ***distal integrated*** cultures.

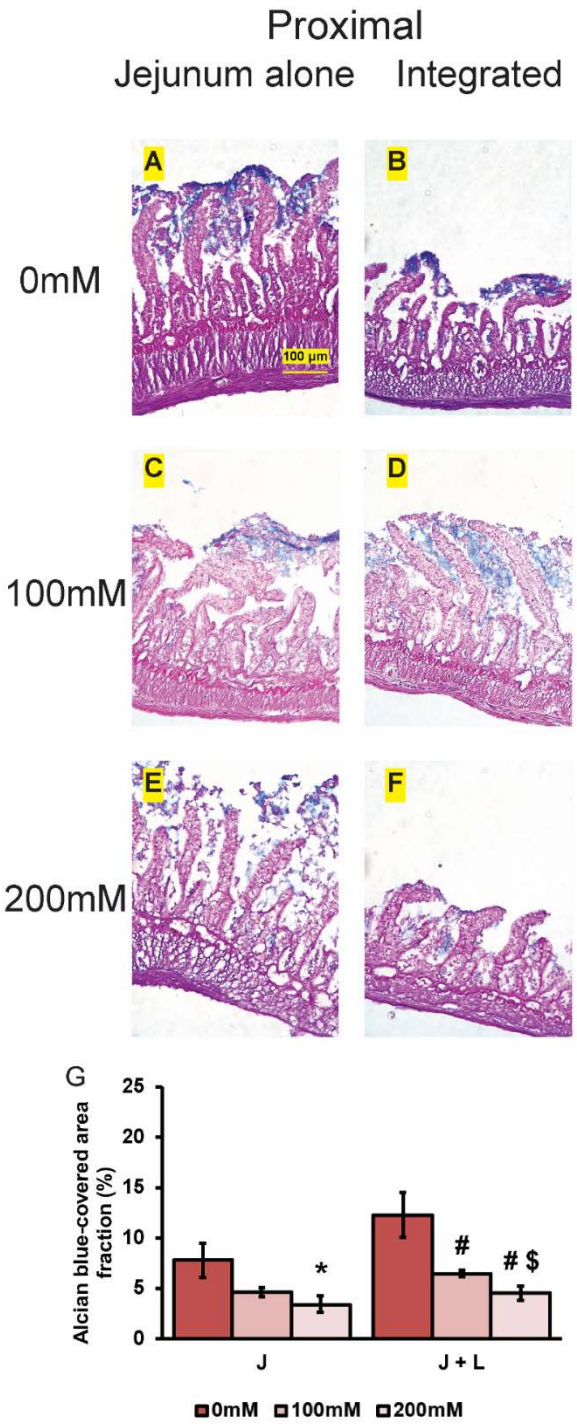

Figure 4.12: (A-F) Effects of EtOH on the proximal jejunum mucus barrier determined through AB/PAS staining and (G) mucin-covered area fractions. * and # denote $p \leq 0.05$ compared to jejunum alone and integrated untreated controls respectively and $ denotes $p \leq 0.05$ relative to integrated 100mM group.

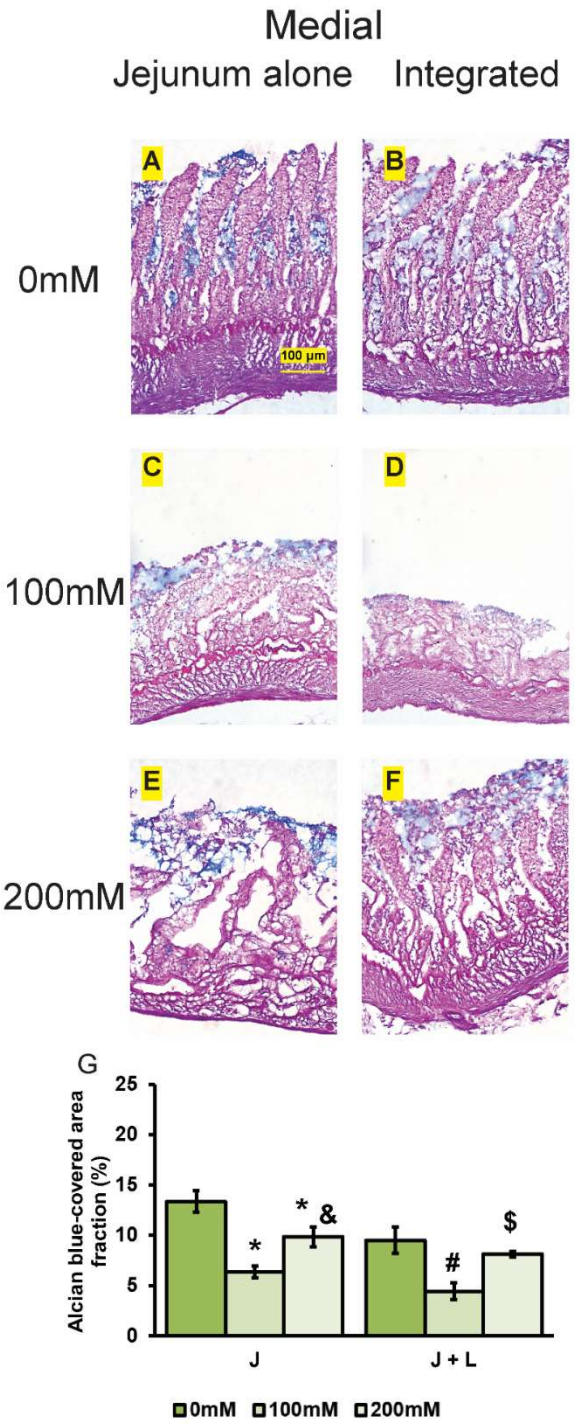

Figure 4.13: (A-F) Effects of EtOH on the medial jejunum mucus barrier determined through AB/PAS staining and (G) mucin-covered area fractions. * and # denote $p \leq 0.05$ compared to jejunum alone and integrated untreated controls respectively; & and $ denote $p \leq 0.05$ relative to alone integrated 100mM groups, respectively.

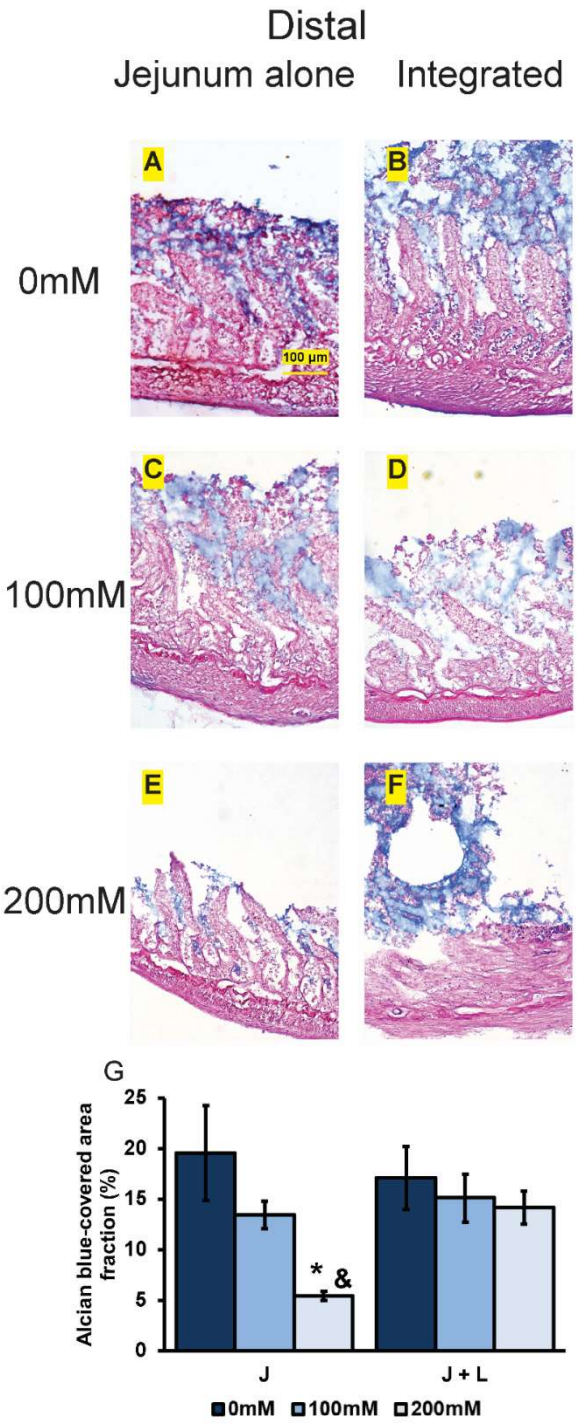

Figure 4.14: (A-F) Effects of EtOH on the distal jejunum mucus barrier determined through AB/PAS staining and (G) mucin-covered area fractions. * and # denote $p \leq 0.05$ compared to jejunum alone and integrated untreated controls respectively and & denotes $p \leq 0.05$ relative to alone 100mM group.

AB/PAS staining was also performed on rat hepatocytes in CS alone cultures treated with EtOH at $LC_{50}/2$ and LC_{50} as controls (**Figure 4.15A-C**). As expected, no mucin deposition was observed in the hepatocyte only cultures with or without EtOH (**Figure 4.15A-C**) (270).

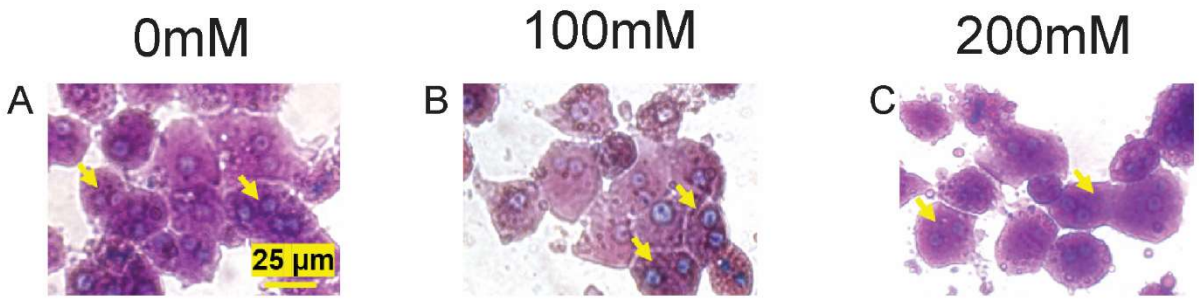

Figure 4.15: AB/PAS staining on CS alone controls. (A) 0 mM, (B) 100 mM and (C) 200 mM EtOH.

4.5 Discussion and Conclusions

The lack of primary, multi-tissue, *in vitro* models of toxicity that mimic the gut-liver connections motivated us to develop an integrated model using primary hepatocytes and jejunum from rats (252-254). This integrated culture model was employed to investigate EtOH toxicity to the gut-liver axis *in vitro.* EtOH was chosen to interrogate these cultures because it is an important toxicant encountered by most humans that affects both the gut and the liver (131-137).

In a previous study, we divided the rat jejunum into three different regions of equal length and reported differences in enterocyte, goblet cell and Paneth cell functions between these regions (265). In this study as well, explants obtained from three different locations - the proximal, medial and distal jejunum - were used to investigate any differences in EtOH toxicity. The effects of EtOH exposure on activities of enzymes such as ALP, ADH and lysozyme were investigated in addition to jejunum villus morphology, mucus barrier and cytokine secretion. Markers of enterocyte, goblet cell and Paneth cell functions showed significant changes in response to EtOH administration, demonstrating the toxic effects of EtOH to multiple intestinal cell types in culture.

Proximal integrated cultures exhibited decreases in jejunum protein at both 100 mM and 200 mM EtOH. The location and presence of hepatocytes in the cultures could both have played a role. The presence of CS cultures could have led to EtOH metabolism by both the jejunum and the hepatocytes. Hepatocyte protein in distal integrated cultures decreased significantly even at 100 mM EtOH. This could be due to a combined effect of EtOH toxicity and higher endotoxin levels in the distal cultures (131, 271). Endotoxin levels have not been measured in the present study, but further investigations would be performed in the future to understand their importance.

Jejunum and hepatocyte ALP activities increased upon treatment with EtOH. Increase in hepatic ALP activity due to EtOH has been reported *in vivo* and a similar mechanism has been suggested for intestinal ALP activity as well (272). For example, one study reported that hepatic ALP activity increased by ~63% with EtOH treatment in rats *in vivo* (272). Additionally, endotoxins such as lipopolysaccharide (LPS) have been shown to induce both the expression and activity of intestinal ALP (273). Induction of ALP in the intestine has been linked to inflammation (274). Future studies may also benefit from an investigation of gut bacteria-associated changes in ALP activity upon EtOH administration (275). In the distal integrated cultures, potential damage to the hepatocytes at 200 mM EtOH, as evidenced by the loss in hepatocyte protein observed with both 100 mM and 200 mM EtOH, could have led to a decreased ALP activity. Measurement of ALP activity in the culture media could help understand this mechanism as hepatocyte damage may be associated with an increase in media ALP activity due to release of the enzyme form damaged cells into the media (276). It is possible that hepatocyte-derived factors such as bile acids are causing the increased differences in jejunum ALP activity in the integrated cultures. Investigation of secreted factors such as bile acids that are affected by both the hepatocytes and the intestine that may affect ALP activity would elucidate the trends observed in jejunum ALP activity in integrated cultures. For example, bile acids such as taurocholic acid have been shown to induce ALP activity in hepatocytes (277). We have also observed a correlation between ALP activity and taurocholic

acid levels in our studies. In **Chapter 3**, the ALP activity in distal jejunum samples was found to be significantly lower than the proximal and medial jejunum at 4h. Correspondingly, in **Chapter 5**, the concentration of taurocholic acid has been detected to be significantly lower in the distal jejunum compared to the proximal and medial jejunum at 4h. It would be interesting to explore this metabolite in EtOH treated cultures as well.

Lysozyme activity, a marker of Paneth cell function, also increased in response to EtOH. EtOH has been reported to increase both the number of Paneth cells and the secretion of antimicrobial peptides from these cells in the gastrointestinal tract *in vivo* (278, 279). The increase in lysozyme activity observed in the present study could be due to EtOH-induced secretion of antimicrobial peptides from Paneth cells (278). While the present study does not investigate other antimicrobial peptides, more detailed studies would be conducted in the future to understand the effects of EtOH on Paneth cells.

ADH activity was induced in both jejunum explants and hepatocytes in integrated cultures in response to EtOH. Induction of ADH activity due to EtOH in both the intestine and the liver has been demonstrated in *in vivo* studies (280, 281). For example, a ~1.8-fold increase in intestinal ADH activity with EtOH treatment was reported in rats *in vivo* (281). Similarly, a ~40% increase in rat hepatic ADH activity with EtOH treatment was also reported *in vivo* (281). The decrease in hepatocyte ADH activity at 100 mM in may be due to varied effects of different EtOH doses to the ADH isoforms expressed in the liver (282). For example, in the mouse liver, activity of ADH I isoform decreased due to EtOH at lower (millimolar) concentrations, while that of the ADH III isoform increased at higher (molar) concentrations in a dose-dependent manner (282). Since various ADH isoforms are also expressed in rat hepatocytes (283), a delineation of the activities of these different isozymes may be beneficial in further explaining the results observed. Furthermore, the reason for the distal jejunum alone cultures exhibiting a high increase in ADH activity even at 100 mM EtOH is not yet explained. While the other modes of EtOH metabolism

(CYP2E1 and catalase) in the intestine and the liver are less prominent compared to the ADH pathway, their expression as well as activity can be induced by EtOH (284, 285). In the future, measurement of CYP2E1 and catalase activities would provide comprehensive information on the mechanism of EtOH metabolism in the different regions of the jejunum and in hepatocytes. Further insight may be gained by delineation of the different ADH isoforms expressed in the rat intestine (286).

The secretion of pro-inflammatory cytokines such as TNF-α, IL-1β, and IL-6 has been found to be upregulated in the murine small intestine and liver after chronic exposure to EtOH (287). This study focused on measurements of TNF-α in protein lysates from the jejunum explants as intestinal epithelial cells are known to express TNF-α. In the present study, significant increase in TNF-α due to EtOH was observed only in proximal jejunum cultures. Contrary to the expectation of increased expression of TNF-α in medial and distal jejunum explants due to EtOH, gut bacteria and associated endotoxin levels, we did not observe any change in these regions in the present study. Arya *et al* demonstrated that an increase in TNF-α expression due to LPS (endotoxin) in the rat intestinal tissue lysates was time- and location-dependent (288). In their study, the amount of intestinal TNF-α protein increased to a maximum by 1 h of LPS exposure in the jejunum and ileum, and by 2 h of LPS exposure in the duodenum. The TNF-α levels then decreased to close to untreated controls by 3 h. At 3 h and 4 h, the TNF-α levels in the jejunum were higher than the ileum, although not statistically significant (288). This trend is similar to the differences between the proximal, medial and distal jejunum observed in the present study. Increased TNF-α expression, as observed in the proximal jejunum 20h after EtOH treatment in the present study, has been correlated to increased cell death in the intestine (289). The increased sensitivity of proximal jejunum cultures to EtOH in protein measurements could be due to the increased TNF-α expression in the proximal jejunum after EtOH administration in this segment. EtOH-induced

secretion of TNF-α could also have partially played a role in the changes in villus morphology and mucus barrier of the proximal jejunum observed in this study (287).

Morphometric measurements revealed drastic changes in villus area upon EtOH administration. *In vivo,* both acute and chronic EtOH administrations have been shown to cause villus damage that manifests as contraction and shortening of the villi (152, 153). However, the mechanism of this change has not been clearly described. The loss of villus morphology observed in this study correlates with previous reports of damage to villi due to EtOH *in vivo* (152, 153, 290). For example, Baraona *et al* reported a ~24% decrease in villus height as a result of EtOH treatment in rats (152).

EtOH can affect the mucus barrier in different ways. Rats treated with EtOH have higher luminal mucus content and lower mucosal hydrophobicity than the untreated animals, showing that EtOH can modify the mucus barrier by itself (291). In addition, TNF-α is an important regulator of mucin expression and secretion by goblet cells (292). Several mechanisms have been described for this dependence. TNF-α leads to apoptosis of Muc2 producing goblet cells (292). The change in mucus barrier area in the current study could be a result of both direct effects of EtOH and TNF-α -induced effects. The decrease in acidic mucins in medial and distal jejunum cultures cannot be explained by changes in TNF-α. Interestingly, while a decrease in mucin area was consistently observed in proximal jejunum cultures, the integrated cultures of medial and distal jejunum did not show any decrease at 200 mM EtOH. There are different mechanisms that can either cause upregulation or downregulation of mucin expression and secretion in the intestine as a result of EtOH. A combination of these opposing mechanisms working together may explain these results. Grewal *et al* reported an increase in mucin secretion in rats fed EtOH chronically (293). This was also accompanied by an increase in ALP activity detected in the mucins isolated from EtOH-fed rats. In the study, the increase in ALP activity was attributed to enterocyte brush border membranes trapped in the mucus layer (293). Additionally, LPS and other bacterial products from

both gram-negative and gram-positive bacteria have also been shown to upregulate Muc2 expression (294-296). A combination of mechanisms working to increase and decrease mucin production in the cultures could be responsible for the trends observed. Further investigation into the mechanisms responsible for such changes would help understand these results.

In vivo studies have revealed that the effects of acute EtOH toxicity are reversible owing to regeneration of damaged villi (297-299). The present study does not investigate recovery and regeneration of the intestinal mucosa. In the future, a study can be designed in which EtOH-containing media is removed after 10 h of administration and fresh media (without EtOH) is added to the explants for another 10 h before ending the cultures. Samples would be collected for imaging the villi and the acidic mucins as well as measurements of enzymatic activities. This study design would help understand any regeneration and recovery occurring after the toxicant is removed from the cultures.

Direct toxicity effects of EtOH to the intestine were observed in the present study. Similar observations have been reported *in vivo* (152, 153). Direct effects of acute EtOH toxicity on the liver such as its effects on fatty acid oxidation and triacylglycerol synthesis have also been reported *in vivo* (300). In future investigations, fatty acid metabolism and an analysis of corresponding metabolites in CS alone cultures could be explored to understand direct effects of EtOH on the liver. Additionally, the directionality of the effects of EtOH can be investigated by designing an experiment where conditioned media from jejunum alone cultures treated with EtOH is supplemented to hepatocyte only cultures and vice versa.

Taken together, our results from this study highlight two important factors that could affect the of the jejunum and hepatocyte cultures to EtOH toxicity: (1) the location from where the jejunum explants are obtained, and (2) the effect of integration of jejunum explants with hepatocytes. Integrated cultures with explants from the proximal jejunum were the most sensitive to EtOH toxicity *in vitro.* Jejunum and hepatocyte protein, activities of ALP, ADH and lysozyme, and villus

and mucin areas exhibited trends anticipated from *in vivo* reports. These results underscore the importance of integrating the two organs in order to recapitulate the *in vivo* response to EtOH toxicity. Moreover, location along the jejunum could be an important factor affecting the toxic response. In the future, such integrated cultures of the jejunum and hepatocytes could be useful to investigate the toxicity of other drugs and toxicants in the pharmaceutical industry.

Chapter 5: Spatiotemporal Variation in Metabolites in *In Vitro* Cultures of the Rat Jejunum and Hepatocytes

5.1 Abstract

Mass spectrometric (MS) techniques have been used extensively for investigating a range of phenomena including disease and drug metabolism. *In vivo* gut metabolomics studies have commonly been conducted on fecal samples, intestinal contents, urine or blood samples from animals. Despite the presence of numerous metabolomic studies on the intestine *in vivo*, to the best of our knowledge, there are no studies that have investigated spatiotemporal variations in the secreted metabolome of the intestine *in vitro.* Moreover, *in vitro* studies that investigate the metabolites in an integrated intestine-liver model are also lacking. In the present study, we focused on an untargeted analysis of lipophilic compounds (bile acids and fatty acids, and lipophilic media components) in the negative ion mode. The differences in metabolites were evaluated at 2 different time points in culture (4h and 24h), across 3 locations within the jejunum (proximal, medial and distal) and in two different culture types (jejunum explants cultured alone or integrated with hepatocytes in collagen sandwich cultures). Lipids including bile acids, lysophosphatidylcholines and fatty acids were identified in the conditioned culture media and compared to their levels in unconditioned media controls. Spatiotemporal trends were observed within the jejunum *in vitro* that may be correlated to bile acid and fatty acid metabolism pathways in the intestine. More extensive investigations of the pathways involved could provide useful insights into the spatiotemporal trends in the jejunum cultured with and without hepatocytes.

5.2 Introduction

As the metabolite profile of an organism or system most closely aligns with an observed phenotype, assessing the 'metabolome' of a system of interest provides a means to characterize the observed physiology. Mass spectrometric (MS) techniques have been extensively used for investigating the metabolome (154-156), with liquid chromatography-mass spectrometry (LCMS) analyses applied to a wide range of diseases such as osteoarthritis, coronary heart disease, cancer and neurodegenerative diseases such as Alzheimer's disease and Parkinson's disease (155, 157-160). LCMS techniques have also been used to study drug metabolism by the liver, intestine, and the intestinal microbiota (161-163). As the small intestine and the liver regulate several physiological functions including metabolism of oral drugs, bile acid homeostasis, inflammation and nitrogen homeostasis (23, 112), LCMS has been widely used in investigations of drug metabolism, amino acid metabolism as well investigations of several intestinal and serum lipids including bile acids and fatty acids (164-166).

LCMS-based metabolomics can be performed in targeted or untargeted fashion (171, 301). A targeted analysis is performed to quantify specific known compounds of interest (301). Calibration curves are generated using standards for the compounds of interest, and the samples are analyzed to determine their concentrations (301). An untargeted analysis is performed when little is known about the system of interest (171, 302). Samples are obtained and analyzed with the MS operated in either positive or negative ion mode (or both) (303-305). Depending on the class of compounds that needs to be investigated, choices also have to be made with respect to the chromatography media, favoring either polar or non-polar compounds (306). The vast majority of untargeted metabolomics studies utilize a reversed-phase separation (polar compounds elute first), analyzing in both positive and negative ion modes (306).

Electrospray Ionization (ESI) is one of the ways to ionize molecules for MS analysis (307, 308). Depending on the polarity used for ESI, samples can be analyzed in positive or negative ion mode (307, 309). In the positive ion mode, positively charged ions such as protonated molecules (referred to as $[M+H]^+$), or molecules with adducts such as with Na^+ or K^+ ions ($[M+Na]^+$, $[M+K]^+$) may be formed (307). In the negative ion mode, deprotonation ($[M-H]^-$) or formation of molecular adducts with Cl^- ($[M+Cl]^-$) or formate ions may take place (309). Most lipidomics analyses, including identification of fatty acids and taurine-conjugated bile acids, are performed in the negative ion mode (306, 310, 311).

Untargeted metabolomics studies are challenging as there are no streamlined databases to identify compounds, nor is there a full list of all expected metabolites in any system (302). Each ion (and hence metabolite) therefore must be evaluated individually, requiring a retention time vs. mass map from all LCMS runs (312). Knowledge of the potential metabolites present in the samples being analyzed is key to limiting the list of compounds that may be present, as are their retention times on a LC run (312). Employing a high resolution/high mass accuracy MS can aid in identification as high mass accuracy can oftentimes lead to a molecular formula (312). The observed ion at high resolution, along with the retention time on the column, form an exact mass-retention time pair (EMRT), or simply referred to as a feature (313). When coupled with ion intensities, these features and relative abundances can be searched to find differences between samples (313). The differences can be visualized with principal component analyses (PCA) and subsequently ranked according to relative abundance differences (314, 315). Once a ranking has been obtained, efforts are taken to identify the metabolites associated with the observed mass and its fragmentation pattern (312).

Most of the *in vivo* studies on intestinal metabolites have focused on the gut microbiome (162, 167, 168). Chen *et al* (162) and Vernocchi *et al* (167) described the importance of metabolomics studies in understanding host-microbiota interactions in the intestine. *In vivo* gut metabolomics

studies have commonly been conducted on fecal samples or intestinal contents, intestinal tissues or urine or blood samples from animals in both targeted and untargeted manner (165, 168-170).

Recently, Yuan *et al* reported variation in gut metabolites along the length of the baboon small intestine *in vivo* (170). Their study involved an untargeted LCMS-based metabolomics study using tissue samples from different intestinal segments from the duodenum to the distal colon. They correlated the metabolite data with results from 16s-rRNA sequencing from the same tissues. They found that taurine-conjugated bile acids and fatty acids such as linoleic acid and docosahexaenoic acid were present in higher concentrations in the small intestine compared to the colon. On the other hand, metabolites such as cholic acid, lysophosphatidylcholine and sphingomyelin were present at higher concentrations in the colon.

Mass spectrometric analyses of metabolites in *in vitro* intestinal cultures have focused on identification of metabolites of a drug or toxicant administered to Caco-2 cells (172, 173). Similar studies on intestinal drug metabolism using LCMS have been conducted using other *in vitro* systems such as primary enterocytes or intestinal contents (174). Ho *et al* (163) employed LCMS to study the metabolism of several drugs and toxicants including midazolam, paclitaxel and diclofenac by primary human enterocytes. Nepal *et al* (174) incubated gastrodin with intestinal contents from rats to investigate microbial metabolism of the drug *in vitro*.

LCMS has also been used to study the effect of gut bacterial metabolites on hepatocytes *in vitro* (169). In this study, the effect of a tryptophan metabolite formed from bacterial metabolism were studied suing hepatocytes and macrophages. Indole-3-acetate was found to be capable of modulating inflammatory responses from the hepatocytes and the macrophages using cell lines. The importance of enterohepatic circulation between the gut and the liver in the progression of primary sclerosing cholangitis *in vivo* was also investigated by conducting metabolomic analysis of portal blood (316).

Despite the presence of numerous metabolomic studies on the intestine *in vivo*, to the best of our knowledge, there are no studies that have investigated spatiotemporal variations in the secreted metabolome of the intestine *in vitro.* Moreover, *in vitro* studies that investigate the metabolites in an integrated intestine-liver model were also not found.

In **Chapter 3**, it was demonstrated that the spatial variation along the length is not limited to the different longitudinal sections of the small intestine alone. Functional markers for different cell types in the intestinal epithelium vary even within the jejunum *in vitro*. In the present study, we focused on an untargeted analysis of lipophilic compounds (i.e., bile acids and fatty acids, and lipophilic media components) in both positive and negative ion modes. We hypothesized that the secretion, metabolism or both of metabolites in *in vitro* jejunum cultures would vary with the location of intestinal explants, time in culture, and with integration with hepatocytes. The differences in metabolites were evaluated at 2 different time points in culture (4h and 24h), across 3 locations within the jejunum (proximal, medial and distal) and in two different culture types (jejunum explants cultured alone or integrated with hepatocytes in collagen sandwich cultures).

5.3 Materials and Methods

Calcium chloride, chloroform, collagenase type IV, gentamicin sulfate, glucagon, 4-(2-hydroxyethyl)-piperazine-1-ethanesulfonic acid (HEPES), hydrocortisone were purchased from Sigma-Aldrich (St. Louis, MO). Unless stated otherwise, all other chemicals were purchased from Thermo Fisher Scientific (Waltham, MA).

5.3.1 Collagen extraction

Type I collagen was extracted from rat tail tendons as previously described (231). Briefly, the tendons were dissolved in 3 % (v/v) acetic acid and centrifuged at 13,000 x *g*. Collagen was precipitated from the supernatant with 30 % (w/v) sodium chloride. The suspension of precipitated collagen was further centrifuged at 8,500 x *g* and the pellets were resuspended in 0.6 % acetic

acid. The resulting solution was dialyzed in 1 mN hydrochloric acid. The concentration of collagen in the solution was determined through its absorbance at 280 nm. The pH of the solution was maintained at 3.1. The collagen solution was sterilized with chloroform before using it to cast gels for cell culture.

5.3.2 Isolation and culture of primary rat hepatocytes

Primary hepatocytes were obtained from the livers of female Lewis rats weighing 180-210 g (Envigo, Indianapolis, IN) after an *in situ* two-step collagenase perfusion as described before (231) (234). All animal care and surgical procedures were approved by the Virginia Tech Institutional Animal Care and Use Committee (IACUC). Isolated hepatocyte counts ranged between 100-150 million hepatocytes with ≥ 97% viability. Hepatocytes were seeded in 12-well plates on 1.1mg/mL collagen gels (0.25 mL per well) at a density of 500,000 cells per well. To prepare collagen sandwich (CS) hepatocyte cultures, a second layer of collagen (1.1 mg/mL) was deposited over the hepatocyte monolayer 3h after hepatocyte seeding. Hepatocyte culture medium was added 1h later (3mL per well). Culture medium was composed of phenol red-free liquid Dulbecco's modified Eagle medium (DMEM), supplemented with 10 % (v/v) heat-inactivated fetal bovine serum, 200 U/mL penicillin, 200 µg/mL streptomycin, 4 mM L-glutamine, 0.5 U/mL insulin (MP Biomedical, Santa Ana, CA), 20 ng/mL Epidermal Growth Factor (EGF), 14.28 ng/mL glucagon, and 7.65 µg/mL hydrocortisone. Cultures were incubated at 37°C in a humidified incubator in an atmosphere of 10% carbon dioxide.

5.3.3 Isolation and culture of rat jejunum explants

The small intestine was obtained from the same female Lewis rats from which the liver was excised for hepatocyte isolation. The intestine was stored in ice-cold common culture medium supplemented with 50 µg/mL gentamicin sulfate until explant isolation. Jejunum explants (~1 cm in length) were isolated from the intestine as described previously (222). Approximately 1 cm-long sections of the inverted jejunum were pulled on Matrigel® - coated PDMS rods and transferred to

Millicell® inserts. Thereafter, the inserts were placed in 12-well plates coated with 0.5 mL of 1.1 mg/mL collagen gel. Hepatocyte culture medium supplemented with gentamicin was added to each well to cover the intestinal segment in the Millicell® insert (3 mL per well). Eighteen explants (~ 1 cm in length) could be isolated from the entire jejunum. The top six sections (obtained from the region next to the duodenum) were identified as proximal, the middle 6 as medial and the bottom 6 (from the region right before the ileum) as distal. All explants were cultured in a humidified incubator maintained at 37°C in an atmosphere of 10% CO_2. The media was changed at T = 3 h and T = 4 h. The culture medium (3 mL per well) added to the explants at 0h and 3h was additionally supplemented with 50 µg/mL gentamicin. At T = 4h, the explants were transferred to either new collagen-coated wells with/without hepatocytes to be maintained as integrated/jejunum alone cultures respectively. The culture medium added at 4h was not supplemented with gentamicin. All cultures (CS alone, jejunum, or integrated) were supplemented with 3mL per well of common culture medium. Integrated cultures with proximal, medial and distal jejunum explants have been called 'proximal integrated (J+L)', 'medial integrated (J+L)' and 'distal integrated (J+L)' cultures, respectively.

5.3.4 Sample preparation

The culture media (750 µL aliquot) was collected in microcentrifuge tubes rinsed with distilled ethanol (95% v/v) and chloroform and flash frozen. Frozen media samples were freeze-dried in a lyophilizer (Labconco Freezone 4.5). Freeze-dried samples were resuspended in MS grade methanol (400 µL) (Thermo Fisher Scientific), sonicated in a water bath sonicator for 10 min (5510 Branson), then centrifuged at 13,000 x g for 10 min at 10°C. The supernatant was collected, and the pellet was resuspended in methanol again (400 µL), followed by sonication and centrifugation as before. The supernatants collected from the two steps were combined/pooled. Solid phase extraction (SPE) was performed on the total 800 µL volume collected using octadecyl carbon chain-bonded silica solid phase extraction units (Proto 300 C18, The Nest Group, Inc.). The SPE

units were rinsed with methanol and water by centrifuging to dryness at 100 x *g* for 3 min. Higher molecular weight impurities such as polypeptides were removed by running the methanol-suspended samples through the rinsed SPE units and the flow-through was collected after centrifugation at 100 x *g* for 3 min. The SPE columns were washed with methanol another time to collect any residual hydrophobic molecules. The volume of the collected samples was reduced in a centrifugal concentrator. The samples were further dried under high vacuum before preparing them for LCMS.

5.3.5 Preparation of samples for mass spectrometry (MS)

Vacuum-dried extracted samples were resuspended by sonication in a 400 µL solution of 50:50 methanol:water with 0.1% (v/v) formic acid. This was followed by a 10 min centrifugation at 13,000 x g. An aliquot of the supernatant was transferred to an LCMS vial for mass spectrometric analysis. Master mixes were prepared by combining volumes from multiple samples and included in the MS samples for quality control and MS^E analysis. Each biological replicate was injected in triplicate. Injections were randomized to eliminate bias.

5.3.6 LCMS analysis

For LCMS, Acquity I-class UPLC (Waters, Milford, MA) was used in conjunction with a Synapt G2-S mass spectrometer (Waters, Milford, MA). A binary gradient at a flow rate of 0.2 ml/min of solvent A (water + 0.1% formic acid; Thermo Fisher) and solvent B (acetonitrile + 0.1% formic acid) was used as follows: initial to 1 min 5% B, 1 min-12 min linear gradient to 98% B, 12-13 min hold at 98% B and 13-15 min return to initial conditions. A two µL aliquot was injected onto an Acquity BEH C18 column (50 x 2.1 mm i.d., 1.7 µm; Waters, Mildford, MA) maintained at 35°C (C18 = octadecyl (18)-carbon chain-bonded silica column) (**Figure 5.1**).

The column was eluted into the mass spectrometer operated with an electrospray ionization probe (ESI) (**Figure 5.1**). Samples were independently analyzed in both positive and negative high-

resolution ion modes. Source conditions were the same for positive and negative modes with the exception of the capillary voltage which was 3.0 kV and 1.5 kV for positive and negative respectively, temperature 125°C, cone voltage 30 V, source offset 80, desolvation temperature 350°C, cone gas 50 L/h, desolvation gas 500 L/h, nebulizer gas 6.0 bar, cycle time 0.2 s and mass scan range 100 – 1800 m/z. Leucine-enkephalin at a concentration of 200 ng/mL was continually infused at 5 µL/min through the reference sprayer for accurate mass correction. Master mix samples were additionally analyzed in MS^E mode in order to collect MS and fragmentation data simultaneously.

5.3.7 Data processing and feature annotation

The MS data were processed using MarkerLynx XS software (Waters, Milford, MA) for feature discovery and deconvolution. Features were selected based on statistically significant differences between different experimental groups ($p < 0.05$). Selected features discovered in the negative ion mode were identified using the MS^E fragmentation data by matching against existing databases including the human metabolome database (HMDB) (317), Metlin (318) and Lipid Maps (319) through both parent mass and fragment similarity searches (**Figure 5.1**).

5.3.8 Statistical analyses

Statistical significance was determined by obtaining *p*-values through one-way ANOVA followed by Tukey's HSD test for multiple hypotheses testing. Technical replicate measurements from the three injections were averaged for each biological replicate. Three biological replicates were used per condition. For all tests of statistical significance, $\alpha = 0.05$.

5.4 Results

5.4.1 Feature discovery

Figure 5.1 provides a general overview of the steps involved in metabolite detection and identification. LCMS was performed on culture media samples extracted through reversed-phase

separation. The samples injected into the C18 liquid chromatography column were separated based on their lipophilicity leading to different retention times. After ESI/MS on compounds eluted at different retention times, overall sample chromatograms and mass spectra associated with each retention time were obtained, leading to discovery of various features (sets of retention times and m/z). Subsequent data were analyzed for statistical significance among the discovered features. Processing the raw mass spectrometric data using MarkerLynx XS software in the positive ion mode resulted in 67-109 features while processing in the negative ion mode resulted in 64-81 features as listed in **Table 5.1**. Subsequent results focus on the features identified in the negative ion mode.

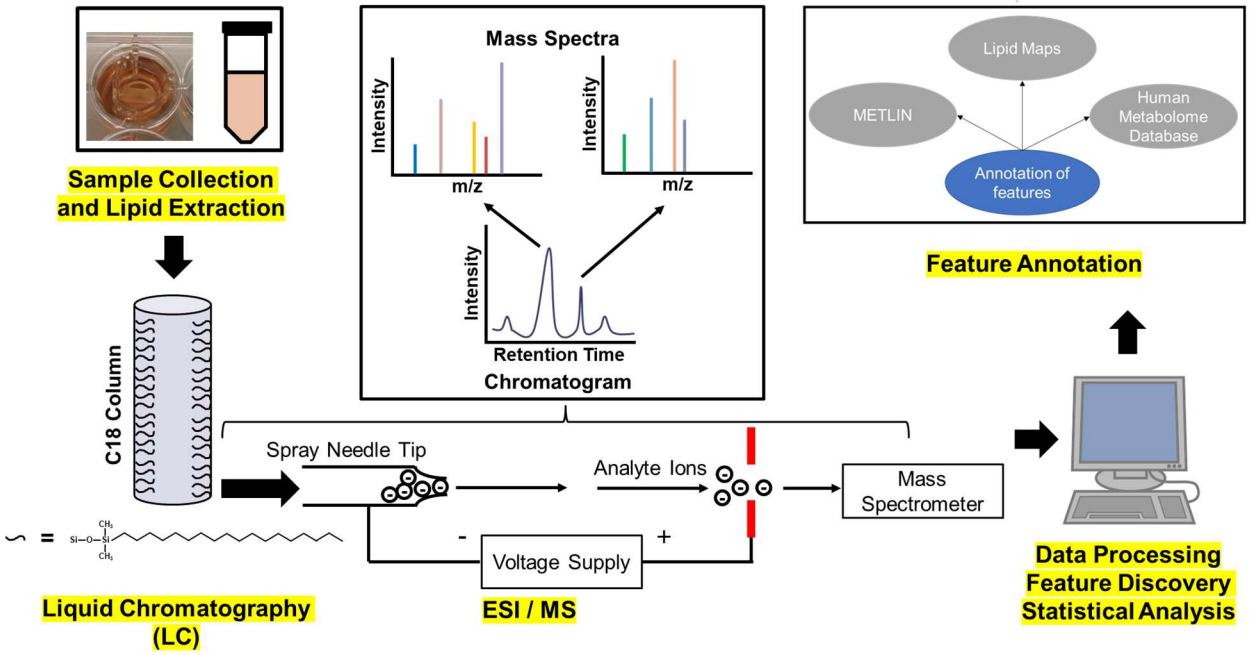

Figure 5.1: Flow diagram of LCMS, data analysis and feature annotation. C18 column refers to octadecyl (18)-carbon chain-bonded silica column. ESI operated in the negative ion mode is depicted in the schematic.

Table 5.1. Number of features discovered in positive and negative ion modes.

Group	Number of features discovered in positive ion mode	Number of features discovered in negative ion mode
Fresh Media (4h)	81	76
Fresh Media (24h)	100	81
CS alone (24h)	100	66
Proximal jejunum alone (4h)	85	76
Medial jejunum alone (4h)	67	64
Distal jejunum alone (4h)	79	71
Proximal jejunum alone (24h)	109	78
Medial jejunum alone (24h)	100	70
Distal jejunum alone (24h)	92	65
Proximal integrated (24h)	90	73
Medial integrated (24h)	96	76
Distal integrated (24h)	98	81

5.4.2 Principal Component Analysis (PCA)

Three levels of comparisons were made between the experimental groups investigated in the LCMS study: (1) location-wise comparisons between proximal, medial and distal jejunum, (2) time-wise comparisons between 4h and 24h time-points, and (3) culture type comparisons between jejunum only, hepatocytes only and integrated cultures (at 24h).

Principal component analyses were performed on the 3 technical replicates of n = 3 biological replicates of each experimental group (total 9 values per group). PCA of jejunum alone cultures at 4h and 24h for location-wise comparisons highlighted location-dependent clustering of LCMS data (**Figure 5.2**). A biological outlier was identified in the distal integrated samples.

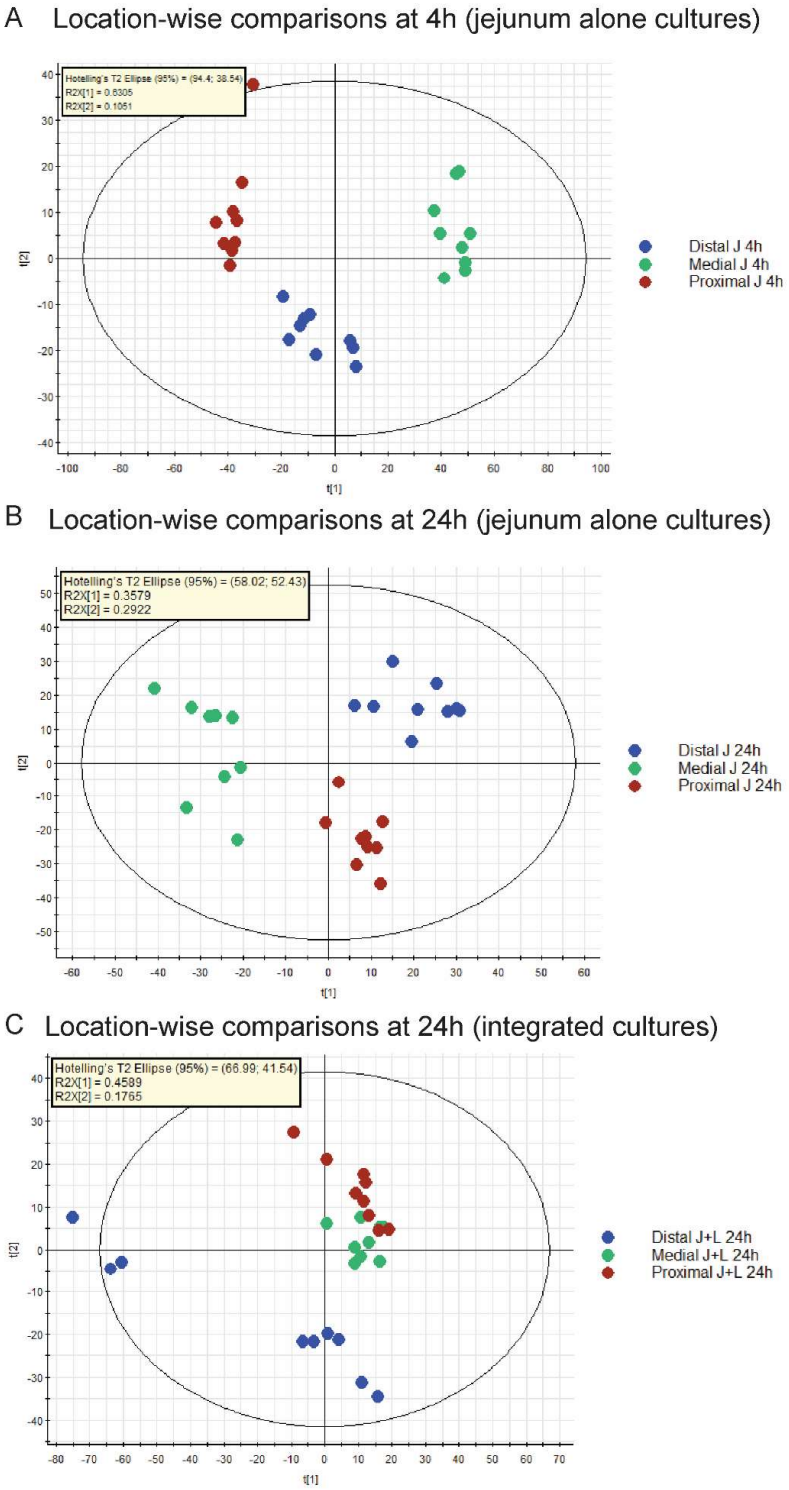

Figure 5.2: PCA of jejunum alone cultures at (A) 4h and (B) 24h, and (C) integrated cultures.

Expectedly, PCA of CS alone and jejunum alone cultures revealed that CS alone cultures grouped separately (**Figure 5.3**).

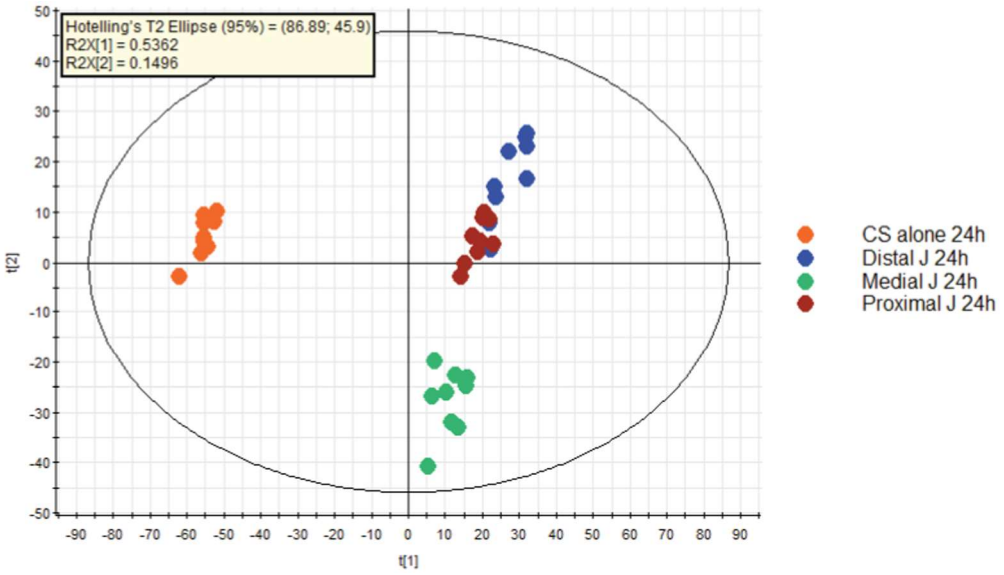

Figure 5.3: PCA of CS alone and jejunum alone cultures.

PCA of comparisons between jejunum alone cultures from proximal, medial and distal jejunum at 4h and 24h time-points revealed greater intergroup variability between 4h and 24h (principal component 1, x-axis) compared to within a given experimental group (principal component 2, y-axis) (**Figure 5.4**).

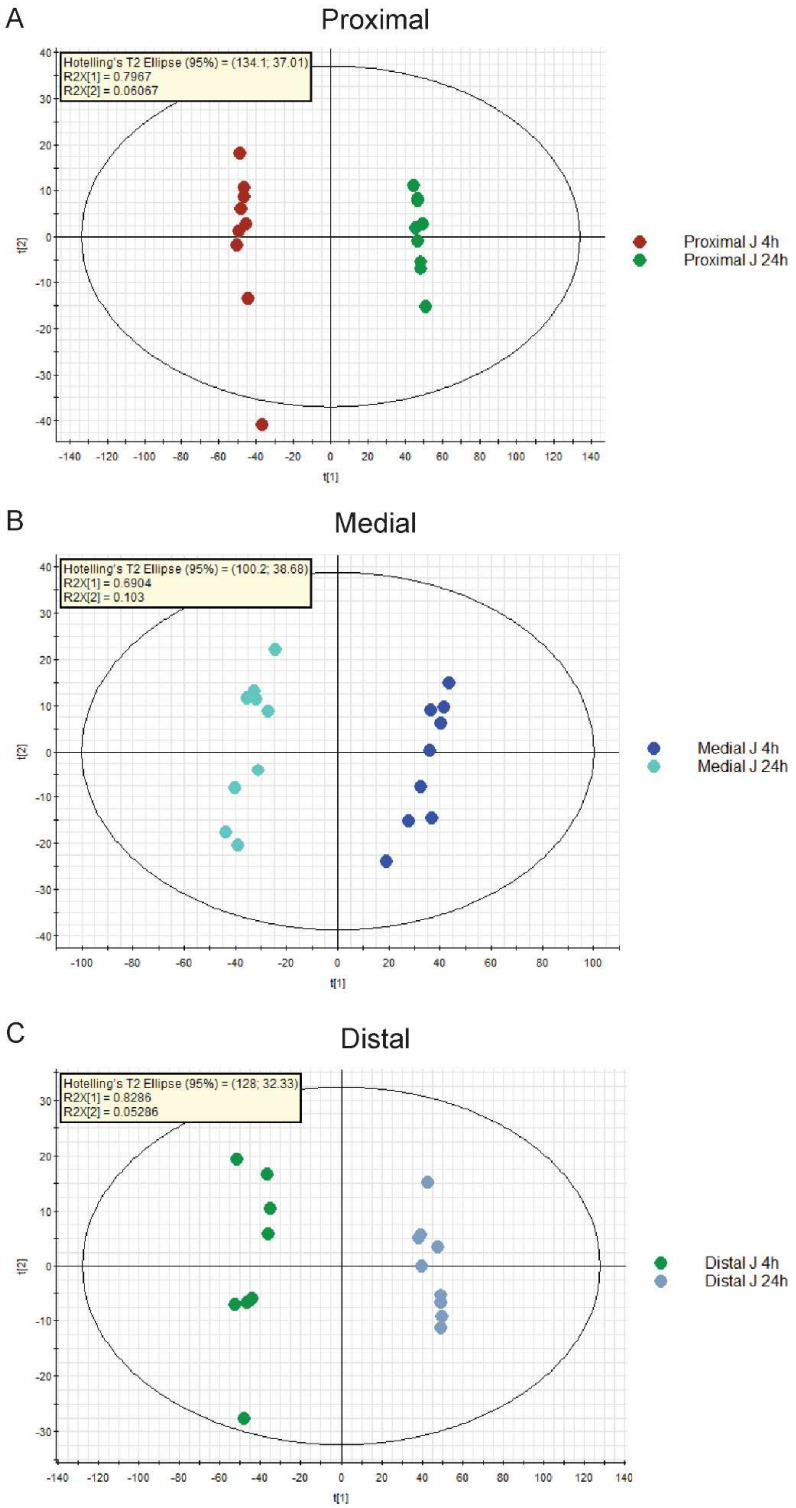

Figure 5.4: PCA of jejunum alone cultures from the (A) proximal, (B) medial, and (C) distal jejunum at 4h and 24h.

Similarly, PCA of comparisons between jejunum alone and integrated cultures from proximal, medial and distal jejunum revealed greater intergroup variability between jejunum alone and integrated cultures (principal component 1, x-axis) compared to within a given experimental group (principal component 2, y-axis) (**Figure 5.5**).

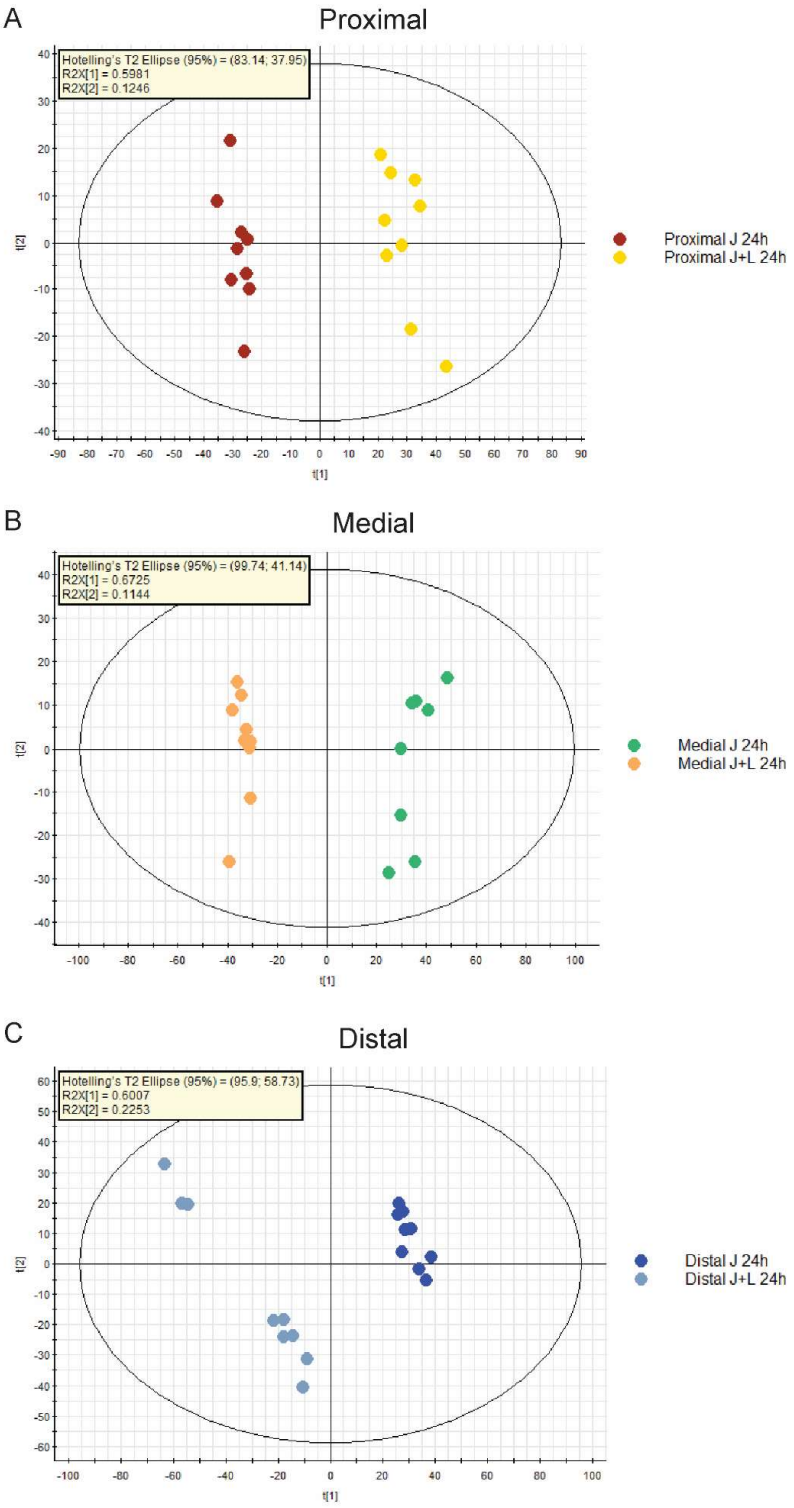

Figure 5.5: PCA of jejunum alone and integrated cultures with (A) proximal, (B) medial and (C) distal jejunum explants.

5.4.3 Annotation of features

Metabolite identification was performed on selected features in the negative ion mode. A sample metabolite identification process is shown in **Figure 5.6** using m/z 614.3455. In **Figure 5.6A**, the extracted ion chromatogram of the selected m/z shows the relevant peak (marked with an arrow). The corresponding mass spectrum is seen in **Figure 5.6B**, where the parent m/z has been identified as the 614 peak. Upon addition of fragmentation energy, the parent mass peak decreases in intensity in **Figure 5.6C**, while the fragments such as 554 increase in intensity. Using the fragmentation pattern and parent mass, metabolites are annotated. In this example, lipid maps was used to identify the metabolite as an LPC (22:5). Two possible structures for the compound are shown in **Figures 5.6D**.

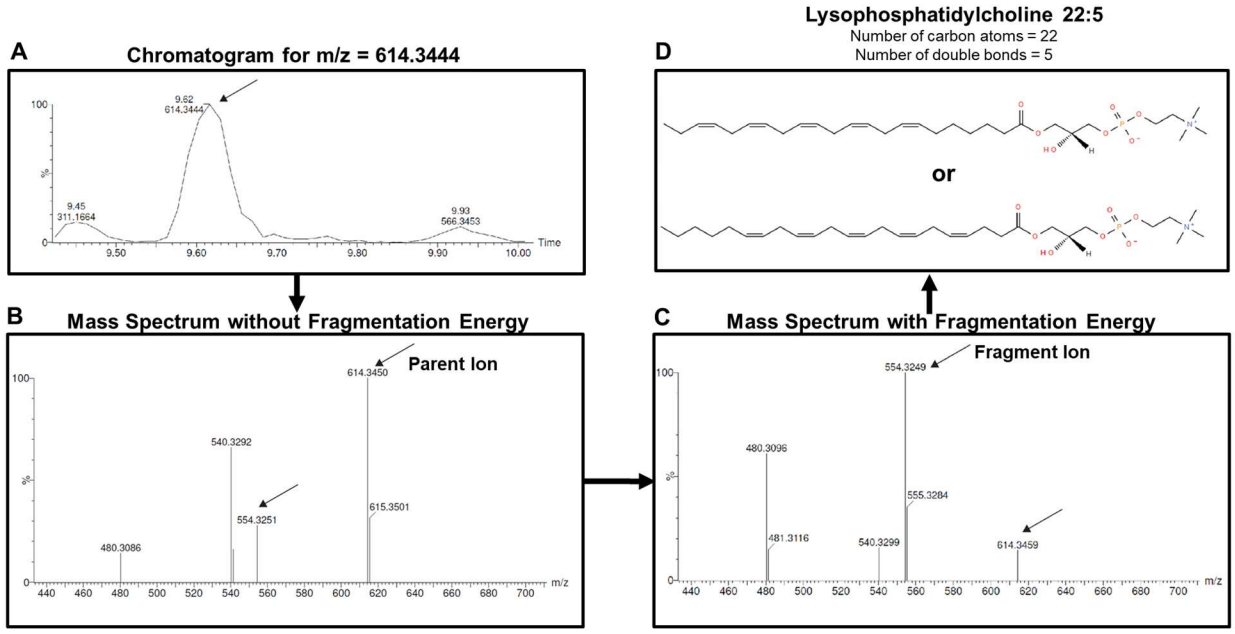

Figure 5.6: Feature annotation example. (A) Extracted ion chromatogram of m/z = 614.3455, (B) Mass spectrum of the chosen peak without fragmentation, (C) Mass spectrum with fragmentation, and (D) chemical structures of possible matched compounds (source: Lipid Maps).

Following this method, different metabolites were identified in the negative ion mode. In **Table 5.2**, identified metabolites have been organized according to the source of the metabolite among the following three categories: (1) unconditioned media; (2) jejunum; and (3) hepatocytes.

Table 5.2: List of sources of metabolites matched in media controls and cultures with jejunum or hepatocytes.

No.	Metabolite	Features (EMRT)	Adduct	Fresh Media	Jejunum	Hepatocytes
1	**Penicillin (methanolyzed)**	6.02_365.1163	M - H	✓		
2	**Phenylalanine**	3.09_164.0706	M - H	✓		
3	**Tryptophan**	3.40_203.0813	M - H	✓		
4	**Tyrosine**	1.82_180.0653	M - H			✓
5	**Pantothenic acid (Vitamin B_5)**	3.25_218.1023	M - H	✓		
6	**Hydrocortisone**	5.78_407.2062	M + formate	✓		
7	**Taurocholic acid/taurourso cholic acid/tauro-β-muricholic acid**	6.07_514.2832	M - H		✓	
8	**Taurosursodeo xycholic acid**	6.73_498.2881	M - H	✓	✓	
9	**LPC(16:0) (lysophosphati dylcholine)**	9.88_540.3293	M + formate	✓		
10	**LPC(20:4) (lysophosphati dylcholine)**	9.39_588.3294	M + formate	✓		
11	**LPC(22:5) (lysophosphati dylcholine)**	9.61_614.3455	M + formate	✓		
12	**Arachidonic acid (AA)**	11.92_303.2313	M - H		✓	
13	**5,8,12-trihydroxy-9-octadecenoic acid**	6.66_329.2313	M - H		✓	
14	**Docosahexaen oic acid (DHA; 22:6 n-3)**	11.72_327.2316	M - H		✓	
15	**FA(23:6(Ke2,Ep ,cyclo))**	12.78_381.1725	M - H		✓	

16	**6-Hydroxy-3-oxotetradecenoic acid**	9.33_277.1431	M + Na - 2H		✓	✓

5.4.4 Known media components identified

5.4.4.1 Antibiotics

The EMRT 6.02 min/365.1163 m/z was identified as **Penicillin (methanolyzed)**. This identity has been assigned by another group previously (320). Penicillin was one of the antibiotics present in the culture media used. The peak areas of this metabolite were significantly lower than the fresh media (24h) control in proximal jejunum alone (24h) and integrated cultures ($p < 0.05$) (a.u. means arbitrary units) (**Figure 5.7**). However, these peak areas only differed by 16-19% compared to the fresh media control. **Table 5.3** at the end of the **Results** section lists the legends for each symbol used to denote statistical significance.

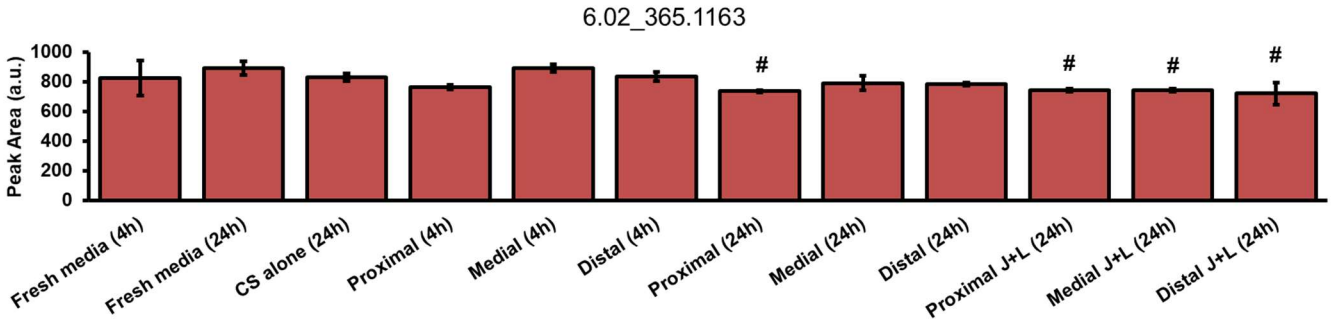

Figure 5.7: Peak areas for the EMRT 6.02 min / 365.1163 m/z (Penicillin)

5.4.4.2 Amino acids

The EMRT 1.82 min/180.0653 m/z was identified as **tyrosine** using Metlin. In the phenol red-free DMEM used in this study, L-tyrosine was present at a concentration of 104 mg/L. Interestingly, tyrosine present in DMEM was below the limit of detection in the fresh media controls (**Figure 5.8**). However, cultures with hepatocytes in them - CS alone and integrated cultures – had significantly higher detectable levels of tyrosine. Synthesis of tyrosine by hepatocytes could

explain its presence in CS containing cultures even though it is not detected in the fresh media (321, 322).

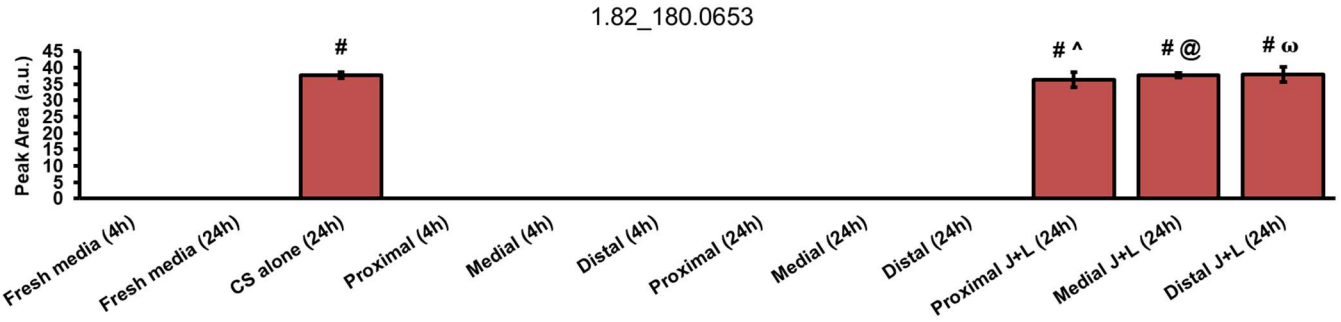

Figure 5.8: Peak areas for the EMRT 1.82 min / 180.0653 m/z (Tyrosine)

Additionally, the EMRT 3.09 min/164.0706 m/z was identified as **phenylalanine** using Metlin. L-phenylalanine is also present in the DMEM used at a concentration of 66 mg/L. The peak area for this amino acid in CS alone cultures was 42% higher than the fresh media (24h) control (**Figure 5.9**). The peak area also increased significantly in medial and distal jejunum alone cultures at 24h by 40% and 35%, respectively. Proximal, medial and distal integrated cultures also showed increases of 61%, 65% and 67% compared to the fresh media control, respectively.

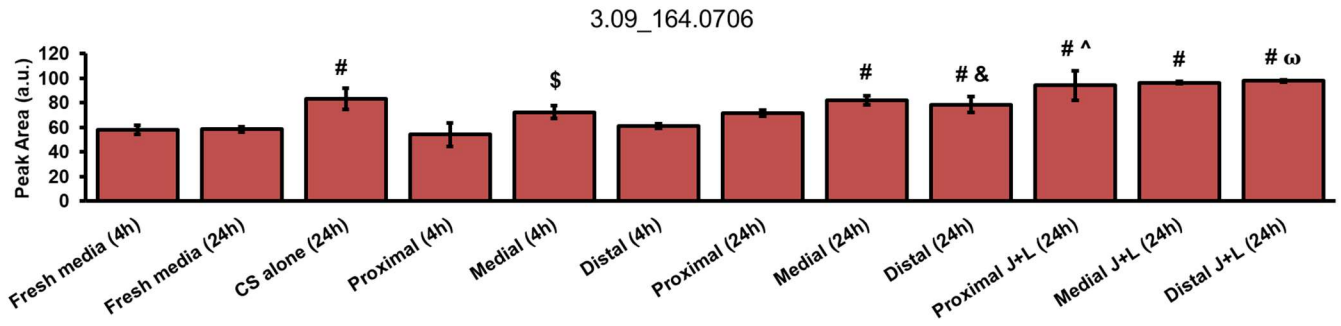

Figure 5.9: Peak areas for the EMRT 3.09 min / 164.0706 m/z (Phenylalanine)

The EMRT 3.40 min/203.0813 m/z was assigned to **tryptophan** using Metlin. L-tryptophan was present in the DMEM at a concentration of 16 mg/L. In the present analysis, while some statistically significant changes in peak areas were observed, many of these changes were not numerically very large (< 20%) (**Figure 5.10**). The peak areas for medial jejunum alone cultures

were higher than proximal cultures by 37% and 30% at 4h and 24h, respectively (p < 0.05). However, a significant change was not observed between proximal and distal jejunum at these time-points.

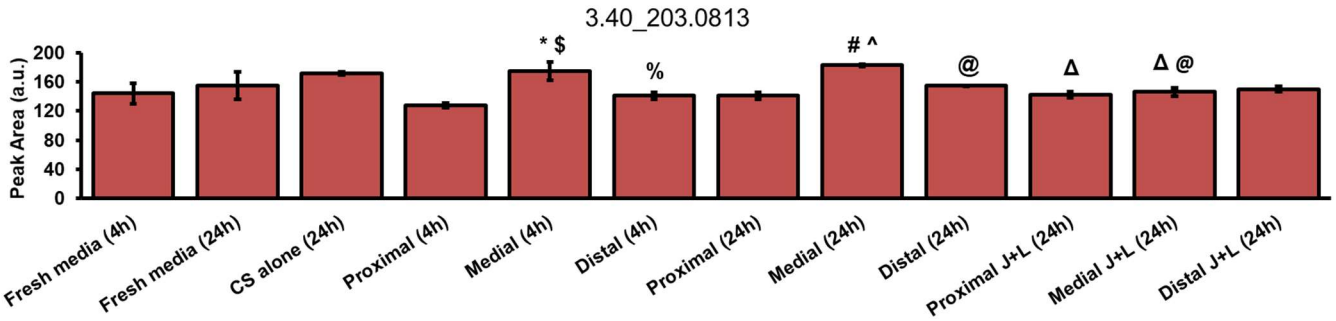

Figure 5.10: Peak areas for the EMRT 3.40 min / 203.0813 m/z (Tryptophan)

5.4.4.3 Vitamin B_5

The EMRT 3.25 min/ 218.1023 m/z was matched to **Pantothenic acid (Vitamin B_5)** using Metlin. Panthothenic acid is a known component of the DMEM used, present at a concentration of 4 mg/L. Similar to the trends with tryptophan, while some statistically significant changes were observed in the comparisons made, these were not numerically very large (**Figure 5.11**).

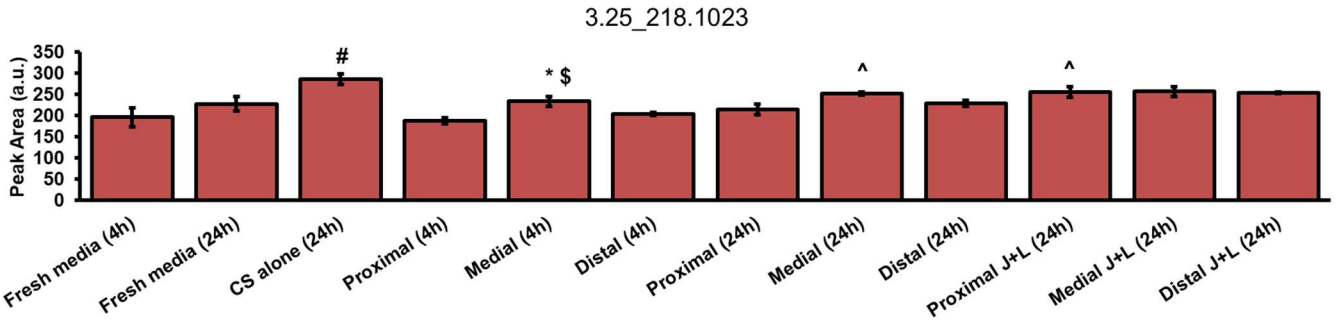

Figure 5.11: Peak areas for the EMRT 3.25 min / 218.1023 m/z (Vitamin B_5)

5.4.4.4 Hydrocortisone

The EMRT 5.78 min / 407.2062 m/z was assigned to **hydrocortisone (cortisol)**, another media component (present at a concentration of 7.65 mg/L), using HMDB. The concentrations of hydrocortisone in the spent culture media from jejunum alone cultures at both 4h and 24h were significantly higher than the respective unconditioned media controls (p < 0.05) (**Figure 5.12**).

Compared to the unconditioned media controls, the peak areas increased by 60%, 85% and 74% in proximal, medial and distal jejunum alone at 4h and by 52%, 64% and 62% in proximal, medial and distal jejunum at 24h, respectively ($p < 0.05$). In the CS alone cultures, the hydrocortisone levels decreased only by 17% ($p > 0.05$). Interestingly, in the integrated cultures from all three jejunum locations, the hydrocortisone concentrations decreased drastically compared to the media control and the respective jejunum alone groups ($p < 0.05$). The peak areas decreased by 16-, 5- and 3-fold in proximal, medial and distal integrated cultures compared to the unconditioned media control at 24h ($p < 0.05$). This suggests metabolism of hydrocortisone in integrated cultures.

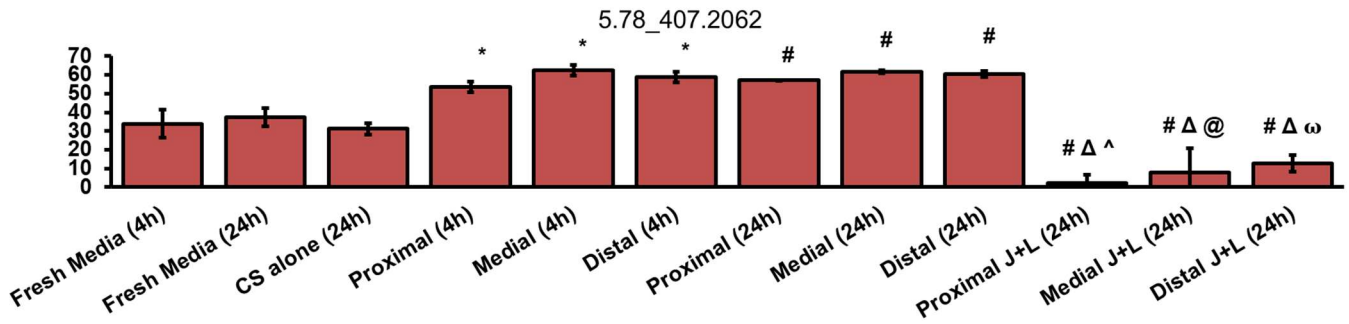

Figure 5.12: Peak areas for the EMRT 5.78 min / 407.2062 m/z (Hydrocortisone)

5.4.5 Bile acids identified

The exact mass/retention time (EMRT) pair 6.07 min/514.2832 m/z was annotated as one of the taurine-conjugated bile acids **taurocholic acid** or **tauroursocholic acid** or **tauro-β-murocholic acid** using the HMDB. This bile acid was absent in the fresh media but increased significantly in the proximal and medial jejunum alone cultures at 4h ($p < 0.05$ for both) (**Figure 5.13**). A spatial variation was observed with the distal jejunum exhibiting ~8-fold lower concentration compared to proximal and medial jejunum at 4h ($p < 0.05$ for both). A similar effect of location was also seen at 24h between proximal and distal jejunum. The peak areas also decreased significantly from 4h to 24h time-points in the proximal and medial jejunum ($p < 0.05$).

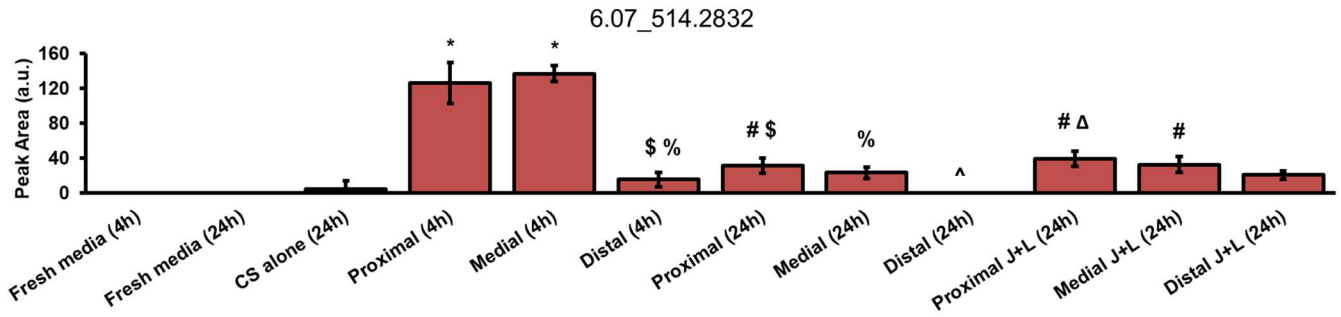

Figure 5.13: Peak areas for the EMRT 6.07 min / 514.2832 m/z (Taurine-conjugated cholic acids)

Another bile acid corresponding to the EMRT 6.73 min/498.2881 m/z was identified as **tauroursodeoxycholic acid** using Metlin. This bile acid was also present in the fresh media controls at 4h and 24h (**Figure 5.14**). In the fresh media, the source of this bile acid would be FBS. The peak area increased significantly in jejunum cultures at 4h compared to the corresponding fresh media control ($p < 0.05$).

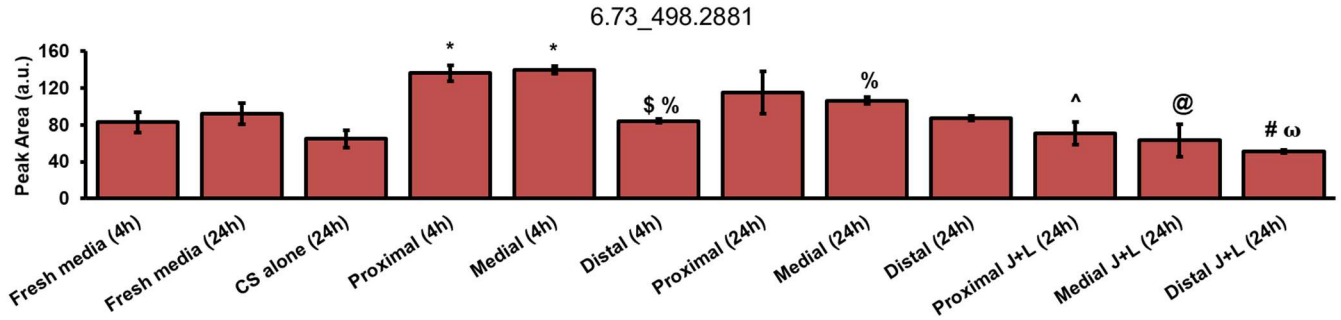

Figure 5.14: Peak areas for the EMRT 6.73 min / 498.2881 m/z (Tauroursodeoxycholic acid)

5.4.6 Lysophosphatidylcholines identified

Three lysophosphatidylcholines were identified using Metlin and Lipid Maps databases. All three were also present in the media, the only possible source being fetal bovine serum. However, the three FBS-derived LPCs were found to be metabolized in culture. The EMRT 9.39 min/588.3294 m/z was identified to be **LPC 20:4**. The peak area for this LPC decreased significantly in proximal,

medial and distal jejunum cultures at 4h compared to the corresponding fresh media control (p < 0.05) (**Figure 5.15**).

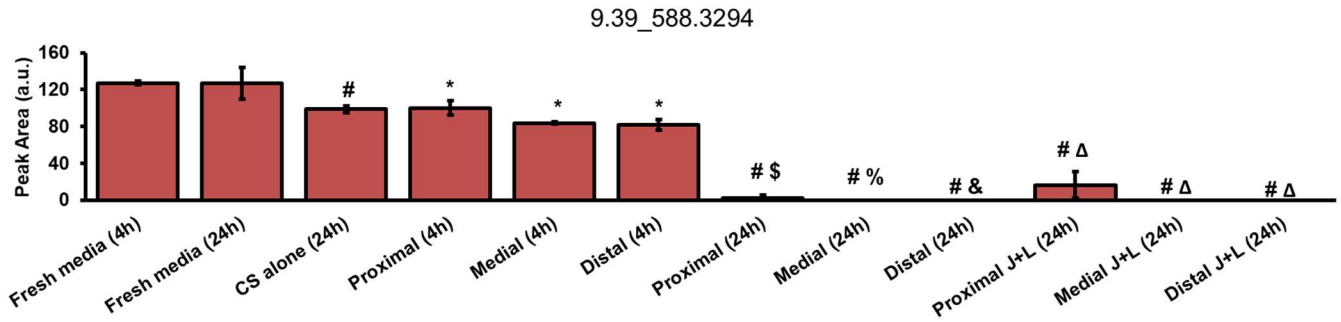

Figure 5.15: Peak areas for the EMRT 9.39 min / 588.3294 m/z (LPC (20:4))

The EMRT 9.88 min/540.3293 m/z was identified as **LPC (16:0)**. The peak area for this LPC decreased significantly in distal jejunum alone and integrated cultures at 24h (p < 0.05; 2.9-fold lower in distal jejunum compared to proximal at 24h; 2.2-fold lower in distal integrated compared to proximal integrated) (**Figure 5.16**). This hints at a location-dependent variation in the metabolism of this LPC by the jejunum.

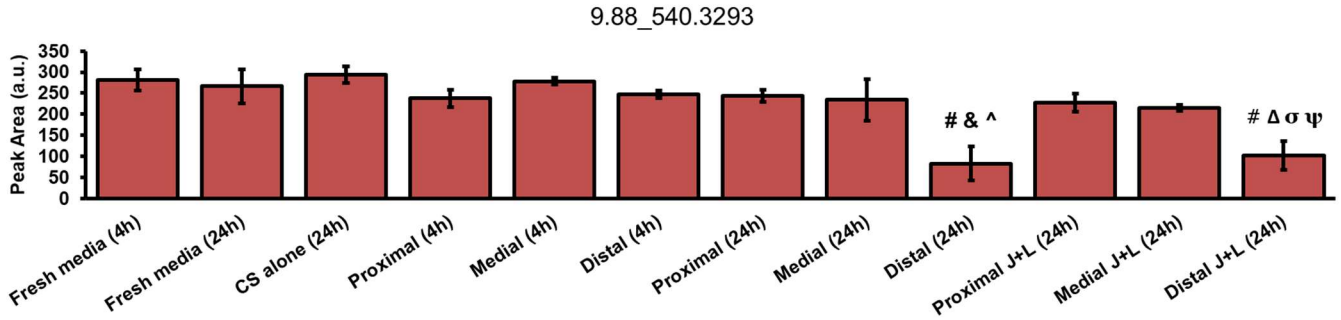

Figure 5.16: Peak areas for the EMRT 9.88 min / 540.3293 m/z (LPC (16:4))

The EMRT 9.61 min/614.3455 m/z was identified as **LPC (22:5)**. LPC (22:5), also present in the fresh media, decreased significantly to levels below the limit of detection in all cultures with jejunum explants at the 24h time-point (p < 0.05) (**Figure 5.17**). This indicates metabolism of the LPC by the jejunum. The peak area for LPC (22:5) also decreased significantly by 24 % in CS

alone cultures compared to the unconditioned media control (p < 0.05), suggesting that hepatocytes may also metabolize this LPC.

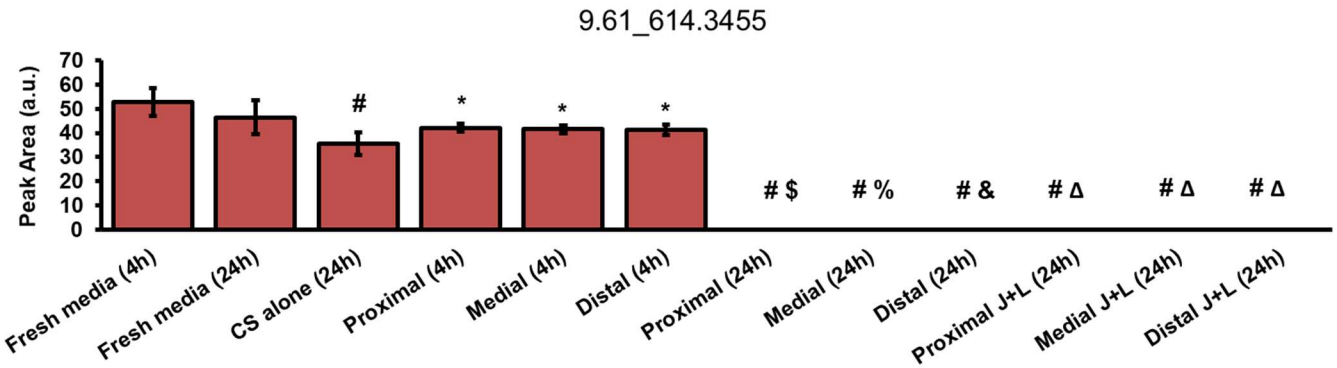

Figure 5.17: Peak areas for the EMRT 9.61 min / 614.3455 m/z (LPC (22:5))

5.4.7 Fatty acids identified

Several fatty acids were also identified in the negative ion mode. These were absent in the fresh media or hepatocyte only cultures but were detected in cultures with jejunum explants. The EMRT 11.92 min/303.2313 m/z was **Arachidonic acid** (AA), assigned using the Metlin database. The peak area increased significantly from proximal to distal jejunum at 4h (p < 0.05) (**Figure 5.18**). The peak areas also increased significantly from 4h to 24h for all 3 jejunum locations (p < 0.05; 3.8-fold and 2.3-fold for medial and distal jejunum, respectively).

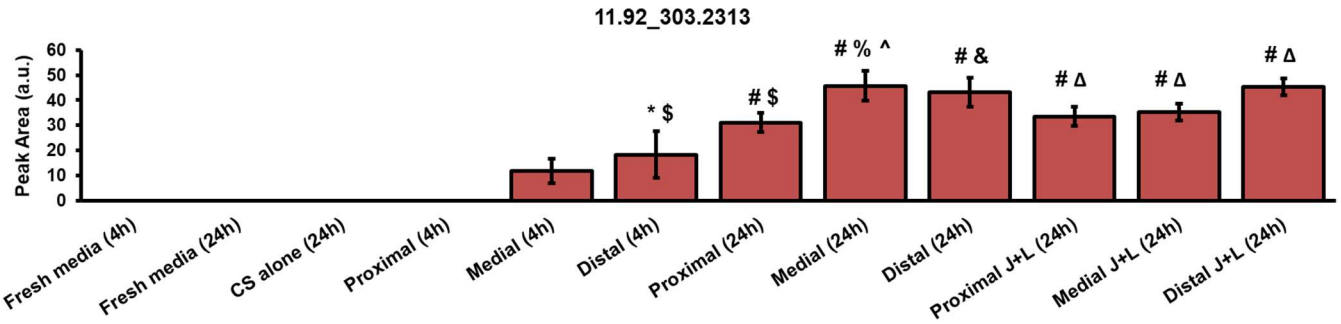

Figure 5.18: Peak areas for the EMRT 11.92 min / 303.2313 m/z (Arachidonic acid)

The EMRT 6.66 min/329.2313 m/z was identified as **5,8,12-trihydroxy-9-octadecenoic acid** using HMDB and Metlin databases. This metabolite was not detected in jejunum cultures at 4h

but increased significantly to detectable levels at 24h (**Figure 5.19**). Moreover, a spatial trend was observed for this metabolite in integrated cultures, where the peak area for medial and distal integrated cultures were 2.5- and 3.3-fold higher than proximal integrated cultures, respectively ($p < 0.05$).

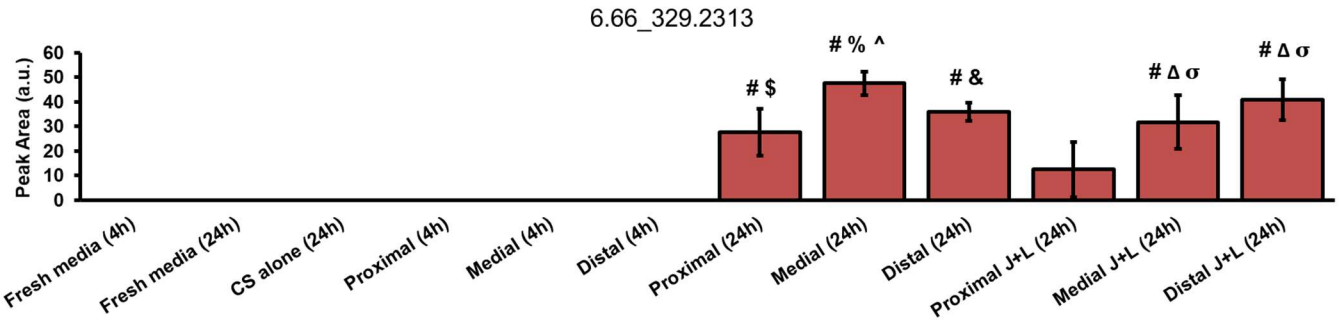

Figure 5.19: Peak areas for the EMRT 6.66 min / 329.2313 m/z (5,8,12-Trihydroxy-9-octadecenoic acid)

The EMRT 11.72 min/327.2316 m/z was identified as **docosahexaenoic acid** (DHA) using Metlin and Lipid Maps. While DHA was below the limit of detection in the jejunum cultures at 4h, it was significantly higher at the 24h time-point ($p < 0.05$) (**Figure 5.20**). Further, a spatial trend was observed in integrated cultures where the peak area for distal integrated cultures was 39% higher than the proximal integrated cultures ($p < 0.05$).

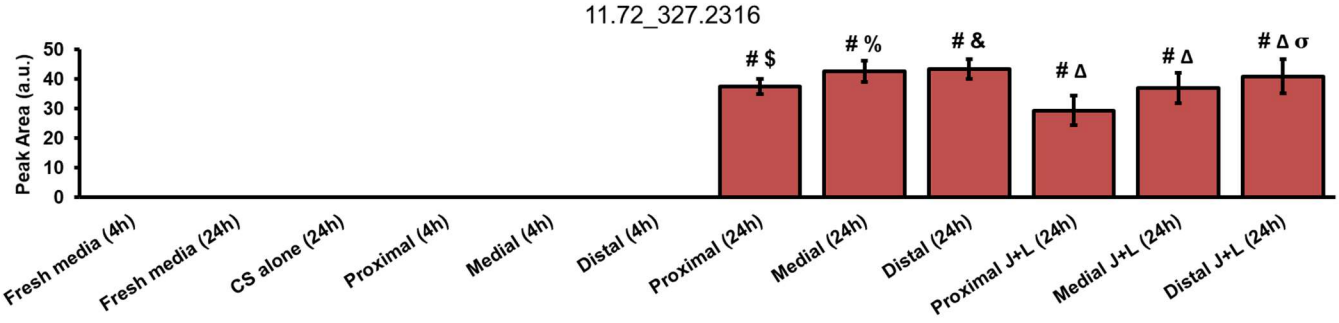

Figure 5.20: Peak areas for the EMRT 11.72 min / 327.2316 m/z (Docosahexaenoic acid)

The EMRT 12.78 min/381.1725 m/z was matched to a fatty acid **FA(23:6(Ke2,Ep,cyclo))** (Ke – keto, Ep – epoxy) using the Metlin and Lipid Maps databases. It was detected at very low levels in the fresh media controls, CS alone cultures and jejunum cultures at 4h (**Figure 5.21**). However, the peak areas for this metabolite increased significantly in the jejunum-containing cultures at 24h compared to the fresh media control ($p < 0.05$). Similarly, the peak areas for proximal, medial and jejunum alone cultures at 24h were respectively 14-, 5- and 8-fold higher than at 4h ($p < 0.05$).

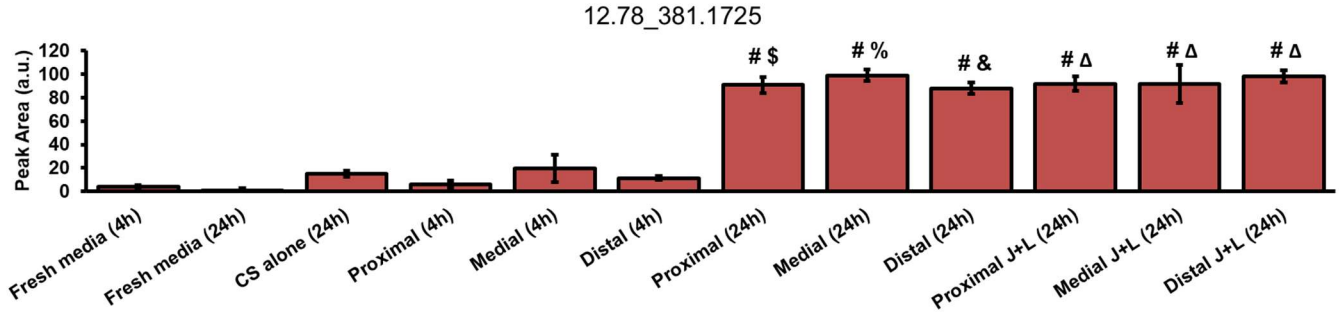

Figure 5.21: Peak areas for the EMRT 12.78 min / 381.1725 m/z (FA(23:6(Ke2,Ep,cyclo)))

The EMRT 9.33 min/277.1431 m/z was matched to the fatty acid **6-hydroxy-3-oxotetradecenoic acid** using HMDB. This fatty acid was not detected in the unconditioned media (**Figure 5.22**). There was a significant increase in the peak area in CS alone cultures, hinting at hepatocyte synthesis of this fatty acid ($p < 0.05$). Jejunum alone cultures also had significantly higher amounts of the fatty acid at both 4h and 24h compared to the respective media controls ($p < 0.05$). Compared to 4h, the peak areas at 24h increased by 2.2-fold in proximal alone cultures, and by 45% and 78% in medial and distal jejunum alone cultures, respectively ($p < 0.05$).

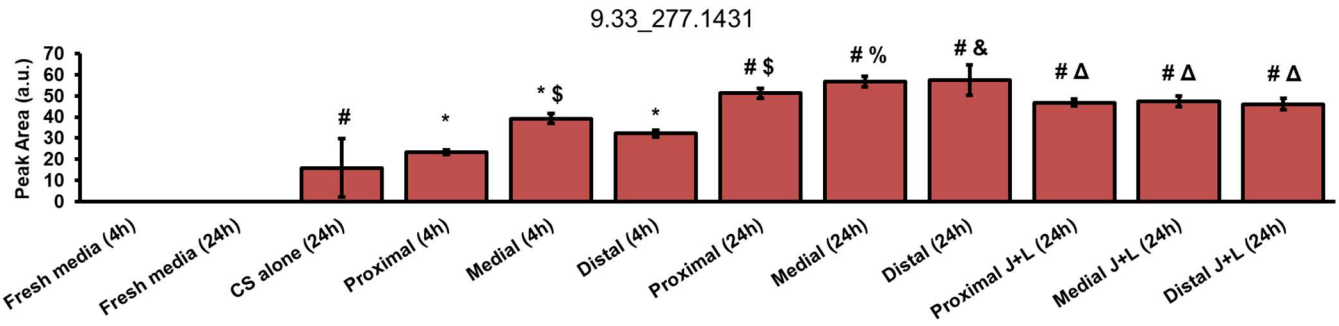

Figure 5.22: Peak areas for the EMRT 9.33 min / 277.1431 m/z (6-Hydroxy-3-oxotetradecenoic acid)

Table 5.3: Legend for statistical comparisons

Symbol	Statistical significance ($p < 0.05$) relative to
*	Fresh media (4h)
#	Fresh media (24h)
$	Proximal Jejunum alone (4h)
%	Medial Jejunum alone (4h)
&	Distal Jejunum alone (4h)
^	Proximal Jejunum alone (24h)
@	Medial Jejunum alone (24h)
ω	Distal Jejunum alone (24h)
Δ	CS alone (24h)
σ	Proximal Integrated (24h)
ψ	Medial Integrated (24h)

5.5 Discussion and Conclusions

The present study describes an investigation of intestinal metabolites using culture media exposed to jejunum explants *in vitro*. The data processed in the negative ion mode helped in identification of several amino acids and lipids in the cultures. The identities assigned to the selected metabolites in the current study fall under level 2 of metabolite identification (323).

Amino acids such as tyrosine, phenylalanine and tryptophan were identified in the media samples. The identities matched other reports of amino acids (170). Although these amino acids are present in the DMEM used for the cultures, tyrosine was below the levels of detection in fresh media controls. However, the increased tyrosine levels in hepatocyte-containing cultures including CS alone and integrated cultures could possibly be due to hepatocyte-mediated tyrosine

synthesis triggered by increased phenylalanine levels in these cultures (321, 322, 324). Since phenylalanine is an essential amino acid that has to be sourced through diet, the increase in phenylalanine in the CS alone and integrated cultures could be a result of protein catabolism (322).

In an LCMS study using cell culture media from *in vitro* using 3D liver models with primary human hepatocytes and Kupffer cells, it was found that 70% of the hydrocortisone added at physiological levels was metabolized by phase II enzymes within 48h of administration (325). Phase II metabolism of hydrocortisone by the enzymes expressed in both the jejunum and hepatocytes together could have caused the decrease in hydrocortisone concentrations in integrated cultures (326). The hydrocortisone observed in jejunum alone cultures could be sourced from bile (327).

Several lipids were also identified in the samples tested. LPCs and tauroursodeoxycholic acid found in fresh media most likely originated from the FBS added. Although a detailed lipid composition analysis of fetal bovine serum was not found, different studies have reported presence of bile acids, fatty acids, phospholipids including LPCs have also been detected in fetal bovine serum (165, 328-336).

Lipids in the intestine are either dietary or sourced from bile or cells shed from the intestinal epithelium (180). Different groups have reported the identification of taurine-conjugated bile acids in the negative ion mode (165, 170). Taurine-conjugated bile acids have been reported to be present in higher quantities in the small intestine compared to the large intestine (170). A similar trend of decreased taurocholic acid in the distal jejunum was observed in the present study.

LPCs are present in both rat and human small intestinal luminal contents (337). The intestinal epithelial cells express LPC-metabolizing enzymes that metabolize them to phosphocholine (PC) and free fatty acids (FAs) such as oleic acid (338). Phospholipase B or lysophospholipase activity detected in the rat small intestine was the most prominent in distal jejunum and the proximal two-

thirds of the ileum (339). In the present study, it was observed that LPCs found in the media were metabolized to levels below the limit of detection when jejunum explants were present. Out of the 3 LPCs identified, LPC (16:0) was present in significantly lower amounts in cultures with the distal jejunum, which could be due to increased lysophospholipase activity in the distal jejunum as reported *in vivo*.

AA and DHA found in intestinal cultures could be synthesized from linoleic and linolenic acids found in FBS, respectively (330, 340, 341). AA is a polyunsaturated omega-6 fatty acid (PUFA) (20:4) present in phospholipids (342). It can be synthesized from linoleic acid or through phospholipase A_2-mediated breakdown of phosphatidylcholines (PCs) (342, 343). DHA is an omega-3 PUFA (22:6), either sourced through diet, or synthesized from alpha-linolenic acid. Yuan *et al* (170) recently identified both AA and DHA in their study on the baboon intestine. DHA concentrations were reported to be higher in the distal regions of the gastrointestinal tract in this study (170). The significant increase in DHA concentrations in the distal integrated cultures observed in the present study is similar to the trend observed *in vivo* (170). The breakdown of LPC (20:4) by lysophospholipase would result in the release of free AA (20:4) (338). In our study, we observe both a decrease in the concentration of LPC (20:4) at 4h and 24h, and a corresponding increase in the concentration of AA in the culture media, which hints at lysophospholipase-mediated breakdown of LPC (20:4) and the corresponding release of AA. On the other hand, the activity of phospholipid-metabolizing enzyme phospholipase A (PLA) varies along the length of the intestine *in vivo* (344, 345). In the rat intestine, the PLA activity increases 3-fold from the duodenum to the ileum (344). Another study reported a 10-fold increase in PLA activity from the duodenum to the ileum in rats (345). PLA_2 activity results in the formation of AA from phospholipids (342). This may be another possible reason for the spatial trends observed from proximal to distal jejunum in the AA levels reported in the present study. The higher AA levels are also linked to an increased pro-inflammatory response (346, 347). The downstream fate of

AA is the synthesis of immunomodulatory eicosanoids such as prostaglandins and leukotrienes (346, 347).

Overall, we were able to identify several classes of lipophilic molecules that were either secreted or metabolized in culture. Spatial, temporal as well as culture-dependent trends were observed in the amounts of different amino acids, bile acids, LPCs and fatty acids. Moreover, the spatial trends in bile acid, LPC and fatty acid metabolism corroborated with *in vivo* reports of lipid metabolism in the intestine.

5.6 Future Work

Overall, this study revealed further spatiotemporal trends within the jejunum *in vitro* that may be correlated to bile acid and fatty acid metabolism pathways in the intestine. The work presented in this chapter can be extended in several ways to further the understanding of lipid and amino acid metabolism pathways in the intestine and hepatocytes *in vitro*. The first step forward would entail targeted and hypothesis-driven work to confirm the identities of the different compounds identified in this study using commercially available standards and running a tandem MS/MS. Fully labeled DMEM kits such as BioExpress® DMEM could be used to incorporate labeled atoms into the metabolites to further help identify metabolites. It would be interesting to elucidate the role of arachidonic acid and its derivative metabolites in the jejunum cultures. The study would benefit from more in-depth investigations to further detect any metabolites from LPC breakdown to validate the hypothesis of spatial differences in lysophospholipase activity leading to differences in LPC levels. Lysophospholipase activity measurements using commercially available ELISA kits on jejunum explant lysates would provide further insight into the metabolism of LPCs by the intestine. A more extensive investigation of the pathways involved would also provide further useful insights into the spatiotemporal trends in the jejunum cultured with and without hepatocytes. Effects of ethanol on the lipids in the metabolome of the spent culture media should

also be investigated as *in vivo* studies have shown ethanol-dependent effects of luminal metabolites (348).

Chapter 6: Conclusion

The research presented in this dissertation focused on the use of rat jejunum explants to perform a range of studies including investigations of spatiotemporal trends in the markers of intestinal function, ethanol toxicity, and secretion and/or metabolism of lipophilic metabolites in *in vitro* cultures of the jejunum and hepatocytes.

In Chapter 2, a method to isolate and culture inverted jejunum explants was described. In Chapter 3, the results from cultures of inverted jejunum explants from different regions of the jejunum were reported. Jejunum explants were cultured for up to 72h. Markers of enterocyte, goblet cell and Paneth cell function in the jejunum were maintained over 24h in culture and followed *in vivo* – like spatial trends reported for the entire small intestine. For the proximal and medial regions of the jejunum, lysozyme activity and mucin area were maintained even after 72h in culture, even though a decline in ALP activity was observed. Jejunum explants were also integrated with hepatocytes to model the intestine-liver axis. Integration of jejunum explants from the proximal region with hepatocytes had a beneficial effect on both hepatocyte urea secretion and jejunum mucin secretion, hinting at communication between these organs in culture.

In Chapter 4, the integrated cultures of the rat jejunum and hepatocytes were used to investigate ethanol toxicity *in vitro*. The trends in biochemical markers such as jejunum and hepatocyte protein, and activities of ALP, ADH and lysozyme in integrated cultures with proximal jejunum explants corroborated with *in vivo* reports on ethanol toxicity. Moreover, the effects of ethanol on morphometric measures such as villus and mucin areas also corresponded to *in vivo* trends. Use of an integrated jejunum-hepatocyte model helped recapitulate the effects of ethanol toxicity observed *in vivo.*

In Chapter 5, various metabolites secreted and/or metabolized by the jejunum alone, hepatocytes alone and integrated cultures were detected and identified using LCMS. The focus of this study

was on lipophilic metabolites due to the increasing importance of lipid markers in investigating the small intestine in health and disease. Location-, time- and culture-dependent trends were observed for several identified metabolites. For example, synthesis of amino acids such as tyrosine was detected in hepatocyte-containing cultures. Similarly, metabolism of known media components such as hydrocortisone by integrated cultures of the jejunum and hepatocytes was observed. Lipid components of the unconditioned media such as LPCs were also metabolized by the tissues in culture. Fatty acids such as AA and DHA, which are important regulators of the intestinal inflammatory response, showed location-dependent trends in concentrations. Confirmatory results were also obtained for the metabolism of LPC (20:4) as a decrease in its concentration was accompanied by a corresponding increase in the concentration of its lysophospholipase product AA. A similar LCMS-based analysis on ethanol-treated samples could provide an insight into the effects of ethanol toxicity on lipid secretion and metabolism.

The overall purpose of integration of the jejunum and the hepatocytes was to take a step towards a holistic model of the intestine-liver axis to recapitulate its physiology and response to drug toxicity *in vitro.* Large-scale animal studies are conducted by and for pharmaceutical companies to investigate the toxicity of drugs and chemicals to the body. It is anticipated that use of holistic *in vitro* models of primary tissues and organs such as the integrated cultures described in this dissertation would help drastically reduce the number of animals required to test drug toxicity while providing *in vivo* – like results. The investigations reported in this dissertation may be extended to human tissues to provide more accurate models of drug toxicity and potentially eliminate the over-reliance on animal studies.

Chapter 7: Future Directions

The research proposed in this thesis can be expanded in future to several other projects.

The hepatocyte model used in the studies performed and proposed for this thesis is a 2D collagen sandwich model with hepatocytes only. While this is a good model for *in vitro* studies on the liver, it lacks the other cell types and the space of Disse architecture that are found in the liver *in vivo*. Integration of gut explants with 3D organotypic multicellular liver models that have been developed by the Rajagopalan group before would provide a more accurate liver mimic (168, 209, 250). In addition to hepatocytes, these models also incorporate non-parenchymal cells such as LSECs, KCs and HSCs in a 3D culture environment.

Incorporation of flow in the cultures would be an important addition to the research pursued in this thesis. To implement this, explants from the jejunum and 2D or 3D liver models could be cultured in different wells and different flows can be applied to each culture system. Peristaltic flow would be beneficial for intestinal culture as it would mimic the *in vivo* environment (251), whereas laminar flow would be used for hepatocyte/liver culture. A bidirectional flow of media, and thus nutrients and metabolites, would be established between the two organs being cultured. It is expected that such a dynamic multi-organ culture system would more accurately mimic the enterohepatic circulation that occurs *in vivo*.

In the studies conducted as part of this dissertation, the jejunum has been used because of its importance in nutrient and drug absorption and metabolism. The study would benefit from an expansion into the ileum as well, particularly if an *in vitro* model of an inflamed gut-liver axis is to be studied. This is because the ileum has Peyer's patches that are involved in mediating immune response.

The integrated *in vitro* gut-liver system developed in the research presented so far can also be expanded to mimic the gut-liver-brain axis *in vitro* as the gut-liver axis affects the brain in several

important ways. Astrocytes and neuronal cells may be incorporated in such a system. Conditioned media obtained from gut-liver cultures could be used to treat a co-culture of astrocytes and neurons and changes in specific astrocytic and neuronal functions can be assessed.

The effect of explant size on spatiotemporal trends and effects of ethanol may be studied. Such a study would help understand the scale of spatiotemporal variation in the intestine. The high standard deviations observed for some data presented in this dissertation may be due to slight variations in explant size. A size-based study would also help understand the variations in data.

Effects of ethanol on other cell types of the intestine such as enteroendocrine cells, stem cells, the neurons of the enteric nervous system and smooth muscle cells could also be investigated *in vitro*. Neurotransmitters such as nitric oxide, dopamine, serotonin and epinephrine are known to be important in maintaining gut homeostasis (210). Ethanol can lead to an increased production of intestinal nitric oxide which results in altered gut motility (209). Further, these effects are known to be location-dependent (209). Synthesis and secretion of serotonin is affected by the gut microbiota (134, 349). It would be interesting to study the spatiotemporal and ethanol-dependent trends in the concentrations of these neurotransmitters *in vitro*.

Numerous trends observed in the data obtained from the research discussed in this dissertation may be affected by the presence of bacteria in the *in vitro* cultures. A detailed analysis of the bacteria present in the cultures may be conducted at different levels. Firstly, a detailed Gram staining analysis of the pellets obtained by centrifuging culture media samples at 10,000 x *g* could reveal the presence of intestinal bacteria in the culture media (350). A fluorescence *in situ* hybridization (FISH) study using the Eub338 probe (universal probe to identify bacteria) may be used to visualize bacteria trapped in the mucus barrier in cryosections (351). Quantification of LPS present in the media using a quantitative limulus amoebocyte lysate (LAL) assay could help delineate the role that LPS may be playing in these cultures with and without EtOH treatment in explants from different locations on the jejunum (352). The role of gut bacteria can further be

studied by performing 16s rRNA gene sequencing of mucosa-associated bacteria as well as the microbiota present in spent culture media (353).

References

1. Reinus, J.F., and Simon, D. Gastrointestinal anatomy and physiology: the essentials. Oxford, UK: John Wiley & Sons; 2014.

2. Reed, K.K., and Wickham, R. Review of the gastrointestinal tract: from macro to micro. Seminars in Oncology Nursing **25**, 3, 2009.

3. McCance, K., and Huether, S. Structure and function of the digestive system. Pathophysiology: The Biologic Basis for Disease in Adults and Children, 2nd ed Baltimore, Md, 1282, 1998.

4. Johnson, L.R., and Gerwin, T.A. Gastrointestinal physiology: Mosby Elsevier Philadelphia; 2007.

5. Treuting, P.M., Arends, M.J., and Dintzis, S.M. Upper Gastrointestinal Tract. Comparative Anatomy and Histology (Second Edition): Elsevier; 2017. pp. 191-211.

6. Gelberg, H.B. Comparative anatomy, physiology, and mechanisms of disease production of the esophagus, stomach, and small intestine. Toxicologic pathology **42**, 54, 2014.

7. Thummel, K.E., Kunze, K.L., and Shen, D.D. Enzyme-catalyzed processes of first-pass hepatic and intestinal drug extraction. Advanced Drug Delivery Reviews **27**, 99, 1997.

8. Kaminsky, L.S., and Zhang, Q.-Y. The small intestine as a xenobiotic-metabolizing organ. Drug metabolism and disposition **31**, 1520, 2003.

9. Rao, J.N., and Wang, J.-Y. Intestinal Architecture and Development. 2010.

10. Ding, X., and Kaminsky, L.S. Human extrahepatic cytochromes P450: function in xenobiotic metabolism and tissue-selective chemical toxicity in the respiratory and gastrointestinal tracts. Annual Review of Pharmacology and Toxicology **43**, 149, 2003.

11. Lin, J.H., Chiba, M., and Baillie, T.A. Is the role of the small intestine in first-pass metabolism overemphasized? Pharmacological Reviews **51**, 135, 1999.

12. Shidoji, Y., and Kim, S.H. Mutually distinctive gradients of three types of intestinal alkaline phosphatase along the longitudinal axis of the rat intestine. Digestion **70**, 10, 2004.

13. Brennan, P.C., McCullough, J.S., and Carr, K.E. Variations in cell and structure populations along the length of murine small intestine. Cells Tissues Organs **164**, 221, 1999.

14. Krause, W.J. Biology of the duodenal (Brunner's) glands. Ultrastructure of the Digestive Tract: Springer; 1988. pp. 67-84.

15. Isenberg, J.I., Wallin, B., Johansson, C., Smedfors, B., Mutt, V., Tatemoto, K., and Emas, S. Secretin, VIP, and PHI stimulate rat proximal duodenal surface epithelial bicarbonate secretion in vivo. Regulatory peptides **8**, 315, 1984.

16. Flemstrom, G., Heylings, J., and Garner, A. Gastric and duodenal HCO3-transport in vitro: effects of hormones and local transmitters. American Journal of Physiology: Gastrointestinal and Liver Physiology **242**, G100, 1982.

17. Iqbal, J., and Hussain, M.M. Intestinal lipid absorption. American Journal of Physiology: Endocrinology and Metabolism **296**, E1183, 2009.

18. Drozdzik, M., Busch, D., Lapczuk, J., Müller, J., Ostrowski, M., Kurzawski, M., and Oswald, S. Protein Abundance of Clinically Relevant Drug-Metabolizing Enzymes in the Human Liver and Intestine: A Comparative Analysis in Paired Tissue Specimens. Clinical Pharmacology & Therapeutics **104**, 515, 2018.

19. Collins, J.T., and Bhimji, S.S. Anatomy, Abdomen, Small Intestine. 2017.

20. Moll, R., and Davis, B. Iron, vitamin B12 and folate. Medicine **45**, 198, 2017.

21. Jung, C., Hugot, J.-P., and Barreau, F. Peyer's patches: the immune sensors of the intestine. International Journal of Inflammation **2010**2010.

22. Tortora, G.J., and Derrickson, B.H. Principles of anatomy and physiology: John Wiley & Sons; 2008.

23. Orbach, S.M., Less, R.R., Kothari, A., and Rajagopalan, P. In vitro intestinal and liver models for toxicity testing. ACS Biomaterials Science & Engineering **3**, 1898, 2017.

24. Umar, S. Intestinal stem cells. Current gastroenterology reports **12**, 340, 2010.

25. Gribble, F.M., and Reimann, F. Enteroendocrine cells: chemosensors in the intestinal epithelium. Annual Review of Physiology **78**, 277, 2016.

26. Clevers, H.C., and Bevins, C.L. Paneth cells: maestros of the small intestinal crypts. Annual Review of Physiology **75**, 289, 2013.

27. Van Der Flier, L.G., and Clevers, H. Stem cells, self-renewal, and differentiation in the intestinal epithelium. Annual Review of Physiology **71**, 241, 2009.

28. Crosnier, C., Stamataki, D., and Lewis, J. Organizing cell renewal in the intestine: stem cells, signals and combinatorial control. Nature Reviews Genetics **7**, 349, 2006.

29. Barker, N., van de Wetering, M., and Clevers, H. The intestinal stem cell. Genes & development **22**, 1856, 2008.

30. Artursson, P. Cell cultures as models for drug absorption across the intestinal mucosa. Crit Rev Ther Drug Carrier Syst **8**, 305, 1990.

31. Rocha, F.G., and Whang, E.E. Intestinal tissue engineering: from regenerative medicine to model systems. J Surg Res **120**, 320, 2004.

32. Ghaemmaghami, A.M., Hancock, M.J., Harrington, H., Kaji, H., and Khademhosseini, A. Biomimetic tissues on a chip for drug discovery. Drug Discov Today **17**, 173, 2012.

33. Artursson, P., and Borchardt, R.T. Intestinal drug absorption and metabolism in cell cultures: Caco-2 and beyond. Pharmaceutical Research **14**, 1655, 1997.

34. Chen, X.-M., Elisia, I., and Kitts, D.D. Defining conditions for the co-culture of Caco-2 and HT29-MTX cells using Taguchi design. Journal of pharmacological and toxicological methods **61**, 334, 2010.

35. Hubatsch, I., Ragnarsson, E.G., and Artursson, P. Determination of drug permeability and prediction of drug absorption in Caco-2 monolayers. Nature Protocols **2**, 2111, 2007.

36. Sambuy, Y., De Angelis, I., Ranaldi, G., Scarino, M., Stammati, A., and Zucco, F. The Caco-2 cell line as a model of the intestinal barrier: influence of cell and culture-related factors on Caco-2 cell functional characteristics. Cell Biology and Toxicology **21**, 1, 2005.

37. Walter, E., Janich, S., Roessler, B.J., Hilfinger, J.M., and Amidon, G.L. HT29-MTX/Caco-2 cocultures as an in vitro model for the intestinal epithelium: In vitro–in vivo correlation with permeability data from rats and humans. Journal of Pharmaceutical Science **85**, 1070, 1996.

38. Hidalgo, I.J., Raub, T.J., and Borchardt, R.T. Characterization of the human colon carcinoma cell line (Caco-2) as a model system for intestinal epithelial permeability. Gastroenterology **96**, 736, 1989.

39. Lesuffleur, T., Porchet, N., Aubert, J.-P., Swallow, D., Gum, J.R., Kim, Y.S., Real, F.X., and Zweibaum, A. Differential expression of the human mucin genes MUC1 to MUC5 in relation to growth and differentiation of different mucus-secreting HT-29 cell subpopulations. Journal of Cell Science **106**, 771, 1993.

40. Schweinlin, M., Wilhelm, S., Schwedhelm, I., Hansmann, J., Rietscher, R., Jurowich, C., Walles, H., and Metzger, M. Development of an Advanced Primary Human In Vitro Model of the Small Intestine. Tissue Engineering Part C Methods **22**, 873, 2016.

41. Prueksaritanont, T., Gorham, L.M., Hochman, J.H., Tran, L.O., and Vyas, K.P. Comparative studies of drug-metabolizing enzymes in dog, monkey, and human small intestines, and in Caco-2 cells. Drug metabolism and disposition **24**, 634, 1996.

42. Sato, T., Vries, R.G., Snippert, H.J., van de Wetering, M., Barker, N., Stange, D.E., van Es, J.H., Abo, A., Kujala, P., and Peters, P.J. Single Lgr5 stem cells build crypt villus structures in vitro without a mesenchymal niche. Nature **459**, 262, 2009.

43. Koo, B.-K., Stange, D.E., Sato, T., Karthaus, W., Farin, H.F., Huch, M., Van Es, J.H., and Clevers, H. Controlled gene expression in primary Lgr5 organoid cultures. Nature methods **9**, 81, 2012.

44. Gjorevski, N., Sachs, N., Manfrin, A., Giger, S., Bragina, M.E., Ordóñez-Morán, P., Clevers, H., and Lutolf, M.P. Designer matrices for intestinal stem cell and organoid culture. Nature **539**, 560, 2016.

45. Kuratnik, A., and Giardina, C. Intestinal organoids as tissue surrogates for toxicological and pharmacological studies. Biochemical Pharmacology **85**, 1721, 2013.

46. Schwank, G., Koo, B.-K., Sasselli, V., Dekkers, J.F., Heo, I., Demircan, T., Sasaki, N., Boymans, S., Cuppen, E., and van der Ent, C.K. Functional repair of CFTR by CRISPR/Cas9 in intestinal stem cell organoids of cystic fibrosis patients. Cell stem cell **13**, 653, 2013.

47. Sato, T., and Clevers, H. Growing self-organizing mini-guts from a single intestinal stem cell: mechanism and applications. Science **340**, 1190, 2013.

48. Yui, S., Nakamura, T., Sato, T., Nemoto, Y., Mizutani, T., Zheng, X., Ichinose, S., Nagaishi, T., Okamoto, R., and Tsuchiya, K. Functional engraftment of colon epithelium expanded in vitro from a single adult Lgr5+ stem cell. Nature medicine **18**, 618, 2012.

49. de Lau, W., Kujala, P., Schneeberger, K., Middendorp, S., Li, V.S., Barker, N., Martens, A., Hofhuis, F., DeKoter, R.P., and Peters, P.J. Peyer's Patch M cells derive from Lgr5+ stem cells require SpiB and are induced by RankL in cultured 'organoids'. Molecular and cellular biology, MCB. 00434, 2012.

50. Evans, G.S., Flint, N., Somers, A., Eyden, B., and Potten, C.S. The development of a method for the preparation of rat intestinal epithelial cell primary cultures. Journal of Cell Science **101**, 219, 1992.

51. Sato, T., and Clevers, H. Primary mouse small intestinal epithelial cell cultures. Epithelial Cell Culture Protocols: Springer; 2012. pp. 319-328.

52. van de Wetering, M., Francies, H.E., Francis, J.M., Bounova, G., Iorio, F., Pronk, A., van Houdt, W., van Gorp, J., Taylor-Weiner, A., and Kester, L. Prospective derivation of a living organoid biobank of colorectal cancer patients. Cell **161**, 933, 2015.

53. Drost, J., Van Jaarsveld, R.H., Ponsioen, B., Zimberlin, C., Van Boxtel, R., Buijs, A., Sachs, N., Overmeer, R.M., Offerhaus, G.J., and Begthel, H. Sequential cancer mutations in cultured human intestinal stem cells. Nature **521**, 43, 2015.

54. Finkbeiner, S.R., Zeng, X.-L., Utama, B., Atmar, R.L., Shroyer, N.F., and Estes, M.K. Stem cell-derived human intestinal organoids as an infection model for rotaviruses. MBio **3**, e00159, 2012.

55. VanDussen, K.L., Marinshaw, J.M., Shaikh, N., Miyoshi, H., Moon, C., Tarr, P.I., Ciorba, M.A., and Stappenbeck, T.S. Development of an enhanced human gastrointestinal epithelial culture system to facilitate patient-based assays. Gut **64**, 911, 2015.

56. Alam, M.A., Al-Jenoobi, F.I., and Al-mohizea, A.M. Everted gut sac model as a tool in pharmaceutical research: limitations and applications. Journal of Pharmacy and Pharmacology **64**, 326, 2012.

57. Bagnall, W., Kelleher, J., Walker, B., and Losowsky, M. The gastrointestinal absorption of paracetamol in the rat. Journal of Pharmacy and Pharmacology **31**, 157, 1979.

58. Arellano, C., Philibert, C., Vachoux, C., Woodley, J., and Houin, G. The metabolism of midazolam and comparison with other CYP enzyme substrates during intestinal absorption: in vitro studies with rat everted gut sacs. Journal of Pharmacy and Pharmaceutical Sciences **10**, 26, 2007.

59. Wilson, T.H., and Wiseman, G. The use of sacs of everted small intestine for the study of the transference of substances from the mucosal to the serosal surface. The Journal of physiology **123**, 116, 1954.

60. Zhang, J.H., Nolan, J.D., Kennie, S.L., Johnston, I.M., Dew, T., Dixon, P.H., Williamson, C., and Walters, J.R. Potent stimulation of fibroblast growth factor 19 expression in the human ileum by bile acids. American Journal of Physiology-Gastrointestinal and Liver Physiology **304**, G940, 2013.

61. Thomas, M.A., Demberg, T., Vargas-Inchaustegui, D.A., Xiao, P., Tuero, I., Venzon, D., Weiss, D., Treece, J., and Robert-Guroff, M. Rhesus macaque rectal and duodenal tissues exhibit B-cell sub-populations distinct from peripheral blood that continuously secrete antigen-specific IgA in short-term explant cultures. Vaccine **32**, 872, 2014.

62. Schmiedlin-Ren, P., Benedict, P.E., Dobbins, W.O., Ghosh, M., Kolars, J.C., and Watkins, P.B. Cultured adult rat jejunal explants as a model for studying regulation of CYP3A. Biochemical Pharmacology **46**, 905, 1993.

63. Kolf-Clauw, M., Castellote, J., Joly, B., Bourges-Abella, N., Raymond-Letron, I., Pinton, P., and Oswald, I.P. Development of a pig jejunal explant culture for studying the gastrointestinal toxicity of the mycotoxin deoxynivalenol: Histopathological analysis. Toxicology in Vitro **23**, 1580, 2009.

64. Shamsuddin, A., Barrett, L., Autrup, H., Harris, C., and Trump, B. Long-term organ culture of adult rat colon. Pathology-Research and Practice **163**, 362, 1978.

65. Finney, K.J., Ince, P., Appleton, D., Sunter, J., and Watson, A. A comparison of crypt-cell proliferation in rat colonic mucosa in vivo and in vitro. Journal of Anatomy **149**, 177, 1986.

66. Finney, K.J., Appleton, D.R., Ince, P., Sunter, J.P., and Watson, A.J. Proliferative status of colonic mucosa in organ culture: 3H-thymidine-labelling studies and computer modelling. Virchows Archiv B **56**, 397, 1988.

67. Nanthakumar, N.N., Young, C., Ko, J.S., Meng, D., Chen, J., Buie, T., and Walker, W.A. Glucocorticoid responsiveness in developing human intestine: possible role in prevention of necrotizing enterocolitis. American Journal of Physiology-Gastrointestinal and Liver Physiology **288**, G85, 2005.

68. Losonsky, G.A., Fantry, G.T., Reymann, M., and Lim, Y. Validation of a gastrointestinal explant system for measurement of mucosal antibody production. Clinical and Diagnostic Laboratory Immunology **6**, 803, 1999.

69. de Kanter, R., Tuin, A., van de Kerkhof, E., Martignoni, M., Draaisma, A.L., de Jager, M.H., de Graaf, I.A., Meijer, D.K., and Groothuis, G.M. A new technique for preparing precision-cut slices from small intestine and colon for drug biotransformation studies. Journal of pharmacological and toxicological methods **51**, 65, 2005.

70. Pham, B.T., van Haaften, W.T., Oosterhuis, D., Nieken, J., de Graaf, I.A.M., and Olinga, P. Precision-cut rat, mouse, and human intestinal slices as novel models for the early-onset of intestinal fibrosis. Physiological Reports **3**2015.

71. MM Groothuis, G., and AM de Graaf, I. Precision-cut intestinal slices as in vitro tool for studies on drug metabolism. Current drug metabolism **14**, 112, 2013.

72. van de Kerkhof, E., de Graaf, I., de Jager, M., Meijer, D., and Groothuis, G. Characterisation of rat small intestinal and colon precision-cut slices as an in vitro system for drug metabolism and induction studies. Drug metabolism and disposition 2005.

73. de Graaf, I.A., Olinga, P., de Jager, M.H., Merema, M.T., de Kanter, R., van de Kerkhof, E.G., and Groothuis, G.M. Preparation and incubation of precision-cut liver and intestinal slices for application in drug metabolism and toxicity studies. Nature Protocols **5**, 1540, 2010.

74. van de Kerkhof, E.G., de Graaf, I.A., de Jager, M.H., Meijer, D.K., and Groothuis, G.M. Characterization of rat small intestinal and colon precision-cut slices as an in vitro system for drug metabolism and induction studies. Drug metabolism and disposition **33**, 1613, 2005.

75. Maresca, M., Pinton, P., Ajandouz, E.H., Menard, S., Ferrier, L., and Oswald, I.P. Overview and Comparison of Intestinal Organotypic Models, Intestinal Cells, and Intestinal Explants Used for Toxicity Studies. 2018.

76. Russo, I., Zeppa, P., Iovino, P., Del Giorno, C., Zingone, F., Bucci, C., Puzziello, A., and Ciacci, C. The culture of gut explants: A model to study the mucosal response. Journal of immunological methods **438**, 1, 2016.

77. Randall, K.J., Turton, J., and Foster, J.R. Explant culture of gastrointestinal tissue: a review of methods and applications. Cell Biology and Toxicology **27**, 267, 2011.

78. van Midwoud, P.M., Merema, M.T., Verpoorte, E., and Groothuis, G.M. A microfluidic approach for in vitro assessment of interorgan interactions in drug metabolism using intestinal and liver slices. Lab on a Chip **10**, 2778, 2010.

79. Arias, I.M., Boyer, J.L., Chisari, F.V., Fausto, M., Schachter, D., and Shafritz, D.A. The Liver: Biology and Pathology. 4th ed. Philadelphia, PA: Lippincott Williams and Wilkins; 2001.

80. Kaplowitz, N., and DeLeve, L. Drug-Induced Liver Disease. Third ed: Academic Press; 2013.

81. Klassen, C.D. Casarett and Doull's Toxicology: The Basic Science of Poisons. New York, NY: McGraw-Hill; 2013.

82. Haschek, W.M., and Rousseaux, C.G. Fundamentals of Toxicologic Pathology: Academic Press; 1997.

83. LeCluyse, E.L., Witek, R.P., Andersen, M.E., and Powers, M.J. Organotypic liver culture models: meeting current challenges in toxicity testing. Critical Reviews in Toxicology **42**, 501, 2012.

84. Godoy, P., Hewitt, N.J., Albrecht, U., Andersen, M.E., Ansari, N., Bhattacharya, S., Bode, J.G., Bolleyn, J., Borner, C., Bottger, J., Braeuning, A., Budinsky, R.A., Burkhardt, B., Cameron, N.R., Camussi, G., Cho, C.S., Choi, Y.J., Craig Rowlands, J., Dahmen, U., Damm, G., Dirsch, O., Donato, M.T., Dong, J., Dooley, S., Drasdo, D., Eakins, R., Ferreira, K.S., Fonsato, V., Fraczek, J., Gebhardt, R., Gibson, A., Glanemann, M., Goldring, C.E., Gomez-Lechon, M.J., Groothuis, G.M., Gustavsson, L., Guyot, C., Hallifax, D., Hammad, S., Hayward, A., Haussinger, D., Hellerbrand, C., Hewitt, P., Hoehme, S., Holzhutter, H.G., Houston, J.B., Hrach, J., Ito, K., Jaeschke, H., Keitel, V., Kelm, J.M., Kevin Park, B., Kordes, C., Kullak-Ublick, G.A., LeCluyse, E.L., Lu, P., Luebke-Wheeler, J., Lutz, A., Maltman, D.J., Matz-Soja, M., McMullen, P., Merfort, I., Messner, S., Meyer, C., Mwinyi, J., Naisbitt, D.J., Nussler, A.K., Olinga, P., Pampaloni, F., Pi, J., Pluta, L., Przyborski, S.A., Ramachandran, A., Rogiers, V., Rowe, C., Schelcher, C., Schmich, K., Schwarz, M., Singh, B., Stelzer, E.H., Stieger, B., Stober, R., Sugiyama, Y., Tetta,

C., Thasler, W.E., Vanhaecke, T., Vinken, M., Weiss, T.S., Widera, A., Woods, C.G., Xu, J.J., Yarborough, K.M., and Hengstler, J.G. Recent advances in 2D and 3D in vitro systems using primary hepatocytes, alternative hepatocyte sources and non-parenchymal liver cells and their use in investigating mechanisms of hepatotoxicity, cell signaling and ADME. Archives of Toxicology **87**, 1315, 2013.

85. Rodes, J., Benhamou, J., Blei, A., Reichen, J., and Rizzetto, M. Textbook of hepatology. From basic science to clinical practice. 3rd. Malden, Mass.: Blackwell.

86. Cotran, R.S., Kumar, V., and Collins, T. Robbins Pathologic Basis of Disease. 6th ed. Philadelphia, PA: Saunders; 1999.

87. Martinez-Hernandez, A., and Amenta, P.S. The hepatic extracellular matrix. I. Components and distribution in normal liver. Virchows Archive A Pathological Anatomy and Histopathology **423**, 1, 1993.

88. Wells, R.G. Function and metabolism of collagen and other extracellular matrix proteins. In: Rodes J., Benhamou J.-P., Blei A., Reichen J., Rizzetto M., eds. The Textbook of Hepatology: From Basic Science to Clinical Practice. Hoboken, NJ: Wiley-Blackwell; 2007.

89. Dunn, J.C., Yarmush, M.L., Koebe, H.G., and Tompkins, R.G. Hepatocyte function and extracellular matrix geometry: long-term culture in a sandwich configuration. FASEB Journal **3**, 174, 1989.

90. Dunn, J.C., Tompkins, R.G., and Yarmush, M.L. Long-term in vitro function of adult hepatocytes in a collagen sandwich configuration. Biotechnology Progress **7**, 237, 1991.

91. Michalopoulos, G., Sattler, C.A., Sattler, G.L., and Pitot, H.C. Cytochrome P-450 induction by phenobarbital and 3-methylcholanthrene in primary cultures of hepatocytes. Science **193**, 907, 1976.

92. Vrzal, R., Zenata, O., Bachleda, P., and Dvorak, Z. The effects of drugs with immunosuppressive or immunomodulatory activities on xenobiotics-metabolizing enzymes expression in primary human hepatocytes. Toxicology in Vitro **29**, 1088, 2015.

93. Lewerenz, V., Hanelt, S., Nastevska, C., El-Bahay, C., Rohrdanz, E., and Kahl, R. Antioxidants protect primary rat hepatocyte cultures against acetaminophen-induced DNA strand breaks but not against acetaminophen-induced cytotoxicity. Toxicology **191**, 179, 2003.

94. den Braver-Sewradj, S.P., den Braver, M.W., Vermeulen, N.P., Commandeur, J.N., Richert, L., and Vos, J.C. Inter-donor variability of phase I/phase II metabolism of three reference drugs in cryopreserved primary human hepatocytes in suspension and monolayer. Toxicology in Vitro **33**, 71, 2016.

95. de Longueville, F., Atienzar, F.A., Marcq, L., Dufrane, S., Evrard, S., Wouters, L., Leroux, F., Bertholet, V., Gerin, B., and Whomsley, R. Use of a low-density microarray for studying gene expression patterns induced by hepatotoxicants on primary cultures of rat hepatocytes. toxicological sciences **75**, 378, 2003.

96. Schyschka, L., Sanchez, J.J., Wang, Z., Burkhardt, B., Muller-Vieira, U., Zeilinger, K., Bachmann, A., Nadalin, S., Damm, G., and Nussler, A.K. Hepatic 3D cultures but not 2D cultures preserve specific transporter activity for acetaminophen-induced hepatotoxicity. Archives of Toxicology **87**, 1581, 2013.

97. Oorts, M., Baze, A., Bachellier, P., Heyd, B., Zacharias, T., Annaert, P., and Richert, L. Drug-induced cholestasis risk assessment in sandwich-cultured human hepatocytes. Toxicology in Vitro **34**, 179, 2016.

98. Liu, C., Sekine, S., and Ito, K. Assessment of mitochondrial dysfunction-related, drug-induced hepatotoxicity in primary rat hepatocytes. Toxicology and Applied Pharmacology **302**, 23, 2016.

99. Kienhuis, A.S., Wortelboer, H.M., Hoflack, J.C., Moonen, E.J., Kleinjans, J.C., van Ommen, B., van Delft, J.H., and Stierum, R.H. Comparison of coumarin-induced toxicity between sandwich-cultured primary rat hepatocytes and rats in vivo: a toxicogenomics approach. Drug metabolism and disposition **34**, 2083, 2006.

100. Jemnitz, K., Veres, Z., Monostory, K., Kobori, L., and Vereczkey, L. Interspecies differences in acetaminophen sensitivity of human, rat, and mouse primary hepatocytes. Toxicology in Vitro **22**, 961, 2008.

101. Farkas, D., and Tannenbaum, S.R. Characterization of chemically induced hepatotoxicity in collagen sandwiches of rat hepatocytes. toxicological sciences **85**, 927, 2005.

102. Cosgrove, B.D., King, B.M., Hasan, M.A., Alexopoulos, L.G., Farazi, P.A., Hendriks, B.S., Griffith, L.G., Sorger, P.K., Tidor, B., Xu, J.J., and Lauffenburger, D.A. Synergistic drug-cytokine induction of hepatocellular death as an in vitro approach for the study of inflammation-associated idiosyncratic drug hepatotoxicity. Toxicology and Applied Pharmacology **237**, 317, 2009.

103. Chatterjee, S., Bijsmans, I.T., van Mil, S.W., Augustijns, P., and Annaert, P. Toxicity and intracellular accumulation of bile acids in sandwich-cultured rat hepatocytes: role of glycine conjugates. Toxicology in Vitro **28**, 218, 2014.

104. Bhatia, S.N., Balis, U.J., Yarmush, M.L., and Toner, M. Effect of cell-cell interactions in preservation of cellular phenotype: cocultivation of hepatocytes and nonparenchymal cells. FASEB Journal **13**, 1883, 1999.

105. Clement, B., Guguen-Guillouzo, C., Campion, J.P., Glaise, D., Bourel, M., and Guillouzo, A. Long-term co-cultures of adult human hepatocytes with rat liver epithelial cells: modulation of albumin secretion and accumulation of extracellular material. Hepatology **4**, 373, 1984.

106. Fraslin, J.M., Kneip, B., Vaulont, S., Glaise, D., Munnich, A., and Guguen-Guillouzo, C. Dependence of hepatocyte-specific gene expression on cell-cell interactions in primary culture. EMBO Journal **4**, 2487, 1985.

107. Griffith, L.G., and Swartz, M.A. Capturing complex 3D tissue physiology in vitro. Nature Reviews Molecular and Cell Biology **7**, 211, 2006.

108. Roberts, M.S., Magnusson, B.M., Burczynski, F.J., and Weiss, M. Enterohepatic circulation. Clinical pharmacokinetics **41**, 751, 2002.

109. Hofmann, A.F. Enterohepatic circulation of bile acids. Comprehensive Physiology 2011.

110. Jones, E., Smallwood, R., Craigie, A., and Rosenoer, V. The enterohepatic circulation of urea nitrogen. Clinical science **37**, 825, 1969.

111. Vajro, P., Paolella, G., and Fasano, A. Microbiota and gut-liver axis: a mini-review on their influences on obesity and obesity related liver disease. Journal of pediatric gastroenterology and nutrition **56**, 461, 2013.

112. Pereira de Sousa, I., and Bernkop-Schnurch, A. Pre-systemic metabolism of orally administered drugs and strategies to overcome it. Journal of Controlled Release **192**, 301, 2014.

113. Niu, X. Precision-cut intestinal slices as an ex vivo model to study NSAID-induced intestinal toxicity. Toxicology in vitro **28**, 1296, 2014.

114. Price, A.B. Pathology of drug-associated gastrointestinal disease. British journal of clinical pharmacology **56**, 477, 2003.

115. Ilett, K.F., Tee, L.B., Reeves, P.T., and Minchin, R.F. Metabolism of drugs and other xenobiotics in the gut lumen and wall. Pharmacology and Therapeutics **46**, 67, 1990.

116. Schaffner, F. Hepatic drug metabolism and adverse hepatic drug reactions. Veterinary Pathology **12**, 145, 1975.

117. Back, D., and Rogers, S. Review: first-pass metabolism by the gastrointestinal mucosa. Alimentary Pharmacology & Therapeutics **1**, 339, 1987.

118. Hall, J.E. Guyton and Hall textbook of medical physiology: Elsevier Health Sciences; 2015.

119. Lee, Y.-P., Liao, J.-T., Cheng, Y.-W., Wu, T.-L., Lee, S.-L., Liu, J.-K., and Yin, S.-J. Inhibition of human alcohol and aldehyde dehydrogenases by acetaminophen: assessment of the effects on first-pass metabolism of ethanol. Alcohol **47**, 559, 2013.

120. Choi, S.H., Fukuda, O., Sakoda, A., and Sakai, Y. Enhanced cytochrome P450 capacities of Caco-2 and Hep G2 cells in new coculture system under the static and perfused conditions:

evidence for possible organ-to-organ interactions against exogenous stimuli. Materials Science and Engineering: C **24**, 333, 2004.

121. Bricks, T., Hamon, J., Fleury, M.J., Jellali, R., Merlier, F., Herpe, Y.E., Seyer, A., Regimbeau, J.M., Bois, F., and Leclerc, E. Investigation of omeprazole and phenacetin first-pass metabolism in humans using a microscale bioreactor and pharmacokinetic models. Biopharmaceutics & Drug Disposition **36**, 275, 2015.

122. Sung, J.H., and Shuler, M.L. A micro cell culture analog (μCCA) with 3-D hydrogel culture of multiple cell lines to assess metabolism-dependent cytotoxicity of anti-cancer drugs. Lab on a Chip **9**, 1385, 2009.

123. Maschmeyer, I., Hasenberg, T., Jaenicke, A., Lindner, M., Lorenz, A.K., Zech, J., Garbe, L.-A., Sonntag, F., Hayden, P., and Ayehunie, S. Chip-based human liver–intestine and liver–skin co-cultures–A first step toward systemic repeated dose substance testing in vitro. European Journal of Pharmaceutics and Biopharmaceutics **95**, 77, 2015.

124. Prot, J.M., Maciel, L., Bricks, T., Merlier, F., Cotton, J., Paullier, P., Bois, F.Y., and Leclerc, E. First pass intestinal and liver metabolism of paracetamol in a microfluidic platform coupled with a mathematical modeling as a means of evaluating ADME processes in humans. Biotechnology and Bioengineering **111**, 2027, 2014.

125. Mahler, G.J., Esch, M.B., Glahn, R.P., and Shuler, M.L. Characterization of a gastrointestinal tract microscale cell culture analog used to predict drug toxicity. Biotechnology and Bioengineering **104**, 193, 2009.

126. Esch, M.B., Mahler, G.J., Stokol, T., and Shuler, M.L. Body-on-a-chip simulation with gastrointestinal tract and liver tissues suggests that ingested nanoparticles have the potential to cause liver injury. Lab on a Chip **14**, 3081, 2014.

127. Lau, Y.Y., Chen, Y.-H., Liu, T.-t., Li, C., Cui, X., White, R.E., and Cheng, K.-C. Evaluation of a novel in vitro Caco-2 hepatocyte hybrid system for predicting in vivo oral bioavailability. Drug metabolism and disposition **32**, 937, 2004.

128. van Midwoud, P.M., Merema, M.T., Verpoorte, E., and Groothuis, G.M. A microfluidic approach for in vitro assessment of interorgan interactions in drug metabolism using intestinal and liver slices. Lab Chip **10**, 2778, 2010.

129. Singal, A.K., Guturu, P., Hmoud, B., Kuo, Y.-F., Salameh, H., and Wiesner, R.H. Evolving frequency and outcomes of liver transplantation based on etiology of liver disease. Transplantation **95**, 755, 2013.

130. Liangpunsakul, S., Haber, P., and McCaughan, G.W. Alcoholic liver disease in Asia, Europe, and North America. Gastroenterology **150**, 1786, 2016.

131. Purohit, V., Bode, J.C., Bode, C., Brenner, D.A., Choudhry, M.A., Hamilton, F., Kang, Y.J., Keshavarzian, A., Rao, R., and Sartor, R.B. Alcohol, intestinal bacterial growth, intestinal permeability to endotoxin, and medical consequences: summary of a symposium. Alcohol **42**, 349, 2008.

132. Maher, J.J. Exploring alcohol's effects on liver function. Alcohol Health and Research World **21**, 5, 1997.

133. Ferrier, L., Bérard, F., Debrauwer, L., Chabo, C., Langella, P., Buéno, L., and Fioramonti, J. Impairment of the intestinal barrier by ethanol involves enteric microflora and mast cell activation in rodents. The American journal of pathology **168**, 1148, 2006.

134. Leclercq, S., Matamoros, S., Cani, P.D., Neyrinck, A.M., Jamar, F., Stärkel, P., Windey, K., Tremaroli, V., Bäckhed, F., and Verbeke, K. Intestinal permeability, gut-bacterial dysbiosis, and behavioral markers of alcohol-dependence severity. Proceedings of the national academy of sciences **111**, E4485, 2014.

135. Yan, A.W., and Schnabl, B. Bacterial translocation and changes in the intestinal microbiome associated with alcoholic liver disease. World journal of hepatology **4**, 110, 2012.

136. Gao, B., and Bataller, R. Alcoholic liver disease: pathogenesis and new therapeutic targets. Gastroenterology **141**, 1572, 2011.

137. Teli, M.R., Day, C.P., James, O., Burt, A., and Bennett, M. Determinants of progression to cirrhosis or fibrosis in pure alcoholic fatty liver. The Lancet **346**, 987, 1995.

138. Lieber, C.S. Alcohol and the liver: metabolism of alcohol and its role in hepatic and extrahepatic diseases. 2000.

139. Salaspuro, M. Acetaldehyde as a common denominator and cumulative carcinogen in digestive tract cancers. Scandinavian Journal of Gastroenterology **44**, 912, 2009.

140. Lieber, C.S. Ethanol metabolism, cirrhosis and alcoholism. Clinica chimica acta **257**, 59, 1997.

141. Lieber, C.S., and DeCARLI, L.M. The role of the hepatic microsomal ethanol oxidizing system (MEOS) for ethanol metabolism in vivo. Journal of Pharmacology and Experimental Therapeutics **181**, 279, 1972.

142. Hawkins, R.D., and Kalant, H. The metabolism of ethanol and its metabolic effects. Pharmacological Reviews **24**, 67, 1972.

143. Zakhari, S. Overview: how is alcohol metabolized by the body? Alcohol Research **29**, 245, 2006.

144. Cederbaum, A.I. Alcohol metabolism. Clinics in liver disease **16**, 667, 2012.

145. Crabb, D.W., Bosron, W.F., and Li, T.-K. Ethanol metabolism. Pharmacology & therapeutics **34**, 59, 1987.

146. Behrens, U., Hoerner, M., Iasker, J., and Lieber, C. Formation of acetaldehyde adducts with ethanol-inducible P450IIE1 in vivo. Biochemical and Biophysical Research Communications **154**, 584, 1988.

147. Rintala, J., Jaatinen, P., Parkkila, S., Sarviharju, M., Kiianmaa, K., Hervonen, A., and Niemelä, O. Evidence of acetaldehyde–protein adduct formation in rat brain after lifelong consumption of ethanol. Alcohol and Alcoholism **35**, 458, 2000.

148. Lin, R.C., Smith, R.S., and Lumeng, L. Detection of a protein-acetaldehyde adduct in the liver of rats fed alcohol chronically. The Journal of clinical investigation **81**, 615, 1988.

149. Seitz, H.K., and Poschl, G. The role of gastrointestinal factors in alcohol metabolism. Alcohol and Alcoholism **32**, 543, 1997.

150. Bode, C., and Bode, J.C. Effect of alcohol consumption on the gut. Best practice & research Clinical gastroenterology **17**, 575, 2003.

151. Israel, Y., Salazar, I., and Rosenmann, E. Inhibitory effects of alcohol on intestinal amino acid transport in vivo and in vitro. The Journal of nutrition **96**, 499, 1968.

152. Baraona, E., Pirola, R.C., and Lieber, C.S. Small intestinal damage and changes in cell population produced by ethanol ingestion in the rat. Gastroenterology **66**, 226, 1974.

153. Beck, I., and Dinda, P. Acute exposure of small intestine to ethanol. Digestive diseases and sciences **26**, 817, 1981.

154. Gowda, G.N., and Djukovic, D. Overview of mass spectrometry-based metabolomics: opportunities and challenges. Mass Spectrometry in Metabolomics: Springer; 2014. pp. 3-12.

155. Lei, Z., Huhman, D.V., and Sumner, L.W. Mass spectrometry strategies in metabolomics. Journal of Biological Chemistry **286**, 25435, 2011.

156. Dettmer, K., Aronov, P.A., and Hammock, B.D. Mass spectrometry-based metabolomics. Mass spectrometry reviews **26**, 51, 2007.

157. Shao, Y., and Le, W. Recent advances and perspectives of metabolomics-based investigations in Parkinson's disease. Molecular neurodegeneration **14**, 3, 2019.

158. Snyder, N.W., Mesaros, C., and Blair, I.A. Translational metabolomics in cancer research. Biomarkers in medicine **9**, 821, 2015.

159. Li, R., Li, F., Feng, Q., Liu, Z., Jie, Z., Wen, B., Xu, X., Zhong, S., Li, G., and He, K. An LC-MS based untargeted metabolomics study identified novel biomarkers for coronary heart disease. Molecular BioSystems **12**, 3425, 2016.

160. Rockel, J., and Kapoor, M. The metabolome and osteoarthritis: possible contributions to symptoms and pathology. Metabolites **8**, 92, 2018.

161. Chen, C., Gonzalez, F.J., and Idle, J.R. LC-MS-based metabolomics in drug metabolism. Drug metabolism reviews **39**, 581, 2007.

162. Chen, M.X., Wang, S.-Y., Kuo, C.-H., and Tsai, I.-L. Metabolome analysis for investigating host-gut microbiota interactions. Journal of the Formosan Medical Association 2018.

163. Ho, M.-C.D., Ring, N., Amaral, K., Doshi, U., and Li, A.P. Human enterocytes as an in vitro model for the evaluation of intestinal drug metabolism: characterization of drug-metabolizing enzyme activities of cryopreserved human enterocytes from twenty-four donors. Drug metabolism and disposition **45**, 686, 2017.

164. Griffiths, W.J. Tandem mass spectrometry in the study of fatty acids, bile acids, and steroids. Mass spectrometry reviews **22**, 81, 2003.

165. Alnouti, Y., Csanaky, I.L., and Klaassen, C.D. Quantitative-profiling of bile acids and their conjugates in mouse liver, bile, plasma, and urine using LC–MS/MS. Journal of Chromatography B **873**, 209, 2008.

166. Chen, Y., Ogundare, M., Williams, C.M., Wang, Y., Wang, Y., Sewell, G.W., Smith, P.J., Rahman, F.Z., O'Shea, N., and Segal, A.W. Shotgun cholanomics of ileal fluid. Biochimie **95**, 461, 2013.

167. Vernocchi, P., Del Chierico, F., and Putignani, L. Gut microbiota profiling: metabolomics based approach to unravel compounds affecting human health. Frontiers in microbiology **7**, 1144, 2016.

168. Li, Z., Quan, G., Jiang, X., Yang, Y., Ding, X., Zhang, D., Wang, X., Hardwidge, P.R., Ren, W., and Zhu, G. Effects of metabolites derived from gut microbiota and hosts on pathogens. Frontiers in cellular and infection microbiology **8**2018.

169. Krishnan, S., Ding, Y., Saedi, N., Choi, M., Sridharan, G.V., Sherr, D.H., Yarmush, M.L., Alaniz, R.C., Jayaraman, A., and Lee, K. Gut microbiota-derived tryptophan metabolites modulate inflammatory response in hepatocytes and macrophages. Cell reports **23**, 1099, 2018.

170. Yuan, C., Graham, M., Staley, C., and Subramanian, S. Mucosal microbiota and metabolome along the intestinal tracts reveals location specific relationship. bioRxiv, 454496, 2019.

171. Vinayavekhin, N., and Saghatelian, A. Untargeted metabolomics. Current protocols in molecular biology **90**, 30.1. 1, 2010.

172. Li, Y., Shin, Y.G., Yu, C., Kosmeder, J.W., Hirschelman, W.H., Pezzuto, J.M., and van Breemen, R.B. Increasing the throughput and productivity of Caco-2 cell permeability assays using liquid chromatography-mass spectrometry: application to resveratrol absorption and metabolism. Combinatorial chemistry & high throughput screening **6**, 757, 2003.

173. Wong, A.K., Ross, B.P., Chan, Y.-N., Artursson, P., Lazorova, L., Jones, A., and Toth, I. Determination of transport in the Caco-2 cell assay of compounds varying in lipophilicity using LC–MS: enhanced transport of Leu-enkephalin analogues. European journal of pharmaceutical sciences **16**, 113, 2002.

174. Nepal, M.R., Jeong, K.S., Kim, G.H., Cha, D.H., Kang, M.J., Kim, J.S., Kim, J.-H., and Jeong, T.C. Role of Intestinal Microbiota in Metabolism of Gastrodin In Vitro and In Vivo. Metabolites **9**, 69, 2019.

175. Rombouts, C., De Spiegeleer, M., Van Meulebroek, L., De Vos, W.H., and Vanhaecke, L. Validated comprehensive metabolomics and lipidomics analysis of colon tissue and cell lines. Analytica chimica acta **1066**, 79, 2019.

176. Abumrad, N.A., and Davidson, N.O. Role of the gut in lipid homeostasis. Physiological reviews **92**, 1061, 2012.

177. Titz, B., Gadaleta, R., Lo Sasso, G., Elamin, A., Ekroos, K., Ivanov, N., Peitsch, M., and Hoeng, J. Proteomics and lipidomics in inflammatory bowel disease research: from mechanistic insights to biomarker identification. International journal of molecular sciences **19**, 2775, 2018.

178. Kiela, P.R., and Ghishan, F.K. Physiology of intestinal absorption and secretion. Best practice & research Clinical gastroenterology **30**, 145, 2016.

179. Ghazalpour, A., Cespedes, I., Bennett, B.J., and Allayee, H. Expanding role of gut microbiota in lipid metabolism. Current opinion in lipidology **27**, 141, 2016.

180. Wang, T.Y., Liu, M., Portincasa, P., and Wang, D.Q.H. New insights into the molecular mechanism of intestinal fatty acid absorption. European journal of clinical investigation **43**, 1203, 2013.

181. Li, L., Han, J., Wang, Z., Liu, J.a., Wei, J., Xiong, S., and Zhao, Z. Mass spectrometry methodology in lipid analysis. International journal of molecular sciences **15**, 10492, 2014.

182. Correia, B.S.B., Torrinhas, R., Ohashi, W., and Tasic, L. Analytical Tools for Lipid Assessment in Biological Assays. Lipid Metabolism: IntechOpen; 2018.

183. Bowerbank, S.L., Carlin, M.G., and Dean, J.R. A direct comparison of liquid chromatography-mass spectrometry with clinical routine testing immunoassay methods for the detection and quantification of thyroid hormones in blood serum. Analytical and Bioanalytical Chemistry **411**, 2839, 2019.

184. Gandhi, A.S., Budac, D., Khayrullina, T., Staal, R., and Chandrasena, G. Quantitative analysis of lipids: a higher-throughput LC–MS/MS-based method and its comparison to ELISA. Future science OA **3**, FSO157, 2017.

185. Murph, M., Tanaka, T., Pang, J., Felix, E., Thompson, J., and Mills, G. ELISA is advantageous over mass spectrometry analysis of lysophosphatidic acid (LPA) in patient samples for rapid quantification of LPA. AACR; 2008.

186. Kubicek-Sutherland, J., Vu, D., Mendez, H., Jakhar, S., and Mukundan, H. Detection of Lipid and Amphiphilic Biomarkers for Disease Diagnostics. Biosensors **7**, 25, 2017.

187. Savage, D.C. Microbial ecology of the gastrointestinal tract. Annual review of microbiology **31**, 107, 1977.

188. Sender, R., Fuchs, S., and Milo, R. Are we really vastly outnumbered? Revisiting the ratio of bacterial to host cells in humans. Cell **164**, 337, 2016.

189. Luckey, T.D. Introduction to intestinal microecology. The American Journal of Clinical Nutrition **25**, 1292, 1972.

190. Khoruts, A., and Sadowsky, M. Therapeutic transplantation of the distal gut microbiota. Mucosal immunology **4**, 4, 2011.

191. Wikoff, W.R., Anfora, A.T., Liu, J., Schultz, P.G., Lesley, S.A., Peters, E.C., and Siuzdak, G. Metabolomics analysis reveals large effects of gut microflora on mammalian blood metabolites. Proceedings of the national academy of sciences **106**, 3698, 2009.

192. Sayin, S.I., Wahlström, A., Felin, J., Jäntti, S., Marschall, H.-U., Bamberg, K., Angelin, B., Hyötyläinen, T., Orešič, M., and Bäckhed, F. Gut microbiota regulates bile acid metabolism by reducing the levels of tauro-beta-muricholic acid, a naturally occurring FXR antagonist. Cell metabolism **17**, 225, 2013.

193. Shamat, M.A. The role of the gastrointestinal microflora in the metabolism of drugs. International journal of pharmaceutics **97**, 1, 1993.

194. Compare, D., Coccoli, P., Rocco, A., Nardone, O., De Maria, S., Cartenì, M., and Nardone, G. Gut–liver axis: the impact of gut microbiota on non alcoholic fatty liver disease. Nutrition, Metabolism and Cardiovascular Diseases **22**, 471, 2012.

195. Rowland, I., Gibson, G., Heinken, A., Scott, K., Swann, J., Thiele, I., and Tuohy, K. Gut microbiota functions: metabolism of nutrients and other food components. European journal of nutrition, 1, 2017.

196. Seki, E., and Schnabl, B. Role of innate immunity and the microbiota in liver fibrosis: crosstalk between the liver and gut. The Journal of physiology **590**, 447, 2012.

197. Nicholson, J.K., Holmes, E., Kinross, J., Burcelin, R., Gibson, G., Jia, W., and Pettersson, S. Host-gut microbiota metabolic interactions. Science **336**, 1262, 2012.

198. Li, D., Chen, H., Mao, B., Yang, Q., Zhao, J., Gu, Z., Zhang, H., Chen, Y.Q., and Chen, W. Microbial biogeography and core microbiota of the rat digestive tract. Scientific reports **7**, 45840, 2017.

199. Brooks, S.P., McAllister, M., Sandoz, M., and Kalmokoff, M. Culture-independent phylogenetic analysis of the faecal flora of the rat. Canadian journal of microbiology **49**, 589, 2003.

200. Tomas, J., Langella, P., and Cherbuy, C. The intestinal microbiota in the rat model: major breakthroughs from new technologies. Animal Health Research Reviews **13**, 54, 2012.

201. Manichanh, C., Reeder, J., Gibert, P., Varela, E., Llopis, M., Antolin, M., Guigo, R., Knight, R., and Guarner, F. Reshaping the gut microbiome with bacterial transplantation and antibiotic intake. Genome research 2010.

202. Yu, Y., Lu, L., Sun, J., Petrof, E.O., and Claud, E.C. Preterm infant gut microbiota affects intestinal epithelial development in a humanized microbiome gnotobiotic mouse model. American Journal of Physiology-Gastrointestinal and Liver Physiology **311**, G521, 2016.

203. Peck, B.C., Shanahan, M.T., Singh, A.P., and Sethupathy, P. Gut microbial influences on the mammalian intestinal stem cell niche. Stem cells international **2017**2017.

204. Engen, P.A., Green, S.J., Voigt, R.M., Forsyth, C.B., and Keshavarzian, A. The gastrointestinal microbiome: alcohol effects on the composition of intestinal microbiota. Alcohol Research: Current Reviews **37**, 223, 2015.

205. Bode, J., Bode, C., Heidelbach, R., Dürr, H., and Martini, G. Jejunal microflora in patients with chronic alcohol abuse. Hepato-gastroenterology **31**, 30, 1984.

206. Endres, K., and Schäfer, K.-H. Influence of commensal microbiota on the enteric nervous system and its role in neurodegenerative diseases. Journal of innate immunity **10**, 172, 2018.

207. Costa, M., Brookes, S.J., and Hennig, G.W. Anatomy and physiology of the enteric nervous system. Gut **47**, iv15, 2000.

208. Yoo, B.B., and Mazmanian, S.K. The enteric network: interactions between the immune and nervous systems of the gut. Immunity **46**, 910, 2017.

209. Bagyánszki, M., and Bódi, N. Gut region-dependent alterations of nitrergic myenteric neurons after chronic alcohol consumption. World journal of gastrointestinal pathophysiology **6**, 51, 2015.

210. Mittal, R., Debs, L.H., Patel, A.P., Nguyen, D., Patel, K., O'Connor, G., Grati, M.h., Mittal, J., Yan, D., and Eshraghi, A.A. Neurotransmitters: The critical modulators regulating gut–brain axis. Journal of cellular physiology **232**, 2359, 2017.

211. Birchenough, G.M., Johansson, M.E., Gustafsson, J.K., Bergström, J.H., and Hansson, G.C. New developments in goblet cell mucus secretion and function. Mucosal immunology **8**, 712, 2015.

212. Rao, J.N., and Wang, J.-Y. Intestinal Architecture and Development. Regulation of Gastrointestinal Mucosal Growth. San Rafael (CA): Morgan & Claypool Life Sciences; 2010.

213. Collins, J.T., and Bhimji, S.S. Anatomy, abdomen, small intestine. Treasure Island, FL: StatPearls Publishing; 2017.

214. Walter, E., Janich, S., Roessler, B.J., Hilfinger, J.M., and Amidon, G.L. HT29-MTX/Caco-2 cocultures as an in vitro model for the intestinal epithelium: In vitro–in vivo correlation with permeability data from rats and humans. Journal of Pharmaceutical Sciences **85**, 1070, 1996.

215. de Lau, W., Kujala, P., Schneeberger, K., Middendorp, S., Li, V.S., Barker, N., Martens, A., Hofhuis, F., DeKoter, R.P., and Peters, P.J. Peyer's Patch M cells derive from Lgr5+ stem cells require SpiB and are induced by RankL in cultured "miniguts". Molecular and cellular biology **32**, 3639, 2012.

216. Maresca, M., Pinton, P., Ajandouz, E.H., Menard, S., Ferrier, L., and Oswald, I.P. Overview and Comparison of Intestinal Organotypic Models, Intestinal Cells, and Intestinal Explants Used for Toxicity Studies. Current Topics in Microbiology and Immunology. Berlin: Springer; 2018. pp. 1-18.

217. Nik, A.M., and Carlsson, P. Separation of intact intestinal epithelium from mesenchyme. Biotechniques **55**, 42, 2013.

218. Drozdzik, M., Busch, D., Lapczuk, J., Müller, J., Ostrowski, M., Kurzawski, M., and Oswald, S. Protein Abundance of Clinically Relevant Drug-Metabolizing Enzymes in the Human Liver and Intestine: A Comparative Analysis in Paired Tissue Specimens. Clinical Pharmacology and Therapeutics **104**, 515, 2018.

219. Julia, P., Farrees, J., and Pares, X. Characterization of three isoenzymes of rat alcohol dehydrogenase: Tissue distribution and physical and enzymatic properties. European journal of biochemistry **162**, 179, 1987.

220. Damink, S.W.O., Deutz, N.E., Dejong, C.H., Soeters, P.B., and Jalan, R. Interorgan ammonia metabolism in liver failure. Neurochemistry international **41**, 177, 2002.

221. Seo, Y.S., and Shah, V.H. The role of gut-liver axis in the pathogenesis of liver cirrhosis and portal hypertension. Clinical and Molecular Hepatology **18**, 337, 2012.

222. Kothari, A., and Rajagopalan, P. Isolating Rat Intestinal Explants for In Vitro Cultures. Current protocols in toxicology, e79, 2019.

223. Permezel, N., and Webling, D. The length and mucosal surface area of the small and large gut in young rats. Journal of Anatomy **108**, 295, 1971.

224. DeSesso, J., and Jacobson, C. Anatomical and physiological parameters affecting gastrointestinal absorption in humans and rats. Food and Chemical Toxicology **39**, 209, 2001.

225. Stahl, G.E., Mascarenhas, M.R., Fayer, J.C., Shiau, Y.-F., and Watkins, J.B. Passive jejunal bile salt absorption alters the enterohepatic circulation in immature rats. Gastroenterology **104**, 163, 1993.

226. McClintock, C., and Shiau, Y. Jejunum is more important than terminal ileum for taurocholate absorption in rats. American Journal of Physiology: Gastrointestinal and Liver Physiology **244**, G507, 1983.

227. Laval, J., Pradayrol, L., Balas, D., Clemente, F., and Ribet, A. The quantitative distribution of certain enzymes along the small intestine of the rat and its correlation with the villous area and the Paneth cells. Digestion **17**, 309, 1978.

228. Kemper, A.C., and Specian, R.D. Rat small intestinal mucins: a quantitative analysis. The Anatomical record **229**, 219, 1991.

229. Wilson, T., and Wiseman, G. Metabolic activity of the small intestine of the rat and golden hamster (Mesocricetus auratus). The Journal of physiology **123**, 126, 1954.

230. Wada, H., Yagami, I., Niwa, N., HAYAKAWA, T., and TSUGE, H. Distribution and properties of rat intestinal alkaline phosphatase isoenzymes. Experimental animals **50**, 153, 2001.

231. Orbach, S.M., Cassin, M.E., Ehrich, M.F., and Rajagopalan, P. Investigating acetaminophen hepatotoxicity in multi-cellular organotypic liver models. Toxicology In Vitro **42**, 10, 2017.

232. Ford, A.J., Orbach, S.M., and Rajagopalan, P. Fibroblasts stimulate macrophage migration in interconnected extracellular matrices through tunnel formation and fiber alignment. Biomaterials **209**, 88, 2019.

233. Orbach, S.M., Ford, A.J., Saverot, S.-E., and Rajagopalan, P. Multi-cellular transitional organotypic models to investigate liver fibrosis. Acta Biomaterialia 2018.

234. Kim, Y., Larkin, A.L., Davis, R.M., and Rajagopalan, P. The design of in vitro liver sinusoid mimics using chitosan–hyaluronic acid polyelectrolyte multilayers. Tissue Engineering Part A **16**, 2731, 2010.

235. Orbach, S.M., Ehrich, M.F., and Rajagopalan, P. High-throughput toxicity testing of chemicals and mixtures in organotypic multi-cellular cultures of primary human hepatic cells. Toxicology in Vitro **51**, 83, 2018.

236. De Jesus, M., Ahlawat, S., and Mantis, N.J. Isolating and immunostaining lymphocytes and dendritic cells from murine Peyer's patches. Journal of Visualized Experiments: JoVE **73**, e50167, 2013.

237. Fischer, A.H., Jacobson, K.A., Rose, J., and Zeller, R. Hematoxylin and eosin staining of tissue and cell sections. Cold Spring Harbor Protocols **2008**, pdb. prot4986, 2008.

238. Cohen, M., Varki, N.M., Jankowski, M.D., and Gagneux, P. Using unfixed, frozen tissues to study natural mucin distribution. Journal of Visualized Experiments: JoVE **67**, e3928, 2012.

239. Schindelin, J., Arganda-Carreras, I., Frise, E., Kaynig, V., Longair, M., Pietzsch, T., Preibisch, S., Rueden, C., Saalfeld, S., and Schmid, B. Fiji: an open-source platform for biological-image analysis. Nature methods **9**, 676, 2012.

240. Berggren, S., Hoogstraate, J., Fagerholm, U., and Lennernäs, H. Characterization of jejunal absorption and apical efflux of ropivacaine, lidocaine and bupivacaine in the rat using in situ and in vitro absorption models. European journal of pharmaceutical sciences **21**, 553, 2004.

241. Kimura, R.E. Glutamine oxidation by developing rat small intestine. Pediatric research **21**, 214, 1987.

242. Ross, G., and Mayhew, T. Effects of fasting on mucosal dimensions in the duodenum, jejunum and ileum of the rat. Journal of Anatomy **142**, 191, 1985.

243. Holmes, J.L., Van Itallie, C.M., Rasmussen, J.E., and Anderson, J.M. Claudin profiling in the mouse during postnatal intestinal development and along the gastrointestinal tract reveals complex expression patterns. Gene Expression Patterns **6**, 581, 2006.

244. Pelaseyed, T., Bergström, J.H., Gustafsson, J.K., Ermund, A., Birchenough, G.M., Schütte, A., van der Post, S., Svensson, F., Rodríguez-Piñeiro, A.M., and Nyström, E.E. The mucus and mucins of the goblet cells and enterocytes provide the first defense line of the gastrointestinal tract and interact with the immune system. Immunological reviews **260**, 8, 2014.

245. Lallès, J.-P. Intestinal alkaline phosphatase: multiple biological roles in maintenance of intestinal homeostasis and modulation by diet. Nutrition Reviews **68**, 323, 2010.

246. Volman-Mitchell, H., and Parsons, D. Distribution and activities of dicarboxylic amino acid transaminases in gastrointestinal mucosa of rat, mouse, hamster, guinea pig, chicken and pigeon. Biochimica et Biophysica Acta (BBA) - Enzymology **334**, 316, 1974.

247. Williams, J., Duckworth, C., Burkitt, M., Watson, A., Campbell, B., and Pritchard, D. Epithelial cell shedding and barrier function: a matter of life and death at the small intestinal villus tip. Veterinary pathology **52**, 445, 2015.

248. Lehr, C.-M., Poelma, F.G., Junginger, H.E., and Tukker, J.J. An estimate of turnover time of intestinal mucus gel layer in the rat in situ loop. International journal of pharmaceutics **70**, 235, 1991.

249. Specian, R.D., and Oliver, M.G. Functional biology of intestinal goblet cells. American Journal of Physiology Cell Physiology **260**, C183, 1991.

250. Kim, J., and Khan, W. Goblet cells and mucins: role in innate defense in enteric infections. Pathogens **2**, 55, 2013.

251. Lavö, B., Colombel, J.F., Knutsson, L., and Hällgren, R. Acute exposure of small intestine to ethanol induces mucosal leakage and prostaglandin E2 synthesis. Gastroenterology **102**, 468, 1992.

252. Kokoska, E.R., Smith, G.S., Deshpande, Y., Rieckenberg, C.L., and Miller, T.A. Adaptive cytoprotection induced by ethanol in human intestinal cells: role of prostaglandins and calcium homeostasis. Annals of Surgery **228**, 123, 1998.

253. Elamin, E., Jonkers, D., Juuti-Uusitalo, K., van IJzendoorn, S., Troost, F., Duimel, H., Broers, J., Verheyen, F., Dekker, J., and Masclee, A. Effects of ethanol and acetaldehyde on tight junction integrity: in vitro study in a three dimensional intestinal epithelial cell culture model. PloS one **7**, e35008, 2012.

254. Kaushal, N., Goyal, D., and Mahmood, A. In vitro Effects of Ethanol on Intestinal Epithelial Cell Glycosylation in Rats. Nutrition & Food Sciences 2013.

255. Neuman, M.G., Koren, G., and Tiribelli, C. In vitro assessment of the ethanol-induced hepatotoxicity on HepG2 cell line. Biochemical and Biophysical Research Communications **197**, 932, 1993.

256. Henzel, K., Thorborg, C., Hofmann, M., Zimmer, G., and Leuschner, U. Toxicity of ethanol and acetaldehyde in hepatocytes treated with ursodeoxycholic or tauroursodeoxycholic acid. Biochimica et Biophysica Acta (BBA)-Molecular Cell Research **1644**, 37, 2004.

257. Cameron, R., Neuman, M., Shear, N., Katz, G., Bellentani, S., and Tiribelli, C. Modulation of liver-specific cellular response to ethanol in vitro in Hep G2 cells. Toxicology in Vitro **12**, 111, 1998.

258. Karim, S., Liaskou, E., Hadley, S., Youster, J., Faint, J., Adams, D.H., and Lalor, P.F. An in vitro model of human acute ethanol exposure that incorporates CXCR3-and CXCR4-dependent recruitment of immune cells. toxicological sciences **132**, 131, 2013.

259. Pastorino, J.G., and Hoek, J.B. Ethanol potentiates tumor necrosis factor-α cytotoxicity in hepatoma cells and primary rat hepatocytes by promoting induction of the mitochondrial permeability transition. Hepatology **31**, 1141, 2000.

260. Sergent, O., Pereira, M., Belhomme, C., Chevanne, M., Huc, L., and Lagadic-Gossmann, D. Role for membrane fluidity in ethanol-induced oxidative stress of primary rat hepatocytes. Journal of Pharmacology and Experimental Therapeutics **313**, 104, 2005.

261. Casini, A., Galli, A., Di Lollo, S., Orsini, B., Arganini, L., Jezequel, A.M., and Surrenti, C. Ethanol-induced alterations of matrix network in the duodenal mucosa of chronic alcohol abusers. Virchows Archiv **434**, 127, 1999.

262. Klaassen, C.D., and Watkins, J.B. Casarett and Doull's toxicology: the basic science of poisons: McGraw-Hill New York; 1996.

263. Huygelen, V., De Vos, M., Willemen, S., Fransen, E., Casteleyn, C., Van Cruchten, S., and Van Ginneken, C. Age-related differences in mucosal barrier function and morphology of the small intestine in low and normal birth weight piglets. Journal of Animal Science **92**, 3398, 2014.

264. Jando, J., Camargo, S.M., Herzog, B., and Verrey, F. Expression and regulation of the neutral amino acid transporter B0AT1 in rat small intestine. PloS one **12**, e0184845, 2017.

265. Kothari, A., and Rajagopalan, P. The assembly of integrated rat intestinal-hepatocyte cultures. Bioengineering and Translational Medicine **doi: 10.1002/btm2.10146** 2019.

266. Langhi, C., Pedraz-Cuesta, E., Haro, D., Marrero, P.F., and Rodríguez, J.C. Regulation of human class I alcohol dehydrogenases by bile acids. Journal of lipid research **54**, 2475, 2013.

267. Cheng, C.F., and Pan, T.M. Monascus-fermented red mold dioscorea protects mice against alcohol-induced liver injury, whereas its metabolites ankaflavin and monascin regulate ethanol-induced peroxisome proliferator-activated receptor-γ and sterol regulatory element-binding transcription factor-1 expression in HepG2 cells. Journal of the science of food and agriculture **98**, 1889, 2018.

268. Elwahab, A.H.A., Ramadan, B.K., Schaalan, M.F., and Tolba, A.M. A novel role of SIRT1/FGF-21 in taurine protection against cafeteria diet-induced steatohepatitis in rats. Cellular Physiology and Biochemistry **43**, 644, 2017.

269. Lindén, S.K., Florin, T.H., and McGuckin, M.A. Mucin dynamics in intestinal bacterial infection. PloS one **3**, e3952, 2008.

270. Buisine, M.-P., Devisme, L., Degand, P., Dieu, M.-C., Gosselin, B., Copin, M.-C., Aubert, J.-P., and Porchet, N. Developmental mucin gene expression in the gastroduodenal tract and accessory digestive glands. II. Duodenum and liver, gallbladder, and pancreas. Journal of Histochemistry & Cytochemistry **48**, 1667, 2000.

271. Zhong, W., Li, Q., Zhang, W., Sun, Q., Sun, X., and Zhou, Z. Modulation of intestinal barrier and bacterial endotoxin production contributes to the beneficial effect of nicotinic acid on alcohol-induced endotoxemia and hepatic inflammation in Rats. Biomolecules **5**, 2643, 2015.

272. Yamada, S., Mak, K.M., and Lieber, C.S. Chronic ethanol consumption alters rat liver plasma membranes and potentiates release of alkaline phosphatase. Gastroenterology **88**, 1799, 1985.

273. Bates, J.M., Akerlund, J., Mittge, E., and Guillemin, K. Intestinal alkaline phosphatase detoxifies lipopolysaccharide and prevents inflammation in zebrafish in response to the gut microbiota. Cell host & microbe **2**, 371, 2007.

274. de Medina, F.S., Martínez-Augustin, O., González, R., Ballester, I., Nieto, A., Gálvez, J., and Zarzuelo, A. Induction of alkaline phosphatase in the inflamed intestine: a novel pharmacological target for inflammatory bowel disease. Biochemical Pharmacology **68**, 2317, 2004.

275. Lassenius, M., Fogarty, C., Blaut, M., Haimila, K., Riittinen, L., Paju, A., Kirveskari, J., Järvelä, J., Ahola, A., and Gordin, D. Intestinal alkaline phosphatase at the crossroad of intestinal health and disease–a putative role in type 1 diabetes. Journal of internal medicine **281**, 586, 2017.

276. Contreras-Zentella, M.L., and Hernández-Muñoz, R. Is liver enzyme release really associated with cell necrosis induced by oxidant stress? Oxidative Medicine and Cellular Longevity **2016**2016.

277. Hatoff, D.E., and Hardison, W.G. Induced synthesis of alkaline phosphatase by bile acids in rat liver cell culture. Gastroenterology **77**, 1062, 1979.

278. Ostaff, M., Schäfer, C., Courth, L., Stebe, S., Ott, G., Stange, E., and Wehkamp, J. Chronic Heavy Alcohol Use is Associated with Upregulated Paneth Cell Antimicrobials in Gastric Mucosa. Clinical and translational gastroenterology **6**, e103, 2015.

279. Gyongyosi, B., Cho, Y., Lowe, P., Calenda, C., Iracheta-Vellve, A., Satishchandran, A., Ambade, A., and Szabo, G. Alcohol-induced IL-17A production in Paneth cells amplifies endoplasmic reticulum stress, apoptosis, and inflammasome-IL-18 activation in the proximal small intestine in mice. Mucosal immunology, 1, 2019.

280. He, L., Ronis, M.J., and Badger, T.M. Ethanol induction of class I alcohol dehydrogenase expression in the rat occurs through alterations in CCAAT/enhancer binding proteins β and γ. Journal of Biological Chemistry **277**, 43572, 2002.

281. Mistilis, S.P., and Garske, A. Induction of Alcohol Dehydrogenase in Liver and Gastrointestinal Tract. Australasian annals of medicine **18**, 227, 1969.

282. Haseba, T., Kameyama, K., Mashimo, K., and Ohno, Y. Dose-dependent change in elimination kinetics of ethanol due to shift of dominant metabolizing enzyme from ADH 1 (Class I) to ADH 3 (Class III) in mouse. International Journal of Hepatology **2012**2011.

283. Harada, S., Tachiyashiki, K., and Imaizumi, K. Effect of sex hormones on rat liver cytosolic alcohol dehydrogenase activity. Journal of nutritional science and vitaminology **44**, 625, 1998.

284. Hakkak, R., Ronis, M.J., and Badger, T.M. Effects of enteral nutrition and ethanol on cytochrome P450 distribution in small intestine of male rats. Gastroenterology **104**, 1611, 1993.

285. Marí, M., and Cederbaum, A.I. Induction of catalase, alpha, and microsomal glutathione S-transferase in CYP2E1 overexpressing HepG2 cells and protection against short-term oxidative stress. Hepatology **33**, 652, 2001.

286. Vaglenova, J., Martínez, S.E., Porté, S., Duester, G., Farrés, J., and Parés, X. Expression, localization and potential physiological significance of alcohol dehydrogenase in the gastrointestinal tract. European journal of biochemistry **270**, 2652, 2003.

287. Fleming, S., Toratani, S., Shea-Donohue, T., Kashiwabara, Y., Vogel, S.N., and Metcalf, E.S. Pro-and anti-inflammatory gene expression in the murine small intestine and liver after chronic exposure to alcohol. Alcoholism: Clinical and Experimental Research **25**, 579, 2001.

288. Arya, R., Grossie, V.B., Weisbrodt, N.W., Lai, M., Mailman, D., and Moody, F. Temporal expression of tumor necrosis factor-α and nitric oxide synthase 2 in rat small intestine after endotoxin. Digestive diseases and sciences **45**, 744, 2000.

289. Negroni, A., Cucchiara, S., and Stronati, L. Apoptosis, necrosis, and necroptosis in the gut and intestinal homeostasis. Mediators of inflammation **2015**2015.

290. Millan, M., Morris, G., Beck, I., and Henson, J. Villous damage induced by suction biopsy and by acute ethanol intake in normal human small intestine. Digestive diseases and sciences **25**, 513, 1980.

291. Qin, X., and Deitch, E.A. Dissolution of lipids from mucus: A possible mechanism for prompt disruption of gut barrier function by alcohol. Toxicology letters **232**, 356, 2015.

292. Leppkes, M., Roulis, M., Neurath, M.F., Kollias, G., and Becker, C. Pleiotropic functions of TNF-α in the regulation of the intestinal epithelial response to inflammation. International Immunology **26**, 509, 2014.

293. Grewal, R., and Mahmood, A. Ethanol induced changes in glycosylation of mucins in rat intestine. Annals of Gastroenterology, 178, 2009.

294. Cornick, S., Tawiah, A., and Chadee, K. Roles and regulation of the mucus barrier in the gut. Tissue barriers **3**, e982426, 2015.

295. Prakash, R., Raja, S.B., Devaraj, H., and Devaraj, S.N. Up-regulation of MUC2 and IL-1β expression in human colonic epithelial cells by Shigella and its interaction with mucins. PloS one **6**, e27046, 2011.

296. Dohrman, A., Miyata, S., Gallup, M., Li, J.-D., Chapelin, C., Coste, A., Escudier, E., Nadel, J., and Basbaum, C. Mucin gene (MUC 2 and MUC 5AC) upregulation by Gram-positive and Gram-negative bacteria. Biochimica et Biophysica Acta (BBA)-Molecular Basis of Disease **1406**, 251, 1998.

297. Bode, C., and Bode, J.C. Alcohol's role in gastrointestinal tract disorders. Alcohol Health and Research World **21**, 76, 1997.

298. Ito, S., and Lacy, E.R. Morphology of rat gastric mucosal damage, defense, and restitution in the presence of luminal ethanol. Gastroenterology **88**, 250, 1985.

299. Krawitt, E.L. Ethanol and development of disease and injury to tha alimentary tract. Environmental health perspectives **20**, 71, 1977.

300. Lieberman, M., and Peet, A. Marks' basic medical biochemistry: a clinical approach: Wolters Kluwer; 2018.

301. Roberts, L.D., Souza, A.L., Gerszten, R.E., and Clish, C.B. Targeted metabolomics. Current protocols in molecular biology **98**, 30.2. 1, 2012.

302. Schrimpe-Rutledge, A.C., Codreanu, S.G., Sherrod, S.D., and McLean, J.A. Untargeted metabolomics strategies—challenges and emerging directions. Journal of the American Society for Mass Spectrometry **27**, 1897, 2016.

303. Wu, H., Chen, Y., Li, Z., and Liu, X. Untargeted metabolomics profiles delineate metabolic alterations in mouse plasma during lung carcinoma development using UPLC-QTOF/MS in MSE mode. Royal Society open science **5**, 181143, 2018.

304. Commisso, M., Strazzer, P., Toffali, K., Stocchero, M., and Guzzo, F. Untargeted metabolomics: an emerging approach to determine the composition of herbal products. Computational and structural biotechnology journal **4**, e201301007, 2013.

305. Manier, S.K., Keller, A., Schäper, J., and Meyer, M.R. Untargeted metabolomics by high resolution mass spectrometry coupled to normal and reversed phase liquid chromatography as a tool to study the in vitro biotransformation of new psychoactive substances. Scientific reports **9**, 2741, 2019.

306. Murphy, R.C., and Axelsen, P.H. Mass spectrometric analysis of long-chain lipids. Mass spectrometry reviews **30**, 579, 2011.

307. Castro-Perez, J.M., Kamphorst, J., DeGroot, J., Lafeber, F., Goshawk, J., Yu, K., Shockcor, J.P., Vreeken, R.J., and Hankemeier, T. Comprehensive LC− MSE lipidomic analysis using a shotgun approach and its application to biomarker detection and identification in osteoarthritis patients. Journal of proteome research **9**, 2377, 2010.

308. Banerjee, S., and Mazumdar, S. Electrospray ionization mass spectrometry: a technique to access the information beyond the molecular weight of the analyte. International journal of analytical chemistry **2012**2012.

309. Straub, R.F., and Voyksner, R.D. Negative ion formation in electrospray mass spectrometry. Journal of the American Society for Mass Spectrometry **4**, 578, 1993.

310. Peng, C., Tian, J., Lv, M., Huang, Y., Tian, Y., and Zhang, Z. Development and Validation of a Sensitive LC–MS-MS Method for the Simultaneous Determination of Multicomponent Contents in Artificial Calculus Bovis. Journal of chromatographic science **52**, 128, 2013.

311. Nichols, K.K., Ham, B.M., Nichols, J.J., Ziegler, C., and Green-Church, K.B. Identification of fatty acids and fatty acid amides in human meibomian gland secretions. Investigative ophthalmology & visual science **48**, 34, 2007.

312. Xiao, J.F., Zhou, B., and Ressom, H.W. Metabolite identification and quantitation in LC-MS/MS-based metabolomics. TrAC Trends in Analytical Chemistry **32**, 1, 2012.

313. Dunn, W.B., Erban, A., Weber, R.J., Creek, D.J., Brown, M., Breitling, R., Hankemeier, T., Goodacre, R., Neumann, S., and Kopka, J. Mass appeal: metabolite identification in mass spectrometry-focused untargeted metabolomics. Metabolomics **9**, 44, 2013.

314. Worley, B., and Powers, R. Multivariate analysis in metabolomics. Current Metabolomics **1**, 92, 2013.

315. Werth, M.T., Halouska, S., Shortridge, M.D., Zhang, B., and Powers, R. Analysis of metabolomic PCA data using tree diagrams. Analytical biochemistry **399**, 58, 2010.

316. Tietz-Bogert, P., Kim, M., Cheung, A., Tabibian, J., Heimbach, J., Rosen, C., Nandakumar, M., Lazaridis, K., LaRusso, N., and Sung, J. Metabolomic Profiling of Portal Blood and Bile Reveals Metabolic Signatures of Primary Sclerosing Cholangitis. International journal of molecular sciences **19**, 3188, 2018.

317. Wishart, D.S., Tzur, D., Knox, C., Eisner, R., Guo, A.C., Young, N., Cheng, D., Jewell, K., Arndt, D., and Sawhney, S. HMDB: the human metabolome database. Nucleic acids research **35**, D521, 2007.

318. Smith, C.A., O'Maille, G., Want, E.J., Qin, C., Trauger, S.A., Brandon, T.R., Custodio, D.E., Abagyan, R., and Siuzdak, G. METLIN: a metabolite mass spectral database. Therapeutic drug monitoring **27**, 747, 2005.

319. Fahy, E., Sud, M., Cotter, D., and Subramaniam, S. LIPID MAPS online tools for lipid research. Nucleic acids research **35**, W606, 2007.

320. Podniesińska, L., Frański, R., and Frańska, M. Comparison of the electrospray ionization (ESI) responses of penicillins with ESI responses of their methanolysis products. European Journal of Mass Spectrometry **25**, 357, 2019.

321. Shiman, R., and Gray, D.W. Formation and Fate of Tyrosine: Intracellular Partitioning of Newly Synthesized Tyrosine in Mammalian Liver. Journal of Biological Chemistry **273**, 34760, 1998.

322. Matthews, D.E. An overview of phenylalanine and tyrosine kinetics in humans. The Journal of nutrition **137**, 1549S, 2007.

323. Salek, R.M., Steinbeck, C., Viant, M.R., Goodacre, R., and Dunn, W.B. The role of reporting standards for metabolite annotation and identification in metabolomic studies. GigaScience **2**, 13, 2013.

324. Udenfriend, S., and Cooper, J.R. The enzymatic conversion of phenylalanine to tyrosine. Journal of Biological Chemistry **194**, 503, 1952.

325. Sarkar, U., Rivera-Burgos, D., Large, E.M., Hughes, D.J., Ravindra, K.C., Dyer, R.L., Ebrahimkhani, M.R., Wishnok, J.S., Griffith, L.G., and Tannenbaum, S.R. Metabolite profiling and pharmacokinetic evaluation of hydrocortisone in a perfused three-dimensional human liver bioreactor. Drug metabolism and disposition **43**, 1091, 2015.

326. George, C.F. Drug metabolism by the gastrointestinal mucosa. Clinical pharmacokinetics **6**, 259, 1981.

327. Morris, D.J., and Brem, A.S. Role of gut metabolism of adrenal corticosteroids and hypertension: clues gut-cleansing antibiotics give us. Physiological genomics **51**, 83, 2019.

328. Villard, P.-H., Barlesi, F., Armand, M., Pascussi, J.-M., Fouchier, F., Champion, S., Dufour, C., Ginies, C., Khalil, A., and Amiot, M.-J. CYP1A1 induction in the colon by serum:

involvement of the PPARα pathway and evidence for a new specific human PPREα site. PloS one **6**, e14629, 2011.

329. Boettcher, R.T., Stadler, I., and Smith, T.A.D. Preparation of Lipid-Stripped Serum for the Study of Lipid Metabolism in Cell Culture. Developmental Cell 2016.

330. Gregory, M.K., King, H.W., Bain, P.A., Gibson, R.A., Tocher, D.R., and Schuller, K.A. Development of a fish cell culture model to investigate the impact of fish oil replacement on lipid peroxidation. Lipids **46**, 753, 2011.

331. Switzer, S., and Eder, H.A. Transport of lysolecithin by albumin in human and rat plasma. Journal of lipid research **6**, 506, 1965.

332. Esko, J.D., and Matsuoka, K. Biosynthesis of phosphatidylcholine from serum phospholipids in Chinese hamster ovary cells deprived of choline. Journal of Biological Chemistry **258**, 3051, 1983.

333. Palmela, I., Correia, L., Silva, R.F., Sasaki, H., Kim, K.S., Brites, D., and Brito, M.A. Hydrophilic bile acids protect human blood-brain barrier endothelial cells from disruption by unconjugated bilirubin: an in vitro study. Frontiers in neuroscience **9**, 80, 2015.

334. Griffiths, W.J., and Sjövall, J. Bile acids: analysis in biological fluids and tissues. Journal of lipid research **51**, 23, 2010.

335. Liu, Y., Rong, Z., Xiang, D., Zhang, C., and Liu, D. Detection technologies and metabolic profiling of bile acids: a comprehensive review. Lipids in health and disease **17**, 121, 2018.

336. Ibrahim, E., Diakonov, I., Arunthavarajah, D., Swift, T., Goodwin, M., McIlvride, S., Nikolova, V., Williamson, C., and Gorelik, J. Bile acids and their respective conjugates elicit different responses in neonatal cardiomyocytes: role of Gi protein, muscarinic receptors and TGR5. Scientific reports **8**, 7110, 2018.

337. Saunders, D.R., Parmentier, C.M., and Ways, P.O. Metabolism of lysolecithin by rat small intestine. Gastroenterology **54**, 382, 1968.

338. Tagesson, C., Telemo, E., Ekström, G., and Weström, B. Development of phospholipase A2 and lysophosphatidylcholine metabolising enzyme activities in the neonatal rat intestine. Gut **28**, 822, 1987.

339. Pind, S., and Kuksis, A. Further characterization of a novel phospholipase B (phospholipase A2–lysophospholipase) from intestinal brush-border membranes. Biochemistry and cell biology **69**, 346, 1991.

340. Minich, D.M., Vonk, R.J., and Verkade, H.J. Intestinal absorption of essential fatty acids under physiological and essential fatty acid-deficient conditions. Journal of lipid research **38**, 1709, 1997.

341. Stoll, L.L., and Spector, A.A. Changes in serum influence the fatty acid composition of established cell lines. In vitro **20**, 732, 1984.

342. Balsinde, J., Winstead, M.V., and Dennis, E.A. Phospholipase A2 regulation of arachidonic acid mobilization. FEBS letters **531**, 2, 2002.

343. Salem Jr, N., Pawlosky, R., Wegher, B., and Hibbeln, J. In vivo conversion of linoleic acid to arachidonic acid in human adults. Prostaglandins, leukotrienes and essential fatty acids **60**, 407, 1999.

344. Mansbach, C.M. Intestinal phospholipase, a novel enzyme. The Journal of clinical investigation **69**, 368, 1982.

345. Shakir, K., Gabriel, L., Sundaram, S.G., and Margolis, S. Intestinal phospholipase A and triglyceride lipase: localization and effect of fasting. American Journal of Physiology-Gastrointestinal and Liver Physiology **242**, G168, 1982.

346. Calder, P.C. Polyunsaturated fatty acids and inflammation. Prostaglandins, leukotrienes and essential fatty acids **75**, 197, 2006.

347. Clarke, G., Fitzgerald, P., Hennessy, A.A., Cassidy, E.M., Quigley, E.M., Ross, P., Stanton, C., Cryan, J.F., and Dinan, T.G. Marked elevations in pro-inflammatory

polyunsaturated fatty acid metabolites in females with irritable bowel syndrome. Journal of lipid research **51**, 1186, 2010.

348. Xie, G., Zhong, W., Zheng, X., Li, Q., Qiu, Y., Li, H., Chen, H., Zhou, Z., and Jia, W. Chronic ethanol consumption alters mammalian gastrointestinal content metabolites. Journal of proteome research **12**, 3297, 2013.

349. Yano, J.M., Yu, K., Donaldson, G.P., Shastri, G.G., Ann, P., Ma, L., Nagler, C.R., Ismagilov, R.F., Mazmanian, S.K., and Hsiao, E.Y. Indigenous bacteria from the gut microbiota regulate host serotonin biosynthesis. Cell **161**, 264, 2015.

350. Shimizu, K., Ogura, H., Tomono, K., Tasaki, O., Asahara, T., Nomoto, K., Morotomi, M., Matsushima, A., Nakahori, Y., and Yamano, S. Patterns of Gram-stained fecal flora as a quick diagnostic marker in patients with severe SIRS. Digestive diseases and sciences **56**, 1782, 2011.

351. Hasegawa, Y., Welch, J.L.M., Rossetti, B.J., and Borisy, G.G. Preservation of three-dimensional spatial structure in the gut microbiome. PloS one **12**, e0188257, 2017.

352. Goris, H., Boer, F.D., and van der Waaij, D. Oral administration of antibiotics and intestinal flora associated endotoxin in mice. Scandinavian journal of infectious diseases **18**, 55, 1986.

353. de Muinck, E.J., Trosvik, P., Gilfillan, G.D., Hov, J.R., and Sundaram, A.Y. A novel ultra high-throughput 16S rRNA gene amplicon sequencing library preparation method for the Illumina HiSeq platform. Microbiome **5**, 68, 2017.